METEOR -Berichte

Rainbow non-boyant hydrothermal plume GEOTRACES study

Cruise No. M176/2

01.09.2021-06.10.2021
Emden (Germany) – Emden (Germany)
Rainbow Plume

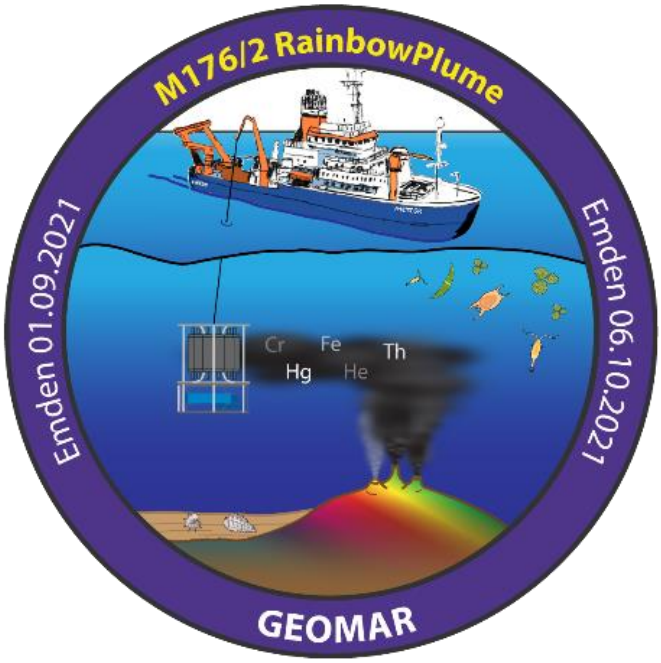

Authors: Prof. Dr. Eric Achterberg and Dr. Zvi Steiner

Chief Scientist: Prof. Dr. Eric Achterberg
GEOMAR Helmholtz Centre for Ocean Research Kiel

2021

Table of Contents

1 Cruise Summary 4
1.1 Summary in English 4
1.2 Zusammenfassung 4
2 Participants 4
2.1 Principal Investigators 4
2.2 Scientific Party 5
2.3 Participating Institutions 5
3 Research Program 6
3.1 Description of the Work Area 6
3.2 Aims of the Cruise 6
3.2 Agenda of the Cruise 7
4 Narrative of the Cruise 9
5 Preliminary Results 11
5.1 Multibeam and Backscatter Mapping of the Rainbow Vent Field and Surround Region. 11
5.2 In-situ mapping of the dispersing Rainbow hydrothermal plume 12
5.2.1 Lateral CTD Survey overview 13
5.3 The control of surface ocean microbial communities by nutrient supply 14
5.3.1 Upper ocean Ti CTD sampling 14
5.3.2 Under-Way Tow-Fish sampling 15
5.3.3 Biological nitrogen fixation 15
5.3.4 Nutrient regulation of phytoplankton growth rates in the North Atlantic 16
5.3.5 Availability of iron to phytoplankton 18
5.4 Deep-water collection with trace metal clean CTD/Rosette 21
5.4.1 Clean lab sampling 21
5.4.2 On-deck sampling 22
5.4.3 Oxygen 22
5.4.4 Particulate and dissolved siderophores 22
5.4.5 Aluminium 23
5.4.6 Dissolved Chromium 24
5.4.7 Stable barium isotopes and rare earth elements (REEs) 24
5.4.8 Mercury 26
5.4.9 Water sampling for dissolved trace-metals, HFSE, Cr and V speciation and organic Fe, Zn and Cu ligands in different size fractions 30
5.4.10 Major elements 31
5.4.11 Nutrients 32
5.5 Suspended particles and radiogenic tracers 33
5.5.1 Subsampling of in-situ pump filters 33
5.5.2 Metal mineralogy sampling 33
5.5.3 Radium Isotopes 34
5.5.4 Thorium 35
5.6 Sediment and porewater 36
5.6.1 Living foraminiferal abundance 37
5.6.2 Porewater 37
5.6.3 MUC video observations 39
5.6.4 Description of the >125 µm fraction of surface sediments 41
5.7 Aerosol sampling 41
5.8 Study of ammonium dynamics, pathways and its controlling factors 42
6 Ship's Meteorological Station 43
6.1 Weather for cruise M176/2. 43

6.2 Transit to the research area 43
6.3 Research work to the southwest of the Azores. 44
6.4 Transit to Emden 45
7 Station List M176/2 46
7.1 Overall Station List 46
8 Data and Sample Storage and Availability 51
9 Acknowledgements 52
10 References 52
11 Abbreviations 58
12 Appendices 60
12.1 Turbidity profiles measured during the Tow-Yo casts 60
12.2 Vertical CTD LADCP Measurements 65
12.3 Biological nitrogen fixation 72
12.4 Plume titanium CTD casts 76
12.5 On-deck sampling of the trace metal Niskin bottles 77
12.6 Chromium samples 84
12.7 In-situ pumps 86
12.8 Radium 87
12.9 Thorium 88
12.10 Sediment and porewater 91
12.11 Aerosols 92
12.12 Nutrients 93
12.13 Ammonium dynamics samples 94
12.14 JUB samples 95

1 Cruise Summary

1.1 Summary in English

On cruise M176/2 we conducted detailed water column surveys in close vicinity to the Rainbow hydrothermal vent field and up to a distance of 60 km along the hydrothermal plume flow. Our aim was to determine the fate of hydrothermally derived trace elements and isotopes (TEIs) with increasing distance from the source, including an assessment of changes in physical and chemical speciation. We assessed to what extent TEIs are controlled by vent supply, particle removal processes and advection. Sampling of Th, Ra and He isotopes was conducted to facilitate quantification of hydrothermal fluxes and removal of TEI and fingerprint sources to elucidate TEI distributions. Atmospheric and deep water (micro)nutrient supply to the surface ocean was assessed to investigate controls on microbial ecosystem functioning, including productivity and diazotrophy. In addition, the role of dissolved organic nitrogen (DON) as a N source to phytoplankton was assessed. The work used GEOTRACES trace metal clean sampling and analysis approaches and the cruise forms a GEOTRACES Process Cruise.

1.2 Zusammenfassung

Wir haben detaillierte Untersuchungen der Wassersäule in unmittelbarer Nähe des Hydrothermal-system und in bis zu 60 km Entfernung durchgeführt, um das Schicksal der hydrothermal abgeleiteten TEIs mit zunehmender Entfernung von der Quelle zu bestimmen, einschließlich einer Bewertung der Veränderungen der physikalischen und chemischen Speziation. Wir beurteilen, inwieweit TEIs durch Eintrag aus den Vent-Quellen, Partikelentfernungsprozesse und Advektion kontrolliert werden. Die Beprobung von Th, Ra- und He-Isotopen wird helfen, hydrothermale Flüsse und Entfernung (Scavenging) von TEI zu quantifizieren und Fingerabdrücke von Quellen zu erstellen, um die TEI-Verteilung zu klären. Die Zufuhr von (Mikro-)Nährstoffen aus der Atmosphäre und dem Tiefenwasser in den Oberflächenozean wird auch untersucht, um den Einfluss auf die Funktion des mikrobiellen Ökosystems, einschließlich Produktivität und Diazotrophie, zu untersuchen. Zusätzlich wird die Rolle von gelöstem organischem Stickstoff (DON) als N-Quelle für das Phytoplankton untersucht. Die Arbeit wird GEOTRACES spurenmetallfreie Probenahme- und Analyseansätze verwenden und die Fahrt bildet eine GEOTRACES Prozessstudie.

2 Participants

2.1 Principal Investigators

Name	Institution
Achterberg, Eric P., Prof. Dr.	GEOMAR
Frank, Martin, Prof. Dr.	GEOMAR
Browning, Thomas, Dr.	GEOMAR
Koschinsky, Andrea, Prof. Dr.	Jacobs University, Bremen

2.2 Scientific Party

Name	Discipline	Institution
Achterberg, Eric, Prof. Dr.	Mar. Biogeochemistry/ Chief	GEOMAR
Pöhle, Sandra, Dr.	Scientist	Jacobs Uni
Blum, Lea	Marine Biogeochemistry	GEOMAR
Mutzberg, Andre	Marine Biogeochemistry	GEOMAR
Schott, Thorsten	Marine Biogeochemistry	GEOMAR
Zhang, Zhouling, Dr.	Marine Biogeochemistry	GEOMAR
Klose, Lukas	Marine Geochemistry	Jacobs Uni
Menon, Vignesh	Marine Biogeochemistry	Jacobs Uni
Steiner, Zvi, Dr.	Marine Biogeochemistry	GEOMAR
Jia, Qi	Marine Biogeochemistry	GEOMAR
Gosnell, Kati, Dr.	Marine Geochemistry	GEOMAR
Jasinski, Dominik	Marine Biogeochemistry	GEOMAR
Torres-Rodriquez, Natalia	Marine Biogeochemistry	Uni Marseille
Vieira, Lucia, Dr.	Marine Biogeochemistry	CAU/GEOMAR
Wen, Zouzhu, Dr.	Marine Biogeochemistry	GEOMAR
Yuan, Zhongwei	Biological Oceanography	GEOMAR
Li, Fengjie, Dr.	Marine Biogeochemistry	GEOMAR
Zhou, Linbin, Dr.	Marine Biogeochemistry	GEOMAR
Galley, Chris	Marine Biogeochemistry	Memorial Uni
Rohleder, Christian	Marine Geophysics	DWD
Krüger, Sarah	Meterology	GEOMAR
Liu, Jing	Marine Biogeochemistry	GEOMAR
Battermann, Paul	Marine Biogeochemistry	GEOMAR
Glock, Nicolas, Dr.	Marine Geology	Uni Hamburg
Von Keitz, Tabea	Marine Biogeochemistry	GEOMAR
Gilliard, Delphine	Marine Biogeochemistry	Uni Lausanne
Reza, Zawad	Marine Biogeochemistry Biological Oceanography	GEOMAR

2.3 Participating Institutions

GEOMAR	Helmholtz-Zentrum für Ozeanforschung Kiel
CAU	Christian-Albrechts-Universität zu Kiel
DWD	Deutscher Wetterdienst, Geschäftsfeld Seeschifffahrt
Jacobs	Jacobs University Bremen
Marseille	University of Marseille
Lausanne	University of Lausanne
Hamburg	University of Hamburg

3 Research Program

3.1 Description of the Work Area

The Rainbow hydrothermal vent field is situated outside the Portuguese EEZ at 36°13.80' N, 33°54.14' W and its hydrothermal activity is well studied. The hot discharging fluids show a strong metal enrichment, especially of Fe, and form a pronounced plume in the water column (German et al., 1996). The Rainbow hydrothermal vent field is located at ~2300 m depth on the western flank of the non-volcanic Rainbow ridge situated in an offset between the South AMAR and AMAR segments of the MAR (Douville et al., 2002). The hydrothermal vent field is composed of multiple (at least 13) black smokers discharging high temperature fluids (up to 370°C) in an area of approximately 100 by 300 m (Edmonds and German, 2004). The surface waters in the study region over the Rainbow field site are influenced by an eastward flowing component of the N Atlantic anticyclonic nutrient depleted subtropical gyre, the Azores Current, which has split from the Gulf Stream in the western North Atlantic (Talley et al., 2011). The water masses encountered in our study region include tropical surface waters, with below the North Atlantic Central Water (NACW) which forms the main pycnocline in the subtropical ocean. Mediterranean Water (MW) is found below NACW as a salty warm layer between ~800-1200 m, with Labrador Sea Water (LSW) down to ~2 km. The North Atlantic Deep Water (NADW) is situated below the LSW (Talley et al., 2011) and forms the waters (S ~34.95 and Pot. T ~2.5°C) surrounding the hydrothermal plume at Rainbow.

3.2 Aims of the Cruise

The main scientific aim was to obtain a mechanistic and quantitative understanding of the processes that set the hydrothermal flux of trace elements and their isotopes (TEIs) to the deep ocean interior on the Mid-Atlantic Ridge (MAR) at the Rainbow site.

We have the following major goals that we want to achieve for the cruise:

• Obj 1. Determine the distribution, and physical and chemical speciation of TEIs, including micronutrients (such as Cd, Co, Cu, Fe, Mn, Mo, Ni, V, Zn, Cr), non-biologically essential elements (such as Al, Pb, Hg, Ti, Zr, Hf, Nb, U, W and REEs), major elements (F, Ca, Mg, Sr, K, S, Li) and a range of isotope systems (incl. Th, Ra, Ba, Fe) in high resolution sampling along the Rainbow plume.

• Obj 2. Quantify the fluxes of these TEIs and micronutrients to the deep ocean from the ocean crust and away from the Rainbow venting sites, and assess the role of physical and chemical speciation of TEIs for their fluxes and flux attenuation.

• Obj 3. Assess, using chemical tracers and physical oceanography, the mixing and advection of these TEIs away from the Rainbow hydrothermal vent sites into the ocean interior.

• Obj 4. Determine the supply of TEIs (including micronutrients) to the surface ocean from atmospheric deposition, and measure their surface ocean concentrations.

• Obj 5. Explore the relationship between macro- and micro-nutrient concentrations and fluxes, irradiance, ocean productivity, phytoplankton community composition, nutrient utilization and limitation, and diazotrophy in the North Atlantic Ocean.

3.3 Agenda of the Cruise

It had been hypothesized in the early 1990s that hydrothermal vents would impact global ocean biogeochemistry (Kadko, 1993), but not until the emergence of GEOTRACES was clear evidence provided. GEOTRACES revealed in recent years that there is a widespread release of dissolved Fe and a range of other elements from hydrothermal vents to the deep ocean (Saito et al., 2013). In case of the Southern East Pacific Rise (SEPR) it was shown that the hydrothermal vent derived dissolved and particulate Fe and Mn persisted for thousands of kilometers across the S Pacific (Resing et al., 2015). Iron is a micronutrient that limits primary productivity of phytoplankton in about 40% of the world's surface oceans (Moore et al., 2013) and manganese (Mn) has recently been shown to be co-limiting alongside Fe in the Southern Ocean (Browning et al., 2021). Supply of hydrothermally-sourced Fe/Mn through isopycnal upwelling could hence potentially stimulate productivity in Fe/Mn limited regions. This mechanism was indicated for the Fe limited North Pacific and Southern Ocean based on GEOTRACES observations and biogeochemical model studies (Resing et al., 2015).

There is currently a lack of understanding of the processes that set the fluxes of hydrothermally sourced trace elements. The initial consideration of full removal of Fe in the direct vicinity of hydrothermal vents (German C. R. et al., 1991) appears incorrect, with processes appearing more complex. In addition, the older studies (1980-1990s) focused on processes occurring within tens to hundreds of meters from individual vents and thereby missing the processes that determine distal plume spread. The more recent GEOTRACES studies have a spatial resolution of ca. 100 km and therefore miss the key processes that result in removal and stabilization of trace elements occurring in the first kilometers away from the vents. The Rainbow Plume cruise has conducted detailed sampling of the Rainbow hydrothermal plume system on the Mid Atlantic Ridge (MAR) over a distance up to 60 km, using state of the art GEOTRACES protocols and laboratory techniques, complemented by supporting analyses (e.g. He, Th and Ra isotopes, metal-binding ligands, metal redox speciation, Fe isotopes, O_2, POC, DOC). The new knowledge will be combined with a global biogeochemical model (University of Liverpool) to obtain new understanding of the impact of hydrothermal TEI supply on ocean biogeochemistry. Slow-spreading ridges are a much more significant oceanic Fe source than ^{3}He fluxes and spreading rates had previously suggested based on relationships at the EPR. Since slow-spreading ridges account for more than half of the submarine ridge system, such a constant emanation of hydrothermal fluids would make hydrothermal vent systems on slow spreading ridges a medium- to long-term stable source of Fe and other micronutrients to the ocean.

Iron and Manganese Biogeochemistry in Hydrothermal Plumes

Hydrothermal fluids have Fe and Mn concentrations more than three orders of magnitude higher than deep ocean waters and, thus, have great potential to influence global marine biogeochemical cycles (Tagliabue et al., 2010). Iron and Mn are often reported together because they both emanate from reducing systems such as sediment porewaters and hydrothermal fluids. However, while both are redox active and are more soluble in their reduced forms, there are also a range of differences in their chemical speciation and reactivity. In the open ocean, Fe(II) is rapidly oxidized to Fe(III) in the presence of oxygen (Hopwood et al., 2020), and dissolved Fe is thought to be >99% bound by natural organic ligands and/or colloidal nanoparticles (Gledhill and Buck, 2012), with ~50% of the dissolved Fe falling into the operationally defined colloidal size

range (Wu et al., 2001). Oxidation of Mn(II) to Mn(IV), however, mostly occurs through microbial and surface catalysis (Mandernack and Tebo, 1993) and is kinetically inhibited (Nealson et al., 1988). Mn(II) is hence able to persist in the dissolved phase because of the slower oxidation rates, mostly as free Mn^{2+} cation (Byrne, 2002) that is operationally soluble-sized (i.e. not colloidal) and not thought to be bound by organic ligands.

The recent data from GEOTRACES section cruises have indicated dissolved Fe plumes in deep ocean waters of every basin (e.g. (Saito et al., 2013; Nishioka et al., 2013; Resing et al., 2015)). There are therefore indications that hydrothermal dissolved Fe must be kept in solution (stabilized) by one or more mechanisms including: 1) complexation by organic ligands that protect Fe from precipitation (Bennett et al., 2008); 2) formation of colloidal-sized nanoparticles (Yucel et al., 2011); 3) exchange among suspended particles and POC (Fitzsimmons et al., 2017; Toner et al., 2009).

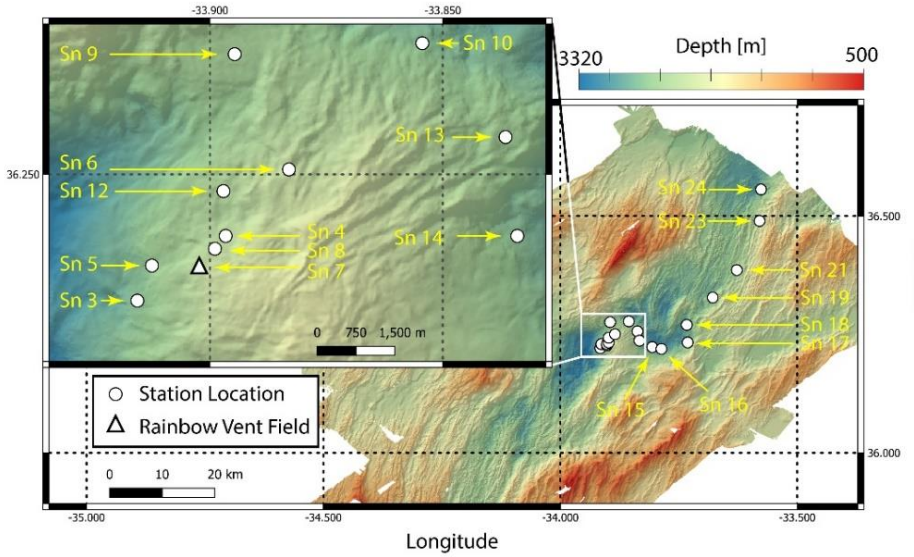

Fig. 3.1 Bathymetric map of the study region. Rainbow vent field is marked with a triangle. CTD stations are marked with white circles.

Recent work in the Pacific on GEOTRACES cruise GP16 has shown that Fe and Mn precipitation takes place to form large sinking particles which drives the non-conservative removal of dissolved Fe and Mn near ridge-axes (Lee et al., 2018). We have collected particulate samples for synchrotron analysis (by Brandy Toner) to assess the changes in mineralogy over the distance of the spreading plume. However, particulate Fe and Mn derived from hydrothermal vents persist alongside their dissolved fractions in the distal plume in the S Pacific (Resing et al., 2015). Whilst Fe particles sink slowly, a fraction remains in suspension as a result of a small size and association with buoyant organic matter (Hoffman et al., 2018). A simultaneous slow sinking of dissolved Fe suggests reversible exchange between dissolved and particulate Fe (Milne et al., 2017; Fitzsimmons et al., 2017). Dissolved and particulate Mn do however not sink through the water column, and therefore there is a decoupling of long range transport hydrothermal Fe and Mn, with consequences for metal fluxes into the ocean and scavenging of multiple other elements (Fitzsimmons et al., 2017).

Particulate Fe investigations have indicated a change in association of hydrothermal Fe oxyhydroxides with organic carbon in the Pacific, from a high Fe:C ratios to a low Fe:C ratio beyond 100 km off-axis. A transition of dissolved Fe speciation was observed within the colloidal phase over the same length scale, from ~90% nano-particulate Fe oxy-hydroxides close to vents to a predominantly ligand-bound Fe phase down-plume (Fitzsimmons et al., 2017). In the Pacific,

inorganic Fe nano-particles are therefore lost to scavenging more rapidly than ligand-bound dissolved Fe in a plume. This effect sets the ultimate hydrothermal Fe flux to the ocean. Processes in dispersing hydrothermal plumes in the N Atlantic will differ from the Pacific due to differences in physico-chemical conditions. Formation of polymetallic sulfides will occur within minutes in hydrothermal systems in both the N Atlantic and Pacific Ocean, and hence on length and timescales that are quite short compared to the approximate time it takes for buoyant plumes to rise (Rudnicki and Elderfield, 1993). The high Fe:S ratios at Rainbow compared to other MAR sites (Charlou et al., 2002) will nevertheless facilitate a greater amount of Fe to escape primary FeS precipitation and potentially become solubilized as organic complexes. However, deep water oxygen concentrations and pH values are higher in the N Atlantic than the Pacific which results in a more rapid (likely in 2-3 minutes (Rudnicki and Elderfield, 1993)) formation of Fe-oxyhydroxides (Millero et al., 1987) in the plume following entry of the vent fluids into the ocean interior. In the Pacific, the predicted half-time for Fe(II) oxidation is ~7 hours on the Juan de Fuca Ridge (Statham et al., 2005), resulting in a slower formation of particulate phases. Fe isotopes will be used as net source tracers.

Elements other than Fe and Mn will be studied to assess whether the transformations affecting Fe and Mn also determine the behaviours and fate of other elements in the dispersing hydrothermal plume. These include Al, Cd, Cu, Ni, Pb, Zn, U, Mo, V, Cr but also high field strengths elements and Hg and Ba isotopes.

The control of surface ocean microbial communities by (micro) nutrient supply

In addition to the deep ocean geochemical studies, atmospheric and deep-water (micro)nutrient supply to the surface ocean was assessed to investigate controls on microbial ecosystem functioning, including productivity and diazotrophy. In addition, the role of dissolved organic nitrogen (DON) as a N source to phytoplankton was assessed.

4 Narrative of the Cruise

August 30-31, 2021. Mobilisation and departure- Cruise M176/2 mobilised in Emden on August 30 and 31, 2021. A group of GEOMAR scientists and technicians travelled to the vessel on the morning of August 30 to unload the containers and set up the equipment for the cruise. The CTD sensors, LADCP and other instruments were installed on August 30. A smaller GEOMAR party had already set up and tested the GEOMAR winch container with a new cable guiding deckblock on the Meteor in July (prior to cruse M176). On August 31, the remaining cruise participants travelled from Jacobs University and Kiel to the Meteor in Emden and assisted with mobilization, and installed their laboratories. We sailed in the morning of September 1 with very calm weather in the North Sea. In the North Sea the wind and waves were still a little demanding for some of the cruise participants, but all got over their sea-sickness within the first few days of the cruise.

We conducted a test station on September 4 (2021) once we were in international waters southwest of Ireland. We tested the new GEOMAR titanium (Ti) CTD with new Niskin bottles and also with older Go Flo bottles, and also the GEOMAR stainless steel (SS) CTD with LADCP. The test station was important and a range of challenges with the CTD systems were identified and rectified.

September 4-27, 2021- The cruise started sampling surface waters from our trace metal clean tow fish for biological and chemical variables as soon as we were in international waters south of Ireland (September 4, 2021). The surface waters were sampled for nitrogen fixation, nutrients and

trace elements to establish the rates of nitrogen fixation, types of diazotrophs present (using nifH gene analysis), and the chemical environment of the diazotrophs. This sampling activity continued until we reached the EEZ of the Azores and had to be halted then until we reached the Rainbow hydrothermal vent region in international waters southwest of the Azores (September 9, 2021). The tow fish was subsequently deployed throughout the cruise whilst the vessel was moving.

In addition, we have sampled for aerosols whilst in international waters. The aerosol collector was placed on the monkey deck of the Meteor and filters changed every 48 h. Sampling was halted on September 27.

The first station to sample the hydrothermal plume that is positioned at about 2100 m near the Rainbow vent field was conducted on September 9, 2021. We had learned a lot from our test stations on September 4 and had fixed some of our problems in the meantime. The first sampling day was therefore very successful, and all equipment and sampling gear worked well.

We have been deploying 3 different CTDs (titanium GEOMAR CTD, stainless steel GEOMAR CTD, stainless steel METEOR CTD) on a daily basis, a multicorer (MUC) and also a set of 6 in situ pumps. The deployments of all CTDs have been successful. The deployment of the in-situ pumps was halted after the first 4 sampling days because of malfunctioning; the in-situ pumps were replaced by large volume water collection using 3 CTD deployments at each station from Sept 13.

Our daily sampling routine started at 0530 h and finished at about 1800 h, and was similar each day. Our nights are occupied by CTD/LADCP surveying operations through the hydrothermal plume. Over the cruise we built up a 3-dimensional picture of the plume movement in the study area, which will provide important context to our geochemical results.

On a daily basis we therefore sampled in detail the non-buoyant hydrothermal plume emanating from the Rainbow vent field using the trace metal clean titanium GEOMAR CTD. This CTD is operated by a dedicated winch system with a Kevlar cable, thereby preventing contamination of the samples during the sample collection. We sampled just above and just below the plume, which means between 1700 m and 2300 m, with the plume maxima being at ca. 2100 m. On our Ti rosette with 24 bottles, we sampled 2 bottles at each depth, and therefore 12 depths above, in and below the plume. Once on deck, 12 Niskin bottles are removed from the frame and taken to our trace metal clean container where the water is filtered into a large number of different bottles for analysis at sea and in the home laboratories. We collected particles from the plume for trace element and synchrotron analyses, and we collected waters that were subsequently filtered on-board through various different filter pore sizes. The collection of various size fractions along the plume will provide detail on chemical transformations and allow us to decipher how much material (e.g. iron) is removed by sinking and remains in solution and may ultimately be available to phytoplankton growth in the surface ocean.

We sampled the other 12 Niskins from the titanium CTD for helium isotopes, DIC, DOC, oxygen, which we will use as a tracer of the hydrothermal fluid inputs to the ocean. Helium is a conservative tracer and allows us to follow the plume and determine the fluxes of elements.

Following the malfunctioning of the in-situ pumps, we deployed instead daily from 13.09.2021 another 3 CTDs (stainless steel) for the collection of Ra and Th isotopes to allow us to assess time scales of plume movement and trace element scavenging processes. Large volume samples (110 L) were obtained from these deployments for Ra isotopes and pumped over Mn

cartridge for short-lived Ra analysis on board and long-lived Ra in Kiel. For Th isotopes, we also measured on-board (Th 234) and subsequently on land (Th 230).

An additional titanium CTD was deployed daily (in the afternoon) to 300 m depth for collection of samples for biological variables. Biological rate experiments of nitrification and di-nitrogen fixation were conducted using the water from the titanium CTD and tow fish. Phytoplankton resource limitation experiments were conducted in the ship-board laboratory and also in incubation tanks on the aft deck.

Each afternoon, a MUC deployment was conducted to obtain sediment cores. These deployments were successful for all stations in obtaining surface sediments. However, the collection of intact cores was not successful in all instances. Nevertheless, on ten occasions we obtained cores which could be used for porewater extraction and slicing.

Our sampling routine was similar over a period of 19 days. On September 27, 2021, we conducted the last sampling station, and after completion of the sampling activities we halted all sampling in the early evening of September 27, 2021.

The last biological experiments on the ship were ended on September 30, 2021. The biological samples were stored for analysis in the home laboratories in Germany.

The weather in the study area has been kind and we have not lost any station time as a result of poor weather.

September 27-October 6, 2021-In this time period we sailed back to Emden, and no sampling was conducted by the ship's science party during this period. The ship's ADCP and TSG were functioning whilst the vessel was in international waters.

5 Preliminary Results

5.1 Multibeam and Backscatter Mapping of the Rainbow Vent Field and Surround Region

(C. Galley[1])
[1]Memorial University of Newfoundland, Canada

While on site bathymetric and backscatter maps from the Dunn et al., 2016 multibeam data set was used to choose the locations of the vertical CTD casts and multicorer sampling (Fig. 5.1), however EM122 multibeam data was also collected during the cruise.

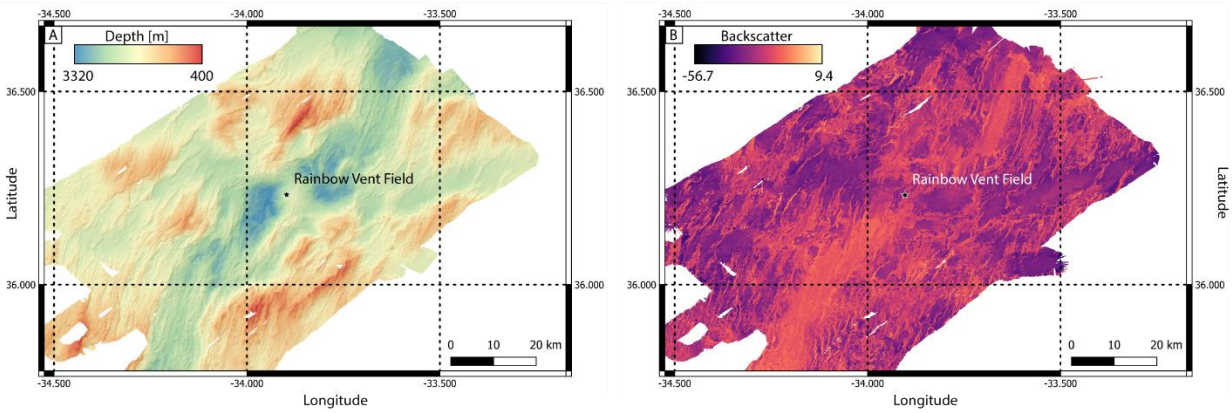

Fig. 5.1 A) bathymetry map of the region surrounding the Rainbow Vent field, with the accompanying, B), backscatter data from the same multibeam data set.

Data collected during this cruise was processed with the MB-system Version 5.7.9beta14 software, to a resolution of 20 m (Fig. 5.2).

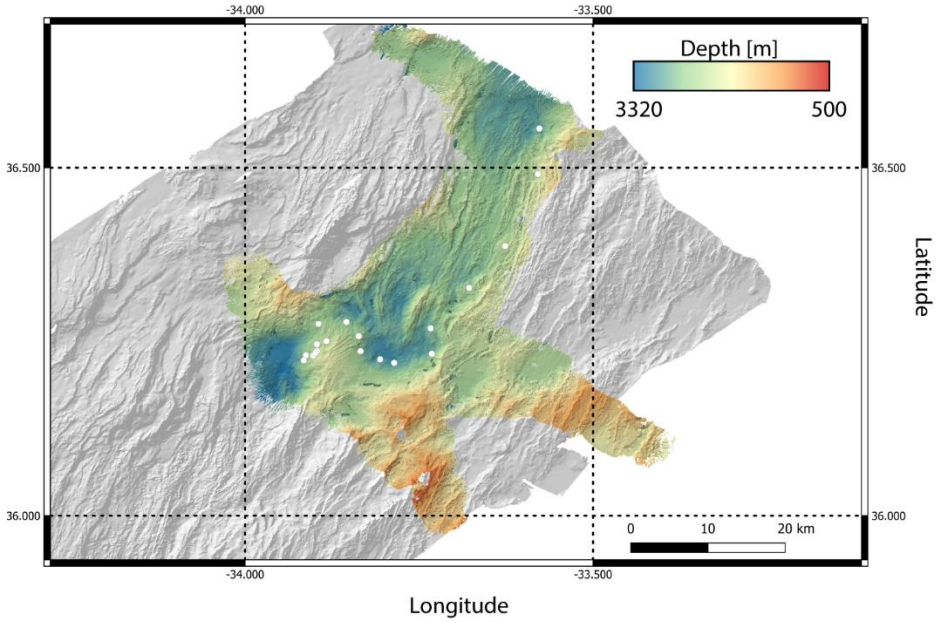

Fig. 5.2 The bathymetry map derived from the EM122 multibeam data collected during the M176/2 cruise. The white dots represent the locations of the 19 stations studied during the cruise.

5.2 In-situ mapping of the dispersing Rainbow hydrothermal plume

(Chris Galley[1] & Lukas Klose[2])
[1]Memorial University of Newfoundland, Canada
[2]Jacobs University, Germany

The Rainbow Vent Field hydrothermal plume was mapped out through a series of 16 cross-sectional CTD surveys beginning over the vent field and ending approximately 60 km down-plume. The CTD surveys were conducted by initially lowering the equipment down to approximately 100 m altitude relative to the seafloor, then with the ship set to sail down the length of the survey line the CTD was raised and lowered in a saw-toothed fashion through the top and bottom of the hydrothermal plume, determining its extents. The primary attribute used to determine the presence of the plume was turbidity, as the many particles that make up the plume scatter light much more intensely than that of the seawater in this area. As such, the plume was identified as a turbidity high anomaly (Fig. 5.3).

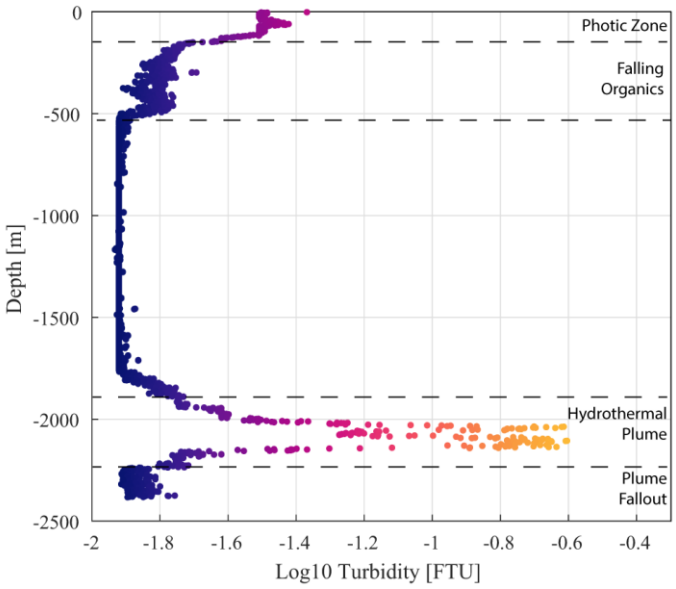

Fig. 5.3 An example of a 1D turbidity distribution with depth, from Station 12. Turbidity varies due to physical and biological processes through the water column, with the signal of a hydrothermal plume sharply standing out.

Originally 13 survey lines were planned, organized in an orthogonal Southwest to Northeast oriented grid. However, soon after the first couple surveys were done it was apparent the plume spread more widely upon leaving the vent field than was anticipated. As a result, the orientation of many of the surveys lines were readjusted and were increased in length to better resolve the lateral extents of the plume. The lateral CTD surveys were then mainly used to plan the next day's biological and geochemical measurement station, choosing the location nearest the cross-sectional center of the plume to best sample its properties.

The CTD stainless-steel frame used during the lateral surveying was equipped with *Sea-Bird Scientific* CTD device, an *AMT Analysentechnik* redox sensor, and a Lowered Acoustic Doppler Current Profiler (LADCP) in place of two Niskin bottles, bringing the frames number of equipped Niskin bottles to 22. Depth information was taken from the CTD sensor, and to determine the CTD's lateral positioning relative to the ship a POSIDONIA Pinger was attached 50 m up-cable from the CTD frame.

5.2.1 Lateral CTD Survey overview

16 lateral CTD surveys were conducted during the 20 days the ship was on station (Fig. 5.4). The lateral CTD surveys were able to compliment the 19 vertical cast stations, where turbidity was also measured with the more sensitive sensor equipped to the titanium-clean CTD used in trace-metals sampling. Information from the lateral surveying could be used to build a model of the dissipating hydrothermal plume as it travels away from the vent field (Fig. 5.4), with the vertical casts being useful in seeing the changes in plume density (using turbidity as a proxy) as one samples down-plume (Fig. 5.5).

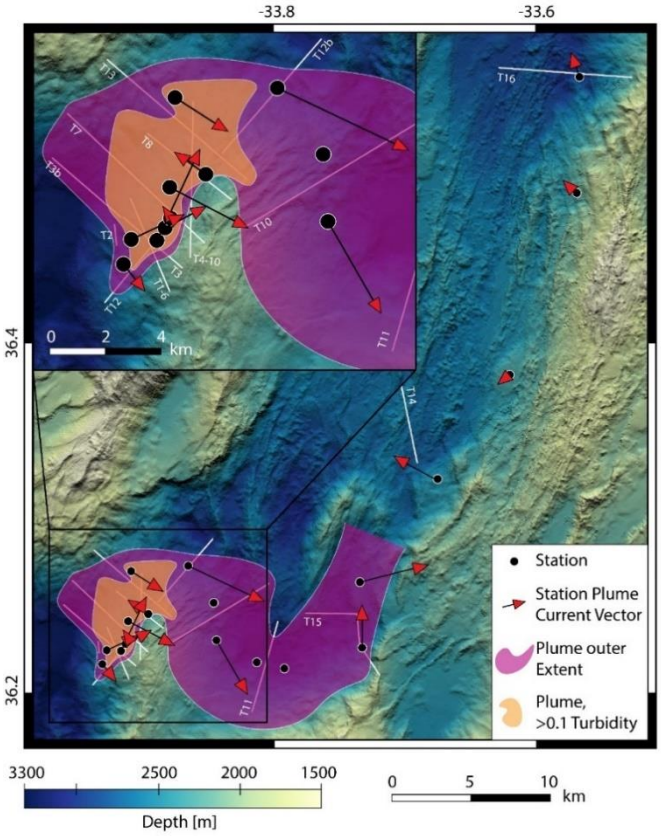

Fig. 5.4 A map of the study region, with the lateral CTD survey lines in white, the interpretation of the plume was drawn in purple to signify the outer extent of the plume, and orange for the inner, higher turbidity section of the plume (>0.1 FTU). The black dots represent the location of the vertical CTD cast stations, with the red arrow heads representing the measured average current vectors present through the depth range that the plume was observed in.

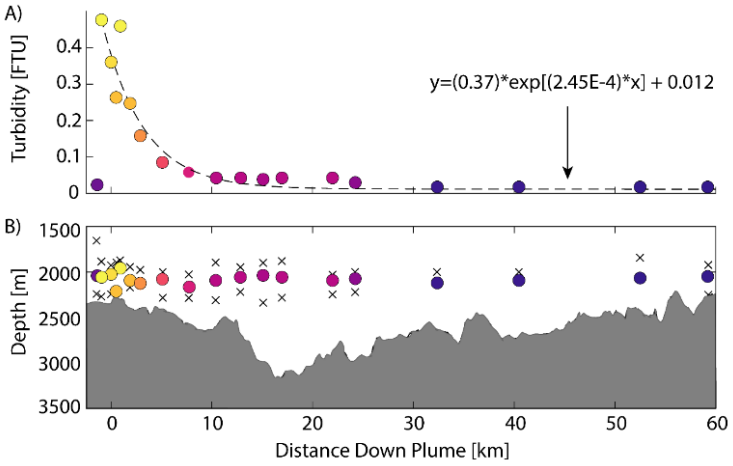

Fig. 5.5 A visualization of the decay in turbidity, and therefore plume density, with distance from the vent field down-plume. A) a turbidity versus distance down-plume from the Rainbow vent field plot, with an exponential fit. B) The locations of the peak turbidity signal from each vertical CTD cast shown coloured based on its turbidity value, with the top and bottom of the plume (when observed) represented by crosses.

5.3 The control of surface ocean microbial communities by (micro) nutrient supply

5.3.1 Upper ocean Ti CTD sampling

(Z. Wen[1] and Z. Yuan[1])
[1] GEOMAR

Samples were collected at 18 stations (Tables 12.1 & 12.4) during this cruise in the region of the Rainbow Vent. Water samples were collected using trace-metal-clean Niskin-X bottles at six depths (ca. 10 m, 20 m, 30 m, 50 m, DCM, 120 m) for the determination of nifH gene abundance, N_2 fixation and primary production incubations, Inorganic and organic nutrients (N, P and Si), Hg, Al, trace metals, Chl a, pigments, flow cytometry and POC/PON. Samples for Chl a were analyzed

on board, these samples were filtered (100 mL), extracted in the dark for over 15 h in 90% acetone at -20°C, and analyzed fluorometrically on a 10AU Turner Designs fluorometer (Fig. 5.6).

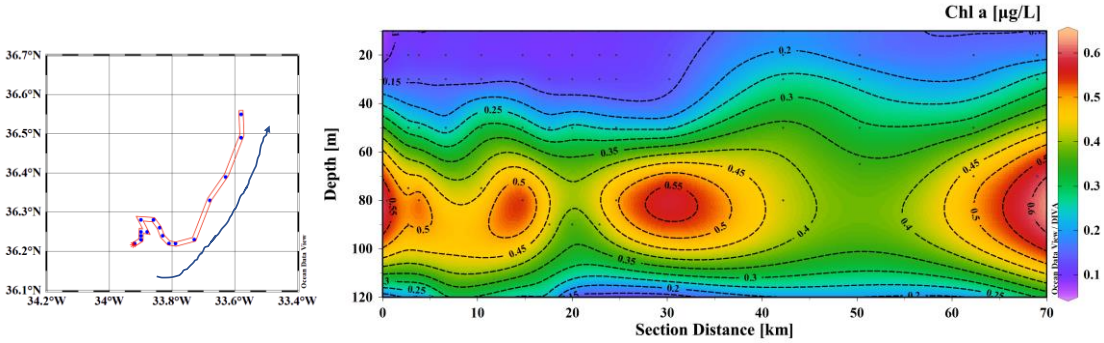

Fig. 5.6 Chl a profile from Rainbow site to the northeast.

5.3.2 Under-Way Tow-Fish sampling

(Zouzhu Wen and Zhongwei Yuan**)**

Trace metal clean sea surface water was sampled from the Tow-Fish sampling device into a trace-metal-clean laboratory via acid-washed tubing and a Teflon diaphragm pump. Regular samplings while sailing to the Rainbow site were conducted appropriately every 8 hours using a 10-liter carboy, then dispensed for the measurement of inorganic and organic nutrients, trace metals, Chl a, flow cytometry, pigments as well as POC/PON (Table 12.1). Macronutrient and trace metal samples were collected filtered (0.2 µm pore size; AcroPak, Pall), macronutrient samples were frozen at -20°C immediately and trace metal samples were acidified within 24 h with 140 µL concentrated HCl to 125 ml seawater sample and stored at room temperature, all concentrations will be determined upon return to a land-based laboratory. Flow cytometry samples were preserved at 1% paraformaldehyde concentration, mixed with a vortex, left for 10 min at room temperature in the dark, and then frozen at -80°C, and later analyzed using a FACSCalibur flow cytometer. Samples for diagnostic pigment analyses were filtered onto glass fiber filters, frozen at -80°C, then later analyzed using a reverse-phase HPLC system. Samples for POC/PON were filtered onto pre-combusted (450°C, 4 h) GF/F filters, frozen at -20°C, then later analyzed using an elemental analyzer coupled to a mass spectrometer. Following the ship's return to port, all frozen samples were transported to the laboratory on dry ice and later analyzed at GEOMAR. A total of 6 bioassay experiments (Table 12.2) were set up using acid-washed Nalgene polycarbonate bottles (4 L). Nutrient amendments at all sites were Fe, P, and Fe+P. The amended Fe and P (chelexed and filter-sterilized) concentrations were 2.5 nM and 100 nM, respectively. Control bottles incubated with no nutrient treatment were included with all experiments. All treatments were conducted with triplicate replicates and incubated for ~2 days in a screened on-deck incubator continuously flushed with surface seawater.

5.3.3 Biological nitrogen fixation

(Z. Wen)

Biological N_2 fixation is a key process which provides bioavailable nitrogen for the growth of phytoplankton that live in the euphotic zone. In some areas of the oligotrophic open ocean, such "new nitrogen" derived by the N_2-fixers can equal to the nitrogen supplied by diffusive processes from the deep water, which substantially supports primary production and subsequently export

production. Despite its importance, few efforts have been conducted to understand the spatial and temporal distribution of N_2 fixation, and a mechanistic understanding of its controlling factors is still lacking, presenting a major barrier to making accurate projections. To address this, I conduct N_2 fixation rate incubations, and DNA sampling for the analysis of the abundances of key diazotrophic phylotypes in this cruise. These efforts are accompanied by a diverse range of ancillary environmental parameters, alongside several nutrient amendment experiments directly testing the response of N_2 fixation rates to supply of potentially limiting nutrients (iron and phosphate).

5.3.3.4 N_2 fixation and primary production measurements

N_2 fixation rates were determined by the $^{15}N_2$ gas dissolution method (Mohr et al., 2010), combined with a primary production assay using $NaH^{13}CO_3$ (99 atom% 13C, Cambridge Isotope Laboratories). The N_2 fixation and primary production incubations were conducted in duplicate 4 L Nalgene polycarbonate bottles. Samples were spiked with 100 mL $^{15}N_2$ enriched filtered seawater from the same site and incubated on-deck for 24h. The final $^{15}N_2$ enriched seawater concentration in the incubation bottles was ~3 atom%. $NaH^{13}CO_3$ solution was added at a concentration of 100 μM. After that, the bottles were covered with neutral-density screen to adjust the light to the levels at sampling depths, and then were incubated for 24 h in an on-deck incubator continuously flushed with surface seawater.

5.3.3.5 nifH gene abundance

~4 L seawater samples for DNA extractions were filtered onto 0.22 μm pore-sized membrane filters (Supor200, Pall Gelman, NY, USA) and then frozen in liquid N_2. DNA will be extracted using the QIAamp® DNA Mini Kit (Qiagen) follow the manufacturer's protocol. The quantitative polymerase chain reaction (qPCR) analysis was targeted on the nifH phylotypes of *Trichodesmium* spp., unicellular cyanobacterial UCYN-A1, UCYN-A2, and UCYN-B, Richelia spp. (het-1), and a gamma-proteobacterium (γ-24774A11), using previously designed primers and probe sets (Church et al., 2005a; 2005b; Moisander et al., 2008; Thompson et al., 2014).

5.3.4 Nutrient regulation of phytoplankton growth rates in the North Atlantic
(Z. Yuan)

Phytoplankton growth rates control how much food is available for higher trophic levels and play a crucial role in regulating biogeochemical cycles. Nutrient addition bioassay experiments have been crucial in demonstrating 'community level' limitation of phytoplankton biomass accumulation (e.g., Browning et al., 2017) and various '-omics' techniques have demonstrated phytoplankton nutrient stress (e.g., Ustick et al., 2021), but growth rates cannot be easily inferred from either of these. The aim of this project is therefore to measure phytoplankton growth rates of different types in situ and following low level nutrient additions within surface waters of the hydrothermal vent plume area. In addition, the efforts will be also devoted to determining a large dataset of related environmental parameters, including inorganic and organic nutrients, trace metals, Chl a, pigments, flow cytometry as well as particulate organic carbon/nitrogen (POC/PON).

5.3.4.1 Standard nutrient addition experiment

One factorial nitrogen–phosphorus–iron addition experiment was conducted at 36°18.063'N, 33°47.514'W. Unfiltered seawater (1 L acid-washed polycarbonate bottles; Nalgene) was collected through the tow-fish sampling device. Before filling the polycarbonate bottles, samples were collected for inorganic and organic nutrients, and trace metals. Approximately 8-liter seawater was collected in a carboy in order to measure initial phytoplankton concentrations and community structure. Incubation bottles were spiked in triplicate with N (1 μM NO_3^- + 1 μM NH_4^+), P (0.2 μM) and Fe (2 nM) in factorial combinations (control, +P, +Fe, +PFe, +N, +NFe, +NP, and +NPFe). Additions were made under a laminar flow hood. Nutrient stocks were previously passed through a prepared column of cation exchange resin to remove trace element contamination (Chelex, BioRad). Bottles were capped, sealed with parafilm, bagged and placed in on-deck incubators for ~48 h. The incubator was screened with blue filters (Lee Filters "Blue Lagoon" screening) and flushed with continuous surface seawater from the ship's underway flow-through supply. Following the incubation period, each triplicate replicate was subsampled for collection/analysis of Chl a and flow cytometry.

5.3.4.2 Dilution experiment

Six low level nitrogen–phosphorus addition experiments were conducted around the Rainbow site, following addition of both nutrients to excess levels (Table 12.5).

Using tow-fish seawater supply and filter (0.2 μm, Pall Acropak) collected ~6 L of filtered seawater in the 8 L Nalgene LDPE bottle, directly after collection filtered seawater, collected 8 L (fill bottle fully) of unfiltered seawater in the second 8 L Nalgene LDPE bottle. Under laminar flow hood, 8 L bottle of filtered seawater agitated to homogenize and poured 94 mL into 48 of the 125 mL polycarbonate bottles, then poured 31 mL of the unfiltered seawater into the bottles containing filtered seawater. The remaining 48 of the 125 mL polycarbonate bottles were filled with 125 mL unfiltered seawater. Incubation bottles were spiked in triplicate with a spectrum of N (0, 50 nM, 100 nM, 150 nM of NH_4^+) and P (0, 10 nM, 20 nM, 30 nM) for experiment 1,2,3,4 , and N (0, 100 nM, 300 nM, 500 nM of NH_4^+) and P (0, 10 nM, 20 nM, 30 nM) for experiment 5,6 to provide 16 treatments. Bottles were capped, sealed with parafilm, bagged and placed in on-deck incubators for 24-36 h. Following the incubation period, each triplicate replicate was subsampled for collection/analysis of Chl a and flow cytometry.

5.3.4.3 Uptake experiment

Two factorial phosphorus–iron addition experiments were conducted around the Rainbow site (Table 12.6). Unfiltered seawater (4 L acid-washed polycarbonate bottles; Nalgene) was collected through the tow-fish sampling device. Incubation bottles were spiked in triplicate with P (0.2 μM) and Fe (2 nM) in factorial combinations (control, +P, +Fe, +PFe). Bottles were capped, sealed with parafilm, bagged and placed in on-deck incubators for ~24 h. Following the incubation period, each triplicate replicate was subsampled 500 mL for collection/analysis of Chl a and flow cytometry. Meanwhile, each remaining triplicate replicate was subsampled into1 L acid-washed polycarbonate bottles for addition of ^{15}N-NH_4^+ and ^{15}N-urea stocks, respectively. Bottles were capped, sealed with parafilm, bagged and placed in on-deck incubators for 1-3 h. Following the incubation period, Samples were filtered onto pre-combusted (450°C, 4 h) GF/F filters, frozen at -20°C, then later analyzed using an elemental analyzer coupled to a mass spectrometer.

5.3.5 Availability of iron to phytoplankton

(F. Liu, Z. Reza)

Other than light and major nutrients, phytoplankton growth and community composition are strongly influenced by availability of the metal iron (Fe). On the FS Meteor M176/2 cruise, we examined two hypotheses: 1, Fe availability to phytoplankton cells depends upon the Fe chemistry in the phycosphere (i.e., driven by local pH, reactive oxygen species ROS, and bacteria and fungi), a micrometer scale space which directly surrounds a phytoplankton cell, rather than the Fe chemistry in the bulk seawater (the long-standing paradigm); and 2, Fe availability has an impact on cellular Fe contents and the composition of phytoplankton community. Hence, two work packages:

5.3.5.1 Work Package 1: A, examine the phycosphere effect from local bacteria and fungi on Fe bio-uptake (The work flow is shown in Fig. 5.7).

Surface seawater (around 2–3 m depth) from the ship's underway supply or from the towed fish before arriving at or between the stations were collected for growing the *in-situ* phytoplankton community (4 transparent carboys * 20 L), and major nutrients (final concentrations: 10 µM NO_3, 1 µM PO_4, 10 µM SiO_3) were added to stimulate the growth of phytoplankton. To maintain the temperature as that of surface seawater, the carboys were submersed in continuously flowing water from the ship's underway system, and the light intensity was set to 30% of natural light via covering a blue film on the top of incubation tanks. The growth of phytoplankton was monitored via measuring raw fluorescence by a Turner Designs Trilogy, and following a 3 to 6 days' growth the phytoplankton was used to determine Fe uptake rate. A subsample was harvested on membrane filters for the analyses of chlorophyll a (pre-combusted GF/F filters), particulate organic carbon POC (pre-combusted GF/F filters), trace metals (polyethersulfone PES filters), 16S RNA (PES filters) and pigment composition (GF/F filters) at GEOMAR.

The exposure medium for the Fe uptake experiments was prepared with 0.2 µm filtered surface seawater (collected in acid-cleaned carboys by the towed fish), and 57-Fe solution (pre-complexed by ethylenediaminetetraacetic acid EDTA, the final concentrations of 57-Fe and EDTA in exposure medium were 5 nM and 5.5 nM, respectively) was added and equilibrated in dark at ambient temperature (17 – 25 Celsius degree) for one week. Each of the six acid-cleaned transparent PC bottles was filled with 6 L the 57-Fe exposure medium for the Fe bio-uptake experiments.

On the day of doing 57-Fe uptake experiments, phytoplankton from the carboys was harvested on the filter membranes and then resuspended into two bottles of 300 mL 0.2 µm filtered surface seawater (one with ampicillin and nystatin to kill any bacteria and fungi associated with phytoplankton cells while the other bottle with heat denatured ampicillin and nystatin as the control) for 25 min. Aliquots of the concentrated phytoplankton were added into the 57Fe-EDTA exposure medium (i.e., 100 ml phytoplankton solution added into 6 L medium, the final concentrations were 55 mg/L ampicillin and 55 mg/L nystatin), and this was recorded as the starting time-point of the Fe bio-uptake. The incubation bottles were kept in the growth chamber at 21 Celsius degree with a constant light intensity of 120 µmol/m^2/s. In the following 10-12 hours, aliquots of exposure medium (2 L per bottle each time) were filtered onto membrane filters, rinsed with 5 mL of a trace metal clean reagent for 5 min per filter (i.e., EDTA-oxalate solution to remove cell surface bound iron, recorded as the end time-point of the Fe bio-uptake), and finally rinsed

with 8 mL of 0.7 M NaCl solution (pre-cleaned with chelex-100 resin) for three times. The filtration was carried out in a laminar hood, and we followed the trace metal clean protocol to avoid possible metal contamination. The filters with phytoplankton were stored in sterile petri-dishes at -80 Celsius degree for the analyses of cellular Fe concentrations at GEOMAR.

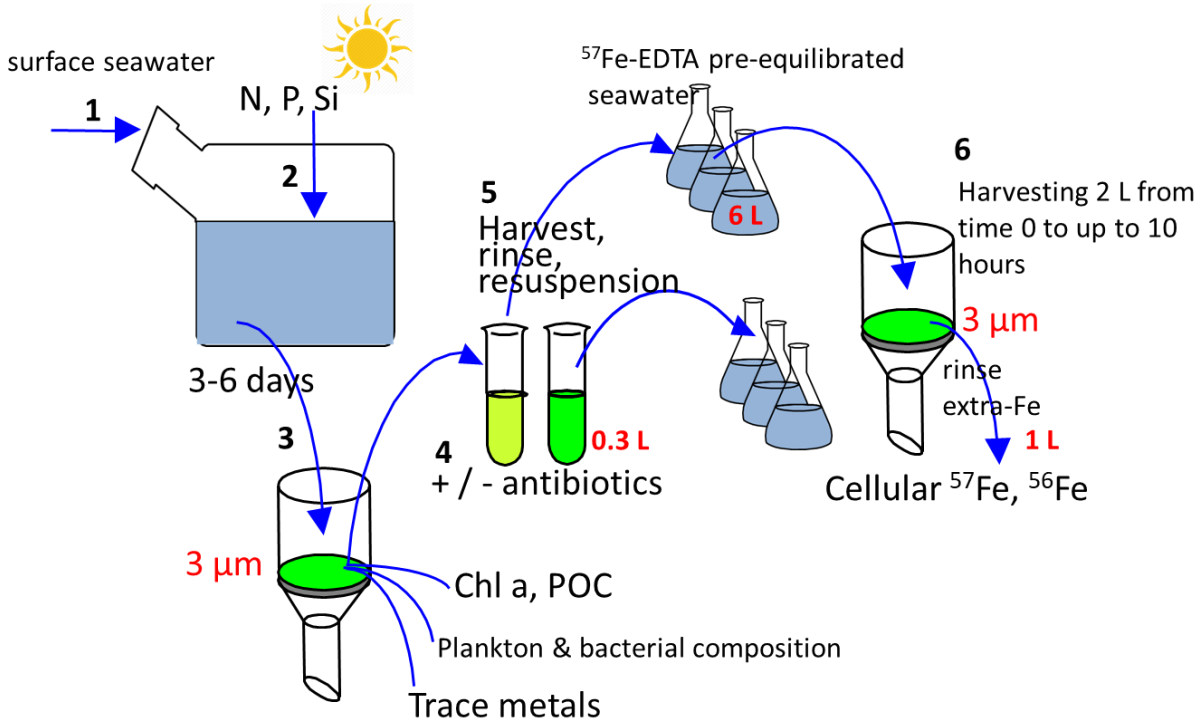

Fig. 5.7 Experimental procedures to examine the influence of phycosphere bacteria and fungi on Fe bio-uptake by the > 3 µm phytoplankton cells.

5.3.5.2 Work Package 1: B, examine the phycosphere pH effect on Fe bio-uptake.

The basic work procedures were similar to those of Fig. 5.7, except for the followings: 37.5 mL 1.6 M 4-(2-hydroxyethyl)-1-piperazineethanesulfonic acid HEPES (cleaned by chelex-100, pH adjusted to 8.18 with trace metal grade NaOH) was added into each of the 6 L 57Fe-EDTA exposure medium as the treatment, while nothing was added in the other three PC bottles as the control.

On the other hand, the whole phytoplankton community was used to examine phycosphere pH effect, and hence 2 L seawater of phytoplankton directly collected from the incubation carboys was added into each of the six PC bottles with 6 L 57Fe-EDTA exposure medium to initiate the Fe uptake experiments. The phytoplankton was collected onto 0.2 µm membrane filters, cleaned and rinsed as descripted above, and finally stored in petri-dishes at -80 Celsius degree for the cellular Fe determination at GEOMAR.

5.3.5.3 Work Package 1: C, examine the phycosphere ROS effect on Fe bio-uptake.

The basic work procedures were similar to those of Work Package 1B, except for the followings: 25 k superoxide dismutase SOD and 64 mg catalase were added into one carboy with 6 L freshly collected algae solution, while the same amounts of heat denatured SOD and catalase were added into the other carboy as the control. Following a 30 min reaction, 2 L of algae solution was added

into each of the six PC bottles with 6 L 57Fe-EDTA exposure medium to initiate the Fe uptake experiments. The Fe uptake experiments were carried out in the same manner as Work Package 1C. The filters with phytoplankton were stored in petri-dishes at -80 Celsius degree for the cellular Fe determination at GEOMAR.

5.3.5.4 Work Package 2: Exponential fed batch EFB cultures of ambient phytoplankton communities to test impact of Fe bioavailability.

The EFB method is a continuous culturing method that adds growth media proportionally to the culture volume in order to maintain a constant dilution rate. For natural communities, the method offers the potential to limit growth rates to those closer to in-situ conditions in nutrient limited environments (~0.1-0.2 /day) and thus potentially prevent the growth of bloom forming phytoplankton in nutrient manipulation experiments.

We carried out a simple experiment consisting of a control and a treatment to test the response of phytoplankton communities to Fe availability in EFB cultures at sea. The control: Unfiltered surface seawater collected from the towed fish on September 4th was used to fill culture vessels (1.4 L * 3 replicates). The 0.2 µm filtered surface seawater was used to fill the reservoir, and the seawater was amended with 20 µM N and 1.25 µM P. The treatment: Unfiltered surface seawater collected from the towed fish on September 4th was used to fill culture vessels (1.4 L * 3 replicates). The 0.2 µm filtered surface seawater was used to fill the reservoir, and the seawater was amended with 20 µM N, 1.25 µM P and 0.5 nM 57-Fe. A subsample of the 0.2 µm filtered seawater was collected into acid-cleaned bottles for the analyses of background concentrations of trace metals and major nutrients at GEOMAR. Also, subsamples of the unfiltered seawater were harvested on membrane filters for the analyses of chlorophyll a (pre-combusted GF/F filters), particulate organic carbon POC (pre-combusted GF/F filters), trace metals (polyether sulfone PES filters), 16S RNA (PES filters) and pigment composition (GF/F filters) at GEOMAR.

In the month on the cruise, the six culture vessels were kept in a growth environmental chamber at 21 Celsius degree with a constant light intensity of 120 µmol/m^2/s for 14 hours per day, and the supply of growth medium from the reservoirs to the culture was controlled by our EFB program (dilution rate was set to 0.1 per day). We sampled 500 mL culture medium from each culture vessel every 3 days in the laminar hood following the trace metal clean procedure, and there were 8 samplings in total. For each sampling, we took:

a, 100 mL medium filtered onto pre-combusted 0.7 µm GF/F filters, store in sealed petri dish at -80 Celsius, for lab analyses of POC/PON or chlorophyll a;

b, 400 mL medium filtered onto acid pre-rinsed 0.8 µm PES filters, store in sealed petri dish at -80 Celsius, for lab analyses of P, Fe and other trace elements.

Also, we took additional samples for 16S RNA analyses at the beginning and end of the EFB experiments.

5.4 Deep-water collection with trace metal clean CTD/Rosette

(S. Poehle[1], K. Gosnell[2], L. Zhou[2], D. Jasinski[2], L. Blum[2])
[1] Jacobs University Bremen
[2] GEOMAR

We used a titanium rosette frame equipped with sensors for conductivity, temperature, depth (CTD), turbidity and oxygen (Seabird Electronics) to ensure trace metal clean collection of seawater samples (TM-clean CTD). Sampling depths were selected based on the turbidity signal, which provides information on the depth range and the intensity of the hydrothermal plume. Deep seawater samples between ca. 1700-2400 m were obtained at 19 stations using the GEOMAR trace metal clean titanium CTD rosette, equipped with 24 trace metal clean Niskin bottles of 12 L each. The titanium CTD water sampling rosette was attached to a conducting plastic-coated Kevlar wire and was operated over the side of the ship via a trace metal clean LEBUS winch system. We closed two bottles at each depth around the plume, one for trace elements and another one for ancillary measurements (see below). The titanium-CTD was equipped with the same standard Seabird sensor package as the GEOMAR and METEOR stainless steel CTD rosettes, which were used for sampling of less contaminant prone metals at the same stations.

After recovery, twelve of the 12 L Go-Flo bottles were immediately carried to the trace metal clean sampling container where unfiltered and filtered seawater samples were collected. The remaining 12 Niskin bottles stayed on deck for sampling of helium, dissolved oxygen, dissolved inorganic carbon (DIC), total alkalinity (TA), ammonium, dissolved organic carbon (DOC), salinity, nutrients and particulate and dissolved siderophore.

5.4.1 Clean lab sampling

Unfiltered samples were collected for mercury species (GEOMAR and Mediterranean Institute for Oceanography - MIO) and sequential filtration approach for trace metals (Jacobs University Bremen). Filtered samples were collected after passing a 0.8/0.2 µm filter cartridge (AcroPak 500, Pall).

Particulate matter (> 0.2 µm) was collected under nitrogen pressurized filtration (approx. 0.5 bar, 99.999% Alphagaz™ 1) for the analysis of trace metals in the particulate fraction (GEOMAR). Therefore, approx. 3–9 L of seawater passed acid-washed 0.2 µm polyethersulfone (PES) filters (25 mm, Pall) which are placed in Swinnex filter holders and directly attached to the outlet tap of the Niskin bottles. The same protocol and filters were used for the collection of particulate matter for minerology analysis via synchrotron.

For the analysis of the soluble fraction of trace metals, filtered subsamples (0.2 µm) were additionally filtered through 0.02 µm filters (25 mm, Anapore) by syringe filtration under the laminar flow bench in the clean laboratory container. The filtrate was collected in 60 ml acid-washed LDPE bottles. Subsamples taken for Fe isotopes, dissolved trace metals and soluble trace metals (all GEOMAR) were acidified with hydrochloric acid (ultrapure grade, Romil) to 0.015 mol/l HCl in the laminar flow bench to stabilize the trace metals until land-based analysis.

All LDPE bottles used to collect the respective subsamples were cleaned prior to the cruise according to the GEOTRACES cleaning recommendations provided in the GEOTRACES cookbook (https://www.geotraces.org/methods-cookbook/).

In total, we collected seawater samples for GEOTRACES key elements, trace metals, isotope systems, major elements, dissolved aluminium and nutrients at 19 different stations (Table 12.6).

5.4.2 On-deck sampling

^{3}He is a conservative tracer for vent supply, which allows us to trace the plume because hydrothermal vents are by far the main source of this isotope to the ocean. As Helium is a very low-density gas, samples for helium isotopes were sampled first. Seawater samples for helium were collected in a copper pipe, which was connected to the Niskin bottle, with water flowing until bubbles in the tube were removed. While the water was flowing, the pipe was closed using an electrical drill and a ratchet to ensure it is tight enough. Helium isotopes will be analysed at the University of Bremen, as part of a contract. In addition, 1.5 L samples for tritium analyses were collected at 3 full depth CTD casts. The samples will be analysed in Bremen too, and the data will serve to correct the He isotope measurements for tritium present in the deep-water.

Dissolved oxygen samples were taken bubble free in 100 mL glass bottles for subsequent Winkler analysis. DIC/TA samples were subsequently collected in 250 mL borosilicates bottles, and poisoned with mercuric chloride (50 microliter of a saturated solution of $HgCl_2$ to 250 ml of seawater). DIC-TA samples will be analysed in Kiel using Apollo DIC and TA instruments.

Ammonium samples were collected and analysed on board using the OPA method with a fluorimeter.

DOC samples were taken after passing through an ashed GF/F filter and acidified to pH 2 in the lab. After station M176/2_14, the DOC samples were not filtered anymore as particle loads in the plume were very low and no contribution of POC to TOC in deep waters was expected. DOC samples will be analysed at GEOMAR using a Shimadzu TOC/TDN instrument.

Salinity, nutrients and particulate and dissolved siderophore samples were taken directly from the Niskin bottles.

5.4.3 Oxygen

(L. Blum[1])

[1] GEOMAR

Oxygen concentrations of the different CTD casts were measured by oxygen sensors attached onto the rosette frames. 119 discrete oxygen samples were collected from different depths of the water column and the CTD casts to calibrate these sensors. For the trace-metal-clean CTD, two samples were taken at the deep cast and two at the shallow cast. For the stainless-steel CTD, five samples were taken at the Tow-Yo cast. Oxygen concentration samples were analysed during the cruise using the Winkler (1888) Method.

5.4.4 Particulate and dissolved siderophores

(L. Blum)

Siderophores are organic ligands that show specificity for iron, and are assumed to play an important role in keeping seawater iron in solution. 2 L samples have been collected in FlexBoys (bloodbags) from the Niskin bottles on deep and shallow casts of the trace metal clean CTD (Table 12.9). Six evenly spread samples were taken in the deep cast, including the turbidity maximum. Three additional samples were taken in the shallow cast, including the deep chlorophyll maximum (DCM) and 15 m above and below the DCM. After adding the internal Standard (160 pM H-

Riboflavin concentration) to the samples, the samples were filtered using Sterivex PVDF filters and Bond Elut ENV 500 mg columns by gravity. The filters were frozen at - 80°C and the columns at - 20°C to be analysed via HPLC-MS after the cruise. The FlexBoys, filters and columns were cleaned with methanol, HCl (0.1 M) and MQ before sampling.

5.4.5 Sampling and analysis of dissolved Al

(L. Zhou[1])
[1] GEOMAR

10 mL seawater was acidified to pH ~2 by adding 10 µL of ultrapure concentrated hydrochloric acid in a clean laminar hood. Dissolved Al in the seawater was analysed within 24 hr of sample collection using the Al-lumogallion complex method following Ren et al. (2001) with a Carey Eclipse fluorometer. High concentrations of dissolved Al are observed in the close vicinity of the hydrothermal vent (Fig. 5.8). Dissolved Al concentration decrease with increasing distance from the vent. The concentrations of dissolved Al in the surface ocean were lower than concentrations in the deep waters, and the lowest dissolved aluminium concentrations were observed at the chlorophyll maximum depth (Figs. 5.9 and 5.6).

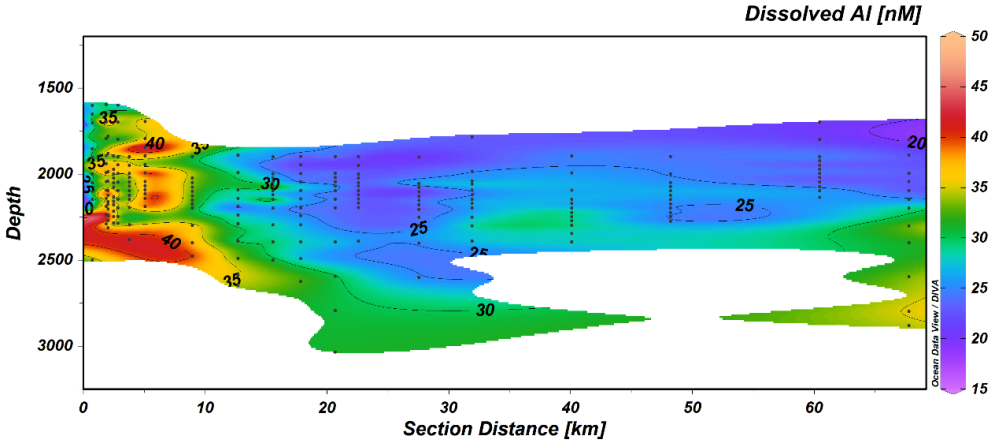

Fig. 5.8 Vertical profiles of dissolved Al concentrations in the deep ocean in the vicinity of the Rainbow hydrothermal vent and up to >60 km distance.

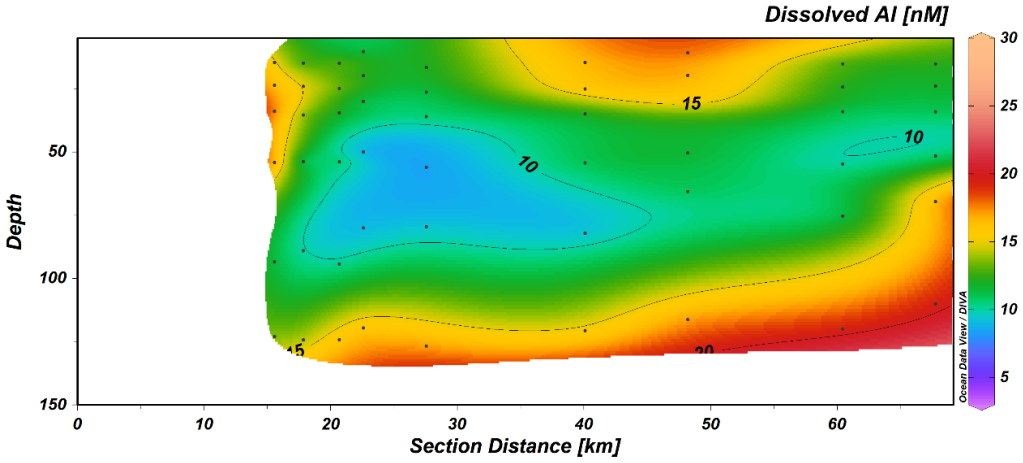

Fig. 5.9 Vertical profiles of dissolved Al concentrations in the surface ocean above the Rainbow hydrothermal vent and up to >60 km distance.

5.4.6 Dissolved chromium

(D. Gilliard[1])

[1] University of Lausanne, Switzerland

During the last decades, chromium (Cr) isotopes found in BIF and carbonates have been used as a proxy for past terrestrial oxygenation ((Crowe et al., 2013; Frei et al., 2009; Frei et al., 2011). Recent studies on dissolved Cr in seawater suggested that Cr redox reactions may be driven by oxygen and/or productivity (e.g. Goring-Harford et al., 2018; Janssen et al., 2020; Scheiderich et al., 2015) instead of atmospheric oxygen. While Cr seems to behave similarly within the seawater column (e.g. low [Cr] and high isotopes values in the upper part and high [Cr] and low isotope values in the lower part e.i. Murray et al., 1983; Goring-Harford et al., 2018; Rickli et al., 2019), its behavior is unknown in hydrothermal plume. In order to better understand Cr cycle into ocean and the contribution of hydrothermal Cr to the oceanic Cr budget, the sampling strategy focused above, within and below the plume. As well as in porewater, and sediments.

Cr has been sampled from the trace-metal clean CTD/rosette into Niskin bottles. Later, the seawater from the Niskin bottles has been filtered with 0.8/0.2 µm Acropack filters in a clean container. The filtered seawater has been stored in 1L LDPE bottles and will be acidified on land. In addition to the 1L LDPE bottles, three times 15mL tubes have been collected for Cr speciation. The Cr speciation, coprecipitation with Mg by adding ~45µL ammonia few hours after receiving the samples from the clean container. Approximately 1 hour/1.5 hours after adding the ammonia, the samples were centrifuged for 5 minutes. Then, dissolution in 1M nitric acid have been provided onboard in the clean lab container. These chemical steps have been processed few hours after receiving the samples from the clean container. Only one sample has been executed in a laminar flow outside the clean container. At the exception of the two first stations, Cr speciation samples were stored in fridge before processing. After processing, all the samples were stored in a dark place. Porewater samples have been collected for Cr speciation, [Cr], and Cr isotopes. They both follow the same procedure than seawater Cr. In total, 8 stations for [Cr] and Cr isotopes, 9 stations for Cr speciation for the seawater, 15 stations for the sediments, and 6 stations for the porewater have been collected.

All the measurements will be process on land. [Cr] and Cr isotopes will be processed following a coprecipitation with Mg and a double spike method. They will be measured on the Neptune ICP-MS. The methods are more details in (Rickli et al., 2019; Janssen et al., 2020). Cr from sediments would be probably leached in order to extract only the Cr adsorbed onto the particles. Nonetheless the leaching method for Cr is currently developed and the use of the method may change in the future.

5.4.7 Stable barium isotopes and rare earth elements (REEs)

(Z. Zhang[1])

[1] GEOMAR

The combined dissolved concentration and stable isotope composition of barium ($\delta^{138/134}$Ba) is a novel tracer for water mass mixing in the Atlantic (Horner et al., 2015) given that Ba behaves essentially conservatively in deep and bottom waters. However, these tracers have also been used to trace continental freshwater inputs and surface water Ba fractionation processes (Cao et al., 2020). Based on data from several hydrothermal vent sites in the Pacific and Atlantic, it has recently been suggested that the effective hydrothermal fluid components after mixing with seawater are isotopically heavy (endmember $\delta^{138/134}$Ba signatures are calculated at +1.7±0.7 ‰)

and may allow the tracing of hydrothermal plumes or even the history of hydrothermal Ba inputs into seawater (Hsieh et al., 2021). These heavy values resulted from significant corrections of the measured Ba isotope compositions of the vent fluids for modification of the original fluid signature by precipitation of barites (Hsieh et al., 2021). These corrections result in a relatively large scatter of the calculated endmember $\delta^{138/134}$Ba signatures of the vent fluids and need further verification by additional measurements. In addition, potential Ba isotope fractionation processes during advection within the plume and interactions with particles may occur and need to be verified before stable Ba isotopes can be used as a reliable tracer of hydrothermal inputs.

Rare earth elements (REEs) are a sequence of 14 naturally occurring elements with coherent chemical properties. In seawater, because the stability of their aqueous complexes increases with their atomic number, the lighter REEs (LREEs) adsorb on particle surfaces more easily (i.e., more particle-reactive) relative to the heavier REEs (HREEs). In such way, they can be used as particle-reactive tracers. In the nonbuoyant plume, Fe and to a lesser extent, Mn oxyhydroxides are dominant and scavenging by these oxyhydroxides will take place. The rare earth elements (REE) are good examples of particle-reactive tracers which may be rapidly and completely removed by adsorption or coprecipitation with hydrothermal precipitates (German et al., 1991; Sherrell et al., 1999). Thus, deep-sea hydrothermal systems might act as a net removal flux for REEs, and the ratios of REEs to Fe increases with distance from the vent site, likely as a result of continuous scavenging by the Fe/Mn oxyhydroxides (German and Von Damm, 2003). The adsorptive scavenging of seawater REEs onto Fe/Mn oxyhydroxides and the inter-element fractionation of REEs need to be examined in a fairly stable nonbuoyant hydrothermal plume.

During cruise M176/2, one of our goals was the determination of the Ba isotope composition, as well as of the Rare Earth Element (REE) distributions within the Rainbow nonbuoyant hydrothermal plume, in order to investigate how dissolved REE deficits & stable Ba isotope signatures evolve with distance from the Rainbow vent site. Therefore, a total of 228 deep-seawater samples (1700 – 2800 m) from 19 stations (Stations 3, 4, 5, 6, 7, 8, 9, 10, 12, 13, 14, 15, 16, 17, 18, 19, 21, 23, 24) were taken for Ba isotopes and REEs measurements covering the entire cruise track. 1 L of seawater from Niskin bottles of the trace-metal clean CTD were collected into 1 L acid-cleaned PE bottles inside of the trace metal clean container. They were collected after passing a 0.8/0.2 µm filter cartridge (AcroPak 500, Pall). Concentrated Ultra-clean HCl was added to the samples to acidify the samples to pH ~2. The bottles were sealed with parafilm and transported to the laboratory at GEOMAR for further ion-chromatographic cleaning and measurement via MC-ICP-MS and ICP-MS.

5.4.7.1 Analytical methods for stable barium isotopes and REEs:

Dissolved Ba concentrations in seawater will be analyzed using isotope dilution ICP-MS, by adding the ^{135}Ba-enriched single spike. Barium isotopic compositions (δ^{138}Ba) of seawater samples will be measured using a double spike technique on a Thermo Scientific Neptune Plus MC-ICP-MS at GEOMAR. A calibrated ^{130}Ba-^{135}Ba double spike will be added to seawater samples. After an equilibration period of 24 hours, Ba will be precipitated from seawater as a carbonate by adding 1.1 M Ba-free Na_2CO_3 solution stepwise. The residual precipitate will be dissolved in 1 M HCl and further purified through Ion exchange chromatography (cation exchange resin: BIORAD® AG50W-X8 resin) twice. Finally, the purified sample solutions will be introduced as a dry aerosol into the plasma using an Aridus desolvator. A three-dimensional data reduction procedure will be

used and each spiked sample measurement of δ^{138}Ba will be normalized to two "bracketing" spiked standard measurements (Yu et al., 2021).

The concentrations of all REEs will be measured with a SeaFAST system (Elemental Scientific Inc.) connected to a Thermo Element XR ICP-MS with a method modified after Hathorne et al. (2012). GEOTRACES inter-calibration samples BATS 15 m and BATS 2000 m will be measured to monitor the external reproducibility.

5.4.8 Mercury collection and analysis from Rainbow Plume and Atlantic surface waters

(K. Gosnell[1] and N. Torres[2])
1 GEOMAR
2 Mediterranean Institute of Oceanography, France

Mercury is delivered to the surface ocean through atmospheric deposition, while hydrothermal vents provide a natural deep-water source. Enriched concentrations of Hg (>10x higher) have been measured in deep waters neighbouring the Mid Atlantic Ridge (Bowman et al., 2015), however it is not yet clear whether the extended Ridge, and specifically the Rainbow plume waters, do actually impact deep waters as a conspicuous geothermal Hg source. Furthermore, only 4 deep water hydrothermal sites have been measured for Hg species as of this time. With this cruise we aimed to assess Hg processes in surface waters and in detail expanding out from the Rainbow plume. Measuring the Hg biogeochemistry and speciation cycling in the water column in high resolution depth profiles of total Hg (HgT), methylmercury (MeHg) and dissolved gaseous mercury (DGM) will help us to resolve and factor the impact of Rainbow plume as a deep-water Hg source.

5.4.8.1 Mercury sampling

Mercury samples were collected directly from the Niskin bottle spigot as unfiltered seawater. Mercury was sampled from every depth for the deep cast (12 total) in order to obtain complete plume profiles. Only 5 depths were sampled from the shallow cast, collected from the surface, deep, chlorophyll maximum, and 2 other variable depths. A total of 18 stations were analyzed for Hg.

Three bottles were used to collect the 3 different mercury speciation measurements. DGM was always collected first into a 125 mL PET bottle. This was followed by the sample for MeHg into a separate 125 mL PET bottle, and finally the HgT was collected into a 60 mL Teflon (PFA) bottle. The Teflon bottles had been acid cleaned and rinsed with milliQ prior to usage, while the 125 mL PET bottles and caps were taken directly out of the package. The HgT sample bottles were used repetitively for sampling throughout the cruise after analysis had been completed, while the DGM and MeHg bottles were all new.

Each sample bottle was filled with ~5% of the water volume and thoroughly shaken with the cap closed in order to rinse the bottle. After 3 rinses the bottles were filled up until slightly overflowing, with care taken to limit the amount of bubbles in the water. The caps were attached tightly and the bottles were placed in separate boxes for transport to the lab for analysis.

5.4.8.2 Mercury Isotopes Sampling (2 stations)

Approximately 40 L of seawater is required to obtain one measurement of Hg isotopes, thus 4 Niskin bottles (12 L each) were required per each depth. Two stations were collected for Hg

isotopes at 4 depths, making a total of 18 samples. Sixteen bottles on the rosette were used to sample the 4 depths for Hg isotopes, with the remaining 8 bottles collected water for ammonium or radium samples. The first station was collected closer to the edge of the plume, while the second station was collected at the peak of the plume signal. At the first isotope station the plume depth was sampled by selecting the depth of the maximum turbidity signal (2100 m), followed by the oxygen minimum (775 m), the chlorophyll maximum (80 m) and a surface sample (5 m). The second plume station followed a similar scheme, with turbidity maximum (2150 m), overlying plume waters (1500 m), oxygen minimum (775 m), chlorophyll max (80 m), and finally surface water collected from the tow fish (~ 1 m).

Two 20 L acid-cleaned glass bottles were used to collect each sample depth. Each bottle was triple rinsed with the unfiltered sample water prior to filling with seawater from a mixture of the 4 bottles from each depth. Unfiltered seawater was filled up to the bottle shoulder, making sure to leave significant headspace in order to prevent bottle breakage from the eventual pressure buildup which occurs as samples sit. Subsamples for DGM, MeHg and HgT were collected out of one Niskin bottles per each depth. The DGM and MeHg samples were collected directly from the spigot. Total Hg was sampled by drawing water out of the 20 L sample using a 30 mL acid cleaned glass pipette and putting it into the 60 mL Teflon bottle. The 20 L isotope samples were double bagged and tightly sealed, then placed in protective storage container and secured for transport and analysis within the next 8 months.

5.4.8.3 At-Sea Analytical work

All ship-board analysis was completed on a Brooks Rand Model-III instrument that was modified for streamlined and mobile ‘on-line’ analysis (US EPA method 1631; Heimburger et al., 2015). The Hg amount was quantified by Cold Vapor Automatic Fluorescence Spectrometry (CVAFS) via a lamp and quartz cuvette (US EPA method 1631). Argon gas flow was set to 1 Bar, and was additionally regulated into the instrument using an AALBORG mass Flow Controller set to 0.15 mL/min. The Model-III sensitivity PMT was set to 900 V.

Gold traps were replaced when the sensitivity dropped significantly, which was typically after 5 days of continuous use. First, all electricity running to the control box and traps was turned off and disconnected. Traps were replaced by first cutting off the silicon tubing ends (which tightly connected the Au trap to the valves) and loosening the valves, then carefully sliding the old trap out of the heating coil. Two pieces of new silicon tubing were cut. One was first attached to the second (end) valve. The new Au trap was then carefully slid through the coil and secured in the new tubing/valve. The second piece of tube was attached to the first valve, and then slid in and carefully secured to the other end of the Au trap. The valves were then secured back in place.

5.4.8.4 Methylmercury (MeHg)

Upon reception, the MeHg samples were acidified using concentrated HCl (620 µL) and the bottles placed in a plastic bag, then put in a box for storage. Methylmercury analysis will be completed via isotope dilution (Monperrus et al., 2005) using an ICPMS in the laboratory at MIO within the next 8 months. A total of 307 samples were collected for MeHg.

5.4.8.5 Total Hg (HgT)

The analytical reagents bromine monochloride (BrCl) and Stannous chloride ($SnCl_2$) were prepared at the beginning of the cruise following US EPA Method 1631. HgT seawater samples were treated with BrCl in order to oxidize and release all Hg species. Stannous chloride was required to reduce Hg species into Hg0 prior to purging and analysis.

To start the analytical day ~30-40 mL of BrCl treated seawater was added to the sparging tube, followed by 1 drop of $SnCl_2$, and the plunger cap was quickly and tightly sealed. Water was repetitively sparged until blank levels were consistent for ~3 peaks. Each HgT run would be sparged for 240 sec (4 min). After this a standard curve was created by pipetting increasing concentrations of NIST Hg standard into the purged water in the sparging tube. Standards followed a typical volume scheme of: 15 µL, 25 µL, 50 µL, 100 µL, 150 µL, 200 µL. Once the standard curve was satisfactorily achieved (r^2 = 0.99xx) two additional standards (300 µL of ERM and next 300 µL OMRS) were measured in order to ensure all values and standards were consistent.

Two drops of BrCl (~40 µL) were added directly into each HgT sample bottle at minimum 1 hour before analysis. For analysis; approximately 30 mL of the sample was poured into the sparging tube and 1 drop of $SnCl_2$ (~30 µL) was added just before tightening. The sample peak area was recorded and quantified after each run ended. After analysis finished the purged water was poured into a measuring tube in order to record the volume. Duplicate analyses were completed for HgT on all samples by analyzing the remaining sample volume amount at a later point. A 50 pg Hg NIST reference standard was analyzed every ~6 samples and at the end of the analysis to track potential drift. Total Hg analysis was performed on 317 samples, with 293 samples analyzed as duplicates.

Pore waters were analyzed for HgT out of select cores, for a total of 72 samples. A drop of BrCl was added to each ~1 mL pore water section aliquot once samples were received. Porewater samples were analyzed by pipetting a 500-1000 µL aliquot into pre-purged seawater and analyzing as usual. Approximately 1 g of sediment was collected for each available sediment section for Hg and MeHg analysis. Sediment subsamples were stored frozen, and will be transported for future analysis on land.

5.4.8.6 Dissolved Gaseous Mercury (DGM)

For DGM analysis a standard curve was first completed using the HgT sparging plunger and setup. Then the sample setup and settings were switched and adjusted for DGM analysis by attaching a bottle cap and sparging bulb were directly into the first valve loop. DGM is volatile and mobile, and rapidly escapes out of collected samples. Accordingly, DGM samples were always analyzed first and as soon as possible. A total of 305 DGM samples were analyzed during the cruise.

The DGM samples are measured as collected using no chemical treatment. It was important to ensure that no water or water vapor can directly reach the intake tube from the top of the sparging cap, as it ruins the Au trap and beyond. Accordingly, head space was formed in each sample by quickly pouring out some water immediately before attaching the sample to the sparging cap for analysis. Water was typically poured out until the sample volume met the 125 mL bottle line. Afterward each sample was attached directly to the online sparging cap for analysis. Each DGM sample was sparged for 752 s (~12.5 min) with Ar. DGM sample analysis was bracketed by standard measurements of 50 µL Hg (NIST) to assess potential drift during the run. After analyzing each DGM sample was acidified with concentrated HCl (500 µL) and placed in a plastic

bag and box for storage until future MeHg analysis could be completed via isotope dilution (Heimburger et al., 2015; Monperrus et al., 2005) at MIO.

5.4.8.7 Preliminary Results Overview:

There was a slight though consistent increase found to match with the plume signal from the turbidity maximum for total Hg (Fig. 5.10A). DGM was consistently lowest in surface and higher amongst the plume stations (Fig. 5.10B). Surface sample measurements were consistently low for HgT (0.2-0.8 pM), and very low for DGM (0.02-0.15 pM).

The Hg plume signal was most distinct at the station directly around the plume (Fig.5.11). Although there was significant scatter between plume stations for both total Hg (0.3-1.2 pM) and DGM values (0.3-0.5 pM).

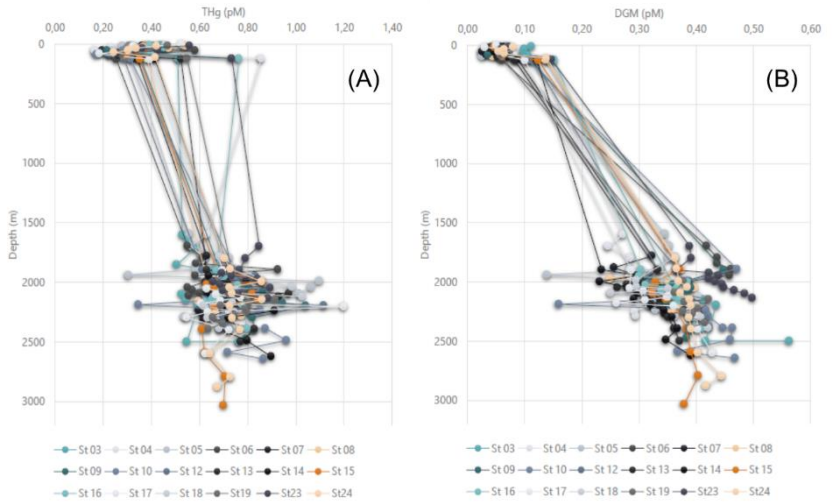

Fig. 5.10 Overview of all of the station measurements for plume and surface casts completed during M176-2 for Total Hg (A) and DGM (B).

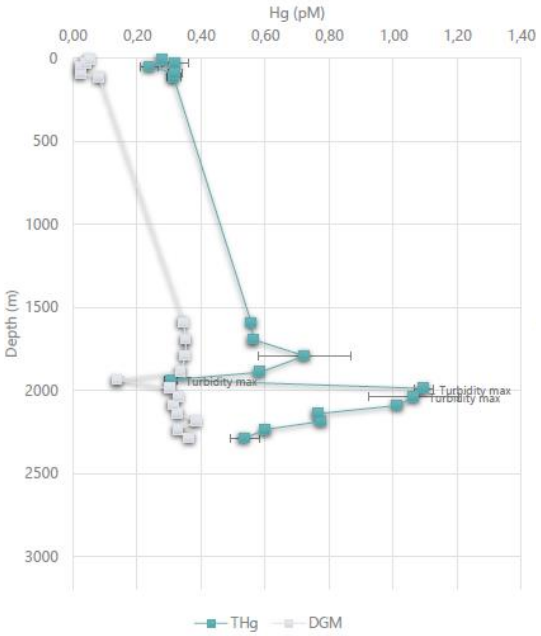

Fig. 5.11 Total Hg measurements for the plume station, illustrating the strong increase in total Hg found around the plume (turbidity maximum).

5.4.9 Water sampling for dissolved trace-metals, HFSE, Cr and V speciation and organic Fe, Zn and Cu ligands in different size fractions

(L. Klose[1], S. Pöhle[1], V. Menon[1])

[1] Jacobs University Bremen

The sampling strategy was designed to determine the distribution of trace-elements and their physical and chemical speciation along the dispersing nonbuoyant hydrothermal plume from the Rainbow vent site. Because of the time-consuming filtration work (sequential filtration and Ultrafiltration, see below) and necessary cleaning and blank processing, we subdivided the stations into two categories, 1) super stations and 2) normal station (Table 12.21). At superstation samples all size fractions were sampled (0.8 µm, 0.2 µm, 0.015 µm and 10 kDa (~0.003 µm)), whereas, at normal stations samples were solely taken in the 0.2 µm fraction (for the detailed sampling list see Table 12.27).

The sampling for dissolved trace-metals (TM), high-field strength elements (HFSE), Pt, speciation analysis of Cr and V as well as organic Fe (FeL), Zn (ZnL) and Cu (CuL) ligands were conducted with a trace-metal clean CTD/rosette. The Niskin bottles were transferred into a clean-lab container and subsequently filtered through 0.8/0.2 µm AcroPak (Pall) filters (for more detailed information on sampling see section 5.4.1). The samples were then transferred to a chemical lab for acidification (TM, HFSE and Pt) inside a laminar flow-bench to a pH of 1.7 using ultra-pure HCl (Roth™) and were subsequently stored cool (4 °C). All samples for speciation analysis (Cr and V) and organic ligand determination were immediately frozen after sampling at -20 °C.

5.4.9.1 Sequential filtration

To determine the different size fractions along the dispersing hydrothermal plume, three samples at each superstation (above, within and below the hydrothermal plume) were chosen (for more details see Table 12.27). For each of these samples, sequential filtration was carried out inside a laminar flow-bench using individual filter-towers (for each size fraction) equipped with 47 mm Nuclepore (Whatmann) membrane filters in the respective size fraction (0.8 µm, 0.2 µm, 0.015 µm). The filter-towers were over pressurized (0.5 to ~1 bar) with nitrogen gas (N_2 99.999% Alphagaz™ 1) to increase filtration speed. All samples were taken unfiltered in the clean lab container and transferred to the chemical lab. Prior to filtration each filter-tower and membrane filter were rinsed with ~ 30 ml of 0.1 M ultrapure HCl (Roth) and DI. The total volume of each sample (1.5 to 2 L) was filtered sequentially through 0.8 µm, 0.2 µm and 0.015 µm filter membranes. At each filtration step, subsamples for FeL (~200 ml), TM (~100 ml), HFSE (~100 ml) and Pt (~100 ml) were taken. Following this filtration process three DI blanks (18.2 MΩ, MillQ® Merck) were also prepared. The filtered sample/blank volume for each filter was noted and the membrane filters were stored frozen for later analysis of particulates. Subsamples for Fe ligand analysis were also frozen immediately (-20 °C), whereas TM, HFSE and Pt samples were acidified using ultra-pure HCl (Roth™) and stored cool (~4 °C).

5.4.9.2 Ultrafiltration

In addition to the sequential filtration, which separates size fractions between 0.8 µm, 0.2 µm and 0.015 µm, we further conducted a cross-flow ultrafiltration (Millipore Pellicon 2 tangential flow ultrafiltration unit) with a molecular weight cut-off (MWCO) of 10 kDa. By following this

approach, we receive information about the distribution between the colloidal (< 0.2 µm) and the truly dissolved (<10 kDa) pool by separating and preconcentrating the colloidal fraction larger than 10 kDa. Six stations along the dispersing hydrothermal plume with the highest turbidity signal were chosen for this extended filtration program (for detailed information see Table 12.27). The ultrafiltration procedure was as follows: A total sample volume (4.5 to 8 L) was filtered through 0.8/0.2 µm AcroPak (Pall) filters and collected in an acid-cleaned 10L carboy inside the clean-lab container and subsequently transferred to the chemical lab for further processing. Prior to sample filtration the pre-cleaned ultrafiltration membrane (10 kDa) was conditioned with ~ 500 ml of sample for 5 minutes and the permeate flow-rate was adjusted to <250 ml min^{-1}. After that, the remaining sample volume was filtered until a concentration factor (CF) < 8 was reached (i.e. retentate volume is at least 8 times lower than permeate volume). As the last step 1L of 30 mM HCl solution (ultra-pure HCl Roth™) were recirculated for 10 minutes (5 min with open permeate line, 5 min with closed permeate line) to remove all remaining colloids from the membranes surface. The same membrane was used for all six stations with complete cleaning cycles in between (DI water-0.1M NaOH-DI water-0.1M HCl-DI water). A blank sample was processed after each cleaning cycle. During sample, blank and cleaning procedure the inlet pressure was monitored and kept at 2 bar by adjusting the pump speed if necessary. Subsamples for FeL, TM, HFSE and Pt were collected from the resulting permeate and retentate volume from all processed samples and blanks. Subsamples for TM, HFSE and Pt analysis were acidified using ultra-pure HCl (Roth™) and stored cool (~4 °C), while FeL samples were immediately frozen (−20 °C).

5.4.9.3 Overview of collected and processed samples

During the 19 days in the working area we sampled eight superstations and normal stations, respectively, from the trace-metal clean CTD/rosette. Subsamples for multiple parameters (TM, HFSE, Pt, Cr and V speciation, FeL, ZnL, CuL, Filter) were collected in different size fractions (0.8 µm, 0.2 µm, 0.015 µm, <10 kDa, >10 kDa). In total 1200 samples were collected and a detailed count is given in Table 12.22. All samples in their respective size fractions will be measured by different analytical procedures. TM and HFSE samples will be pre-concentrated by an offline-seaFAST system and subsequently analysed via ICP-MS. Platinum will be determined by a highly sensitive adsorptive stripping voltammetry (ASV) method (Metrohm 220/3e). Chromium speciation will be done voltammetrically (Sander and Koschinsky, 2000), Vanadium speciation will be determined by solid-phase extraction and subsequent analysis via ICP-MS. Different voltammetric techniques will be used for the analysis of Fe, Cu and Zn binding ligands (Buck et al., 2012; Kim et al., 2015; Kleint et al., 2016). The filters obtained from the sequential filtrations will be analysed on the ICP-MS following HF digestion.

5.4.10 Major elements

(Z. Steiner[1])

[1] GEOMAR

After decades of study, there is still poor agreement between the oceanic residence time of major elements such as calcium and strontium when calculated based on the known inputs and outputs (Broecker and Peng, 1982; Hodell et al., 1990; Lecuyer, 2016; Milliman, 1993; Richter and Turekian, 1993; Tipper et al., 2010). This suggests that we are missing key input or output components in this system. One of the main known sources or sinks of major elements in the ocean are hydrothermal vent systems, which are typically rich in calcium but very poor in magnesium

relative to seawater (Berner, 2004; Humphris and Thompson, 1978). Strontium concentrations in hydrothermal fluids are on average similar to seawater of equivalent salinity but the isotopic composition of the hydrothermal strontium is different, suggesting a very active cycle within these systems (Davis et al., 2003). It is therefore assumed that hydrothermal systems are critical for maintaining the chemical balance of the ocean.

A hypothesis we wish to test in the context of the residence time of major elements in the ocean is that reactions occurring following mixing of the hydrothermal fluids and seawater modify the effective contribution of major elements from hydrothermal fluids to ocean chemistry. Such a mechanism could provide a partial solution to the discrepancy between the known sources and sinks of several major elements. To test this hypothesis, we collected samples for the analyses of major element concentrations in 17 stations along the plume. We also collected samples from two shallow CTD casts (biology casts) as a surface ocean reference to the deep-water data, and from an algal growth experiment to test whether changes in productivity affect the measured dissolved concentrations of major elements. Major element samples were filtered in the clean laboratory and stored in acid cleaned bottles. The major element samples were not acidified.

The ratios of the major dissolved cations magnesium, calcium, strontium, lithium and potassium to sodium will be analysed at GEOMAR using a Varian-720 ICP-OES, using a sample-standard bracketing method (Steiner et al., 2020). We assume that mixing of the hydrothermal fluid and seawater is very rapid, hence sodium to salinity ratios can be considered constant, following the modern definition of seawater salinity (IOC et al., 2010; Millero et al., 2008). A major element of particular interest to this survey is fluorine. Fluorine uptake is strongly influenced by carbonate and oxygen concentrations (Feng et al., 2021), and is particularly enhanced by formation of phosphate rich deposits (Rude and Aller, 1991). Cave et al. (2002) have shown that the Rainbow plume promotes removal of phosphate from the water to sediment; hence, it is likely that fluorine is not conservative in this system. Fluorine concentrations will be analysed using the spectrophotometric method described by Kremling (1999).

5.4.11 Nutrient distribution

(A. Mutzberg[1])

[1] GEOMAR

The distribution of nutrients in seawater is key for understanding biogeochemical processes, and their signatures allow the differentiation between the various water masses in the ocean. In addition, they are used to identify leaking bottles due to their well-defined and oceanographically consistent distributions.

Every Niskin bottle fired from every single cast depth was sampled for nutrient analysis onboard. The seawater was collected in acid cleaned (10% HCl) 15 mL polypropylene sample vials. Containers and caps were rinsed three times with the water of the sample before the actual sampling.

Samples were placed immediately in the fridge after collection (4°C in darkness) in case they could not be immediately analyzed. Analysis of nutrients was undertaken on board by segmented flow injection analysis using a QUAATRO39 (Seal Analytical) auto-analyzer including a XY2-autosampler unit. The system set-up included 4 channels for nitrate + nitrite (TON), silicate, nitrite, and phosphate. The analytical methods followed during the M176/2 Rainbow plume cruise correspond to those described by QuAAtro Applications: Method No. Q-

068-05 Rev. 11 for TON, Q-066-05 Rev. 5 for Silicate, Q-070-05 Rev. 6 for Nitrite and Q-064-05 Rev. 8 for Phosphate. Low nutrient surface seawater collected by towfish during the cruise was used for the calibration standards preparation and as baseline blank for all parameters.

A total of ~450 samples collected by the titanium-geochem-CTD-casts in depths between ~1700 and 2500 m, ~430 samples collected by the titanium-biology-CTD-casts in depths between ~10 and 120 m and ~170 samples collected by the stainless steel GEOMAR and Meteor-CTD-casts in depths between ~1500 and 2500 m were measured. Additionally, ~120 pore- and bottom-water samples collected by the GEOMAR Multicorer and ~ 20 digested foraminifera samples were also measured.

Towfish samples from oceanic surface with expected concentration values lower than ~100 nM for mainly nitrate + nitrite were stored at −20°C to be analyzed back at GEOMAR lab in Kiel by an modified AA3 SEAL segmented flow analyser.

Certified Reference Material for Nutrients in Seawater (RMNS) was used for every run, in order to I) guarantee repeatability and reproducibility between analytical runs and to II) validate the data set in terms of compatibility within the scientific community. Nutrient analyses were validated with KANSO CRM, Lot-No. CL.

5.5 Suspended particles and radiogenic tracers

5.5.1 Subsampling of in-situ pump filters

(Z. Zhang[1])
[1] GEOMAR

Six In-situ pumps were deployed at stations 3, 4, 5, 6 and 7, with 3 pump heads deployed with acid-washed 0.2 µm polyethersulfone (PES) filters, and 3 heads deployed with Quartz filters. Filters were immediately subsampled with porcelaneous punches and knives. 25mm PES filters were punched for Synchrotron analysis, Th isotopes, Hg isotopes and Ba isotopes; 25mm Quartz filters were punched for Ra isotopes, ^{234}Th and POC. The remaining filters were stored in Ziploc bags. Filters for ^{234}Th were immediately measured onboard, and all the other filter samples were stored at −20 °C.

5.5.2 Metal mineralogy sampling (suspended particles and sediments)

(Z. Zhang[1])
[1] GEOMAR

Deep-sea hydrothermal vents are a source of dissolved and particulate metals to the ocean; however, the overall transport potential, speciation, and bioavailability of hydrothermally derived metals is largely unknown. It is important to determine the fate of hydrothermally derived particulate metals with increasing distance from the source, including an assessment of changes in physical and chemical particulate forms.

Metal mineralogy samples were handled, sealed and stored under anoxic conditions using a Captair portable glove bag purged with N_2 gas. Three layers of gloves were worn at operation, 1) cotton gloves on hands to absorb moisture; 2) glove bag attached white gloves; 3) nitrile gloves over the top to keep attached gloves clean and improve dexterity.

Samples were operated, sealed and stored based on following steps: (step 1) filter and all packaging put into glove bag with N_2 (g); (step 2) filter piece goes in petri slide; (step 3) petri slide goes in plastic bag; (step 4) plastic bag goes in mylar and is heat sealed; (step 5) sealed mylar

pouch stored at -20 °C. Filter samples were sealed immediately after sampling. Sediment samples were all sealed at the end of the cruise; they had first been stored frozen in an Eppendorf that had been flushed with N_2 (see details of sediment sampling in Section XXX).

In total, 84 filter samples were taken, including 8 PES filters (25mm punch) from in-situ pumps (Table 12.12), and 76 PES filters (25mm, Pall) from Niskin bottles (Table 12.13). They will be shipped to Brandy Toner's working group at U. Minnesota, US for synchrotron analysis.

5.5.3 Radium Isotopes

(L. H. Vieira[1,2] and P. Battermann[2])
[1] GEOMAR
[2] Christian Albrecht University

The four radium isotopes (^{226}Ra, $T_{1/2}$=1600 y; ^{228}Ra, $T_{1/2}$= 5.75 y; ^{223}Ra, $T_{1/2}$=11.4 d; ^{224}Ra, $T_{1/2}$= 3.66 d) are produced by the decay of particle-bound thorium isotopes in sediments and are soluble in seawater. Ra isotopes present a range of half-lives varying from days to thousands of years and have relative conservative behaviour in the oceans, so they can be applied to study oceanographic processes that occur within this time scale. Elevated Ra activities have been observed in the vicinity of hydrothermal vents (Kadko, 1996; Kadko and Moore, 1988). The low pH and high temperature of the hydrothermal fluids may release Ra when the circulating fluid interacts with basalt, and any water mass that has been in contact with the Ra source will carry its signature. In addition, Ra isotopes were shown to be powerful tools to study inputs of elements to the oceans. Therefore, they are applied here to study the vertical and horizontal water mass transport processes, and, in combination with dissolved TEIs (Fe, Mn, Co, REE), Ra may provide insights into the distribution and behaviour of TEs and quantify their inputs from the Rainbow hydrothermal field into the ocean.

At five stations (Stns. 3 to 7), sampling of Ra isotopes was performed using in-situ Challenger pumps deployed at six depths. The in-situ pumps were equipped with a polyethersulfone membrane filter (PES) and Quartz filters, alternately, to collect suspended particles; the filtrate then passed through MnO_2-coated polypropylene filter cartridges (Mn-cartridges) to extract the Ra isotopes (Henderson et al., 2013). The in-situ pumps were fixed on the steel wire of the CTD-Rosette and lowered to the desired depths (below, within, and above the hydrothermal plume). The pumps operated for approximately 90 min, pumping from 20 to 1000 L of seawater through the Mn-cartridges. Small-volume samples (1 litre) were collected from the CTD cast at the corresponding in-situ pump depths for analysis of ^{226}Ra by mass spectrometry. The in-situ pumps did not work very reliably, and from station M176/2_8 onwards, the large volume Ra samples were obtained from stainless steel CTD casts.

Samples were then collected by draining ~90 to 230 L of seawater from the CTD bottles into barrels. Seawater was then filtered through MnO_2-impregnated acrylic fiber (Mn-fibers) at a flow rate <1 L min^{-1} to extract Ra isotopes quantitatively. Next, the Mn-fibers were rinsed, and air (partially) dried. Analyses of the short-lived radium (^{223}Ra and ^{224}Ra) were conducted onboard using four Ra delayed coincidence counters (RaDeCC) (Moore and Arnold, 1996). The long-lived Ra isotopes will be analysed in the land-based laboratories by gamma spectrometry and mass spectrometry.

Deep-sea sediments are the dominant source of ^{226}Ra to the oceans. Nonetheless, the use of ^{226}Ra as an oceanic tracer requires a better understanding of how the source varies in the

different ocean basins (Ku and Lu, 2008). For that, at certain stations (Table 12.14), pore water samples (30 ml) and overlying waters (1 L) were collected for ^{226}Ra analysis by mass spectrometry. After collection, the samples were acidified with sub-boiled nitric acid to pH 1.6. See section 5.6 for details of the pore water sampling. The overlying waters were filtered through a polyethersulfone membrane filter (PES) to remove particles and dissolved ^{226}Ra was collected. The filters were stored for future analysis.

5.5.4 Technical report ^{234}Th, ^{230}Th, ^{238}U and Stainless steel CTD, Meteor CTD

(D. Gilliard[1])

[1] University of Lausanne, Switzerland

At each station, five samples (4 L) were collected above, within and below the plume for analyses of ^{234}Th activity. For each sample of ^{234}Th, ^{238}U was collected in 15 mL bottles and acidified with 20 µL of HCl. In addition, ~5 to 6 L were collected for future analyses of ^{230}Th. These samples were acidified with concentrated HCl to pH 2.

From Station 3 to 7, the samples were collected from the Stainless steel CTD where in-situ Challenger pumps were attached to the wire and deployed at six depths (section 5.5.1). The ^{234}Th samples were acidified with ~ 9 mL concentrated Nitric acid to obtain a pH of ~1.6 and spiked with 50µL of a yield standard directly after sampling. After a waiting time of 8 hours, ~9 mL ammonia was added to raise the pH to between 8.3 and 8.6, then 50 µL of potassium permanganate and manganese(II) chloride were added in order to coprecipitate Th with MnO_2. After 8 hours, the samples were filtered onto a silver filter (3 µm pore size) and dried for 1-2h at 50°C. Finally, the dissolve ^{234}Th was measured onboard on the Risø low-level beta GM multicounter. Due to the poor functioning of the in-situ Challenger pumps, the sampling plan was redesigned since station 8. Three CTD (one Stainless steel CTD from Geomar and two CTD from Meteor) were deployed instead of one, to provide enough seawater to the Ra group. The first CTD focused on two depths below the plume, the second CTD focused on two depths in the maxima/within the plume, and the last one focused on one depth within and one depth above the plume. For each of the CTD casts, the depths of sampling were adapted in respect to the observed turbidity signal from the plume. Since the samples were collected with a different timing, the waiting time of 8 hours between chemical steps for ^{234}Th could not stand anymore. The first three samples (2 depths below and one within the plume from two CTD) were acidified and spiked together between 1-4 hours after sampling. The two last samples from the last CTD were acidified and spiked approximately one hours after sampling. Due to the time gap between each of the three CTD casts, the decision was taken to add the ammonia, the potassium permanganate, and the manganese(II) chloride the next day at 6 am and the filtration 8 hours later.

From station 14, the turbidity signal was too weak to detect the plume and the sampling plan has been redesigned a second time for Ra. The first CTD cast focused on two deep depths, the second on only one depth where we expected to find the plume and the third cast on two depths above the expected plume. The timing and the chemical procedures for ^{234}Th were the same than described above. In some of the samples, more than 9 mL of nitric acid and ammonia were required to reach the correct pH. After each use, the 4 L bottles were cleaned with 1 N HCl with 1% H_2O_2 solution and rinsed three times with MQ. Before sampling each of the bottles were rinsed three times with the sample water.

Analyses of particulate and dissolved filters for ^{234}Th were conducted on the Risø low-level beta GM multicounter. The filters were measured for several hours until an error term < ±3% or for a maximum of 12-14 hours. Before measurement, the filters were wrapped first in a plastic film and secondly in an aluminum film.

5.6 Sediment and porewater

(Z. Steiner[1], N. Glock[2], Z. Zhang[1], S. Krüger[1])
[1] GEOMAR
[2] University of Hamburg

The confluence of seawater and hydrothermal fluids creates water that is supersaturated for a large array of minerals. Formation of these minerals likely follows different kinetic rates, for example, copper, iron and manganese oxides are expected to nucleate and precipitate out of the seawater sequentially, and each of these oxides adsorbs other elements from seawater (Cave et al., 2002). Removal of metals contributed by the hydrothermal fluid is the process that eventually determines whether hydrothermal fluids have a global or only local influence on ocean biogeochemistry. The removal products settle on the sediment, which serves as a recorder of this process. However, the sediment is not a passive recorder; elements may be trapped in the sediment or released back to the bottom water depending on microbial respiration, redox conditions, and equilibrium reactions.

Sediment samples were retrieved from 18 of the cruise stations to explore the final removal of hydrothermal fluid products and fluxes between the sediment and bottom water (Table 12.16). In 17 of the stations, the sediment was retrieved using the GEOMAR multi-corer equipped with seven liners (60 cm long, 10 cm diameter) and guided by video telemetry. Near the hydrothermal field, sediment was also collected using a Van-Veen grab. Multi-corer cores were handled as follows:

1) A core was sliced, typically at a one cm resolution. Samples from this core were taken for the following analyses: porosity and organic C, N and S (Florian Scholz, GEOMAR), mercury (K. Gosnell and N. Torres), barium and silicon isotopes (Z. Zhang), chromium (D. Gilliard), Platinum (A. Koschinsky), and storage at GEOMAR for future analyses.
2) Samples for metal mineralogy (Brandy Toner, U. Minnesota) were collected by inserting head-cut 2 mL syringes into a core liner with predrilled holes. The sediment samples were directly transferred from the syringes into N_2 purged micro-centrifuge or Eppendorf tubes, and stored frozen in N_2 purged Mylar bags.
3) N. Glock conducted a survey of the living benthic community along the cruise transect, with a focus on benthic foraminifera. This survey covers the top cm of a core from each of the stations. These samples were wet sieved with surface water over a 125 µm mesh and the residue visually analysed under a stereo microscope within a few hours after retrieval of the sediment core. The main aim was to retrieve enough living specimens of monospecific benthic foraminifera to analyse their intracellular phosphate and nitrate storage. In addition, the top five cm of six cores with particularly flat and undisturbed surface were sliced at a one cm resolution. These samples are preserved in ethanol and stained with Rose Bengal for a detailed survey of the benthic foraminifera community at various distances from the hydrothermal field.

Porewater was extracted using Rhizon samplers from up to three additional cores with predrilled liners, when long enough cores with clear overlying water were retrieved. The cores were moved to a cold room (4ºC) shortly after retrieval, and allowed 1-2 hours to cool back to

near bottom water temperatures before sampling commenced. The Rhizon samplers were rinsed in advance with 3 mM HCl and milli-Q water, and soaked in milli-Q water for a few days before use. The overlying water was filtered using 0.2 µm PES filters for analyses, and the remaining overlying water was drained. Rhizon samplers were inserted and used from top to bottom. The first 1 mL was discarded, and the following samples were collected:

4) 5 mL were collected for the analyses of major elements (Z. Steiner), transition and trace elements (Z. Steiner), nutrients (analysed on-board), silicon and barium isotopes (Z. Zhang,), mercury (K. Gosnell and N. Torres, analysed on-board), chromium speciation (D. Gilliard), typically at a two cm resolution. After collection of the first 5 mL from all Rhizon samplers, another 5 mL were collected for analyses of platinum concentrations (A. Koschinsky) or as backup samples for the analyses of silicon isotopes.
5) 30 mL samples were collected at lower resolution (three cm) from a second core for analyses of ^{226}Ra concentrations (L. Viera). 1 mL from each of these samples was taken for analyses of trace and major elements to allow comparison with the higher resolution core.
6) Another 30 mL were collected from a third core in two of the stations for analyses of chromium isotopes at a three cm resolution (D. Gilliard). In these cases, the chromium speciation samples were collected from the chromium isotopes core and not from the first porewater core.

5.6.1 Living foraminiferal abundance

The top five cm of six cores, with particularly flat and undisturbed surface, were sliced at a one cm resolution. The sediment was preserved in ethanol that contained 2 g of Rose Bengal dye with a final ethanol concentration of ~70%/sample (Schönfeld, 2012). The samples cover a transect from close to the rainbow vent site (~200 m) until a distance of 41 km (Fig. 12.6). All stations were in water depths close to the plume between 2180 and 2508 m. After staining for at least 3-4 weeks, abundances and species composition of stained living foraminifera will be analysed within these samples. This will provide data about the influence of the active vent site and the plume on biodiversity and biomass of benthic meiofauna. In addition, foraminiferal assemblages characteristic of hydrothermal activity will be identified and used to reconstruct past hydrothermal activity in the paleorecord. The living stained foraminifera can also be used for calibration of foraminiferal trace element/Ca ratios, since pore and bottom-water concentrations of trace elements will be determined at the same sampling sites.

5.6.2 Porewater

5.6.2.1 Major and trace elements

Samples are stored in acid clean 5 mL PP vials and acidified by addition of 30 µL of concentrated ultra-pure HCl into each vial containing 3-5 mL of porewater solution. Samples for analyses of major element concentrations (Ca, Sr, Mg, K, S, Li) were diluted at a 1:82 ratio with 0.12 M ultra-pure HCl. Major element concentrations will be analysed at GEOMAR for their element to sodium ratios using a Varian 720 ICP-OES (Inductively Coupled Plasma Optical Emission Spectroscopy), using the sample-standard bracketing method described by Steiner et al. (2020). Trace element

concentrations will be analysed at GEOMAR using an Element 2 HR-ICP-MS (High Resolution Inductively Coupled Plasma Mass Spectrometry). For an initial survey of the trace element concentrations, samples were diluted 1:20 with 1 M double distilled HNO_3. Overlying water samples from six cores will be analysed both using the 1:20 dilution, and after isotope dilution and SeaFast separation of transition metals from the sea salt matrix, to cross calibrate between the methods.

5.6.2.2 Nutrients

The concentrations of SRP (soluble reactive phosphorous), nitrate + nitrite, nitrite and silicic acid were analysed on-board following 1:6 dilution with nutrient depleted surface water. The surface water was collected using the tow fish, and its nutrient concentrations were analysed along with the porewater samples for blank correction.

5.6.2.3 Silicon isotopes

Deposition of Fe/Mn oxyhydroxides near the hydrothermal vent field might promote active Si cycling and diagenetic reactions such as authigenic clay formation. Si adsorption onto Fe/Mn oxyhydroxides and incorporation into Fe-Si gels can create substantial Si isotopic fractionation, with lighter Si isotope (^{28}Si) being preferentially enriched in the solid phase (Delstanche et al., 2009; Zheng et al., 2016). The influence of hydrothermal activity on Si early diagenesis and authigenic clay formation can thus be tested using stable Si isotopes. For example, in the Guaymas Basin (Gulf of California), $\delta^{30}Si$ values in porewaters close to the hydrothermal vent field were found to be higher than those at other basin sites (Geilert et al., 2020).

During cruise M176/2, one of our goals was to determine the stable Si isotopes as well as stable Ba isotopes in sediments under the influences of the Rainbow non-buoyant hydrothermal plume in order to investigate early diagenesis of Si and Ba in both near field and far field sediments. A total of 9 stations of overlying-water/porewater samples, 10 stations of sediment samples and an extra 8 stations of surface sediment samples were taken for Si and Ba isotopes (Table 12.16). Overlying-water and porewater samples were stored in a cool room (4°C) and acidified within 12 hours after sampling, and transported to the laboratory at GEOMAR for further isotope analysis.

Silicon isotopic compositions ($\delta^{30}Si$) of overlying water and pore water samples will be measured using sample-standard bracketing and Mg doping technique on a Thermo Scientific Neptune Plus MC-ICP-MS at GEOMAR. Samples will be pre-concentrated prior to isotopic analysis using the Mg-induced co-precipitation (MAGIC) method, by adding 1 M NaOH to pH-neutral samples in two steps. Then the precipitates will be dissolved and purified from the sample matrix using cation-exchange chromatography. Finally, silicon isotope measurements will be performed at medium resolution on a Thermo Scientific Neptune Plus MC-ICP-MS at GEOMAR. Samples will be introduced into the plasma using an Apex desolvator. The samples, reference materials, and bracketing standard will be doped with Mg to correct for the mass bias. Each sample measurement of $\delta^{30}Si$ will be normalized to two “bracketing” standard measurements.

5.6.2.4 Barium isotopes

The barium isotopic composition ($\delta^{138}Ba$) of overlying water and pore water samples will be measured using a double spike technique on a Thermo Scientific Neptune Plus MC-ICP-MS at GEOMAR. A calibrated ^{130}Ba-^{135}Ba double spike will be added to all water samples. After equilibration overnight, Ba will be purified from the sample matrix using cation-exchange chromatography, twice. The purified sample solutions will be introduced as a dry aerosol into the plasma using an Aridus desolvator. A three-dimensional data reduction procedure will be used and each spiked sample measurement of $\delta^{138}Ba$ will be normalized to two "bracketing" spiked standard measurements.

5.6.2.5 Sediments and porewater platinum (Jacobs University Bremen)

Sediment samples were collected from 17 different locations and the samples were immediately frozen after collection until land-based analysis. We will apply a heated acid pressure-digestion approach and use an inductively coupled plasma-mass spectrometric (ICP-MS) method to determine the concentration of platinum (Pt).

Porewater samples were collected at three different sites and acidified with hydrochloric acid (HCl, ultrapure grade, Roth) to 0.015 mol/L and pH1.7. These samples were stored in a cool room at approx. 4°C until analysis in the home laboratory via ICP-MS to determine the dissolved concentration of Pt in porewaters.

Together with data on dissolved Pt derived from the TM clean CTD, we aim to study processes and fluxes of Pt in the hydrothermal plume and along the mixing gradient with seawater.

5.6.3 MUC video observations

Starting with station 8, the observations of the TV-MUC were recorded digitally. The plume was clearly visible as diffusive fog at stations closer to the vent site (Fig. 5.12). The video observations of the TV-MUC matched the turbidity signal of the CTD-casts at the same stations in water depth and intensity. The plume was typically visible between 2000 and 2200 m water depth.

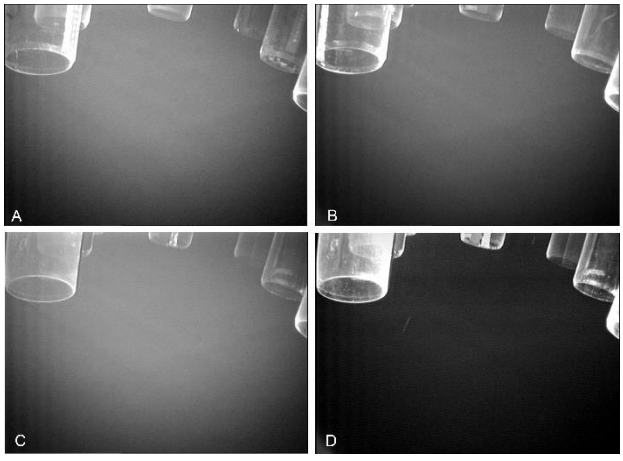

Fig. 5.12: Observations of the rainbow plume by the camera of the TV-MUC. A-C: Video observations of the plume maxima at stations 8 (A), 9 (B) and 12 (C). D: Video observation in the water column above the plume at station 12 (for control).

The abundance of macro- and megafauna, observed by the TV-MUC, apparently decreased with distance from the vent site in parallel with the intensity of the plume. Closer to the vent site we observed megafauna, possibly decapods, crawling relatively fast on the sediment (Fig. 5.13

A&B). Only at Station 10, we observed abundant rocks. These served as substrate for crinoids, possibly *Bourgueticrinida* spp. (Fig. 5.13 C&D).

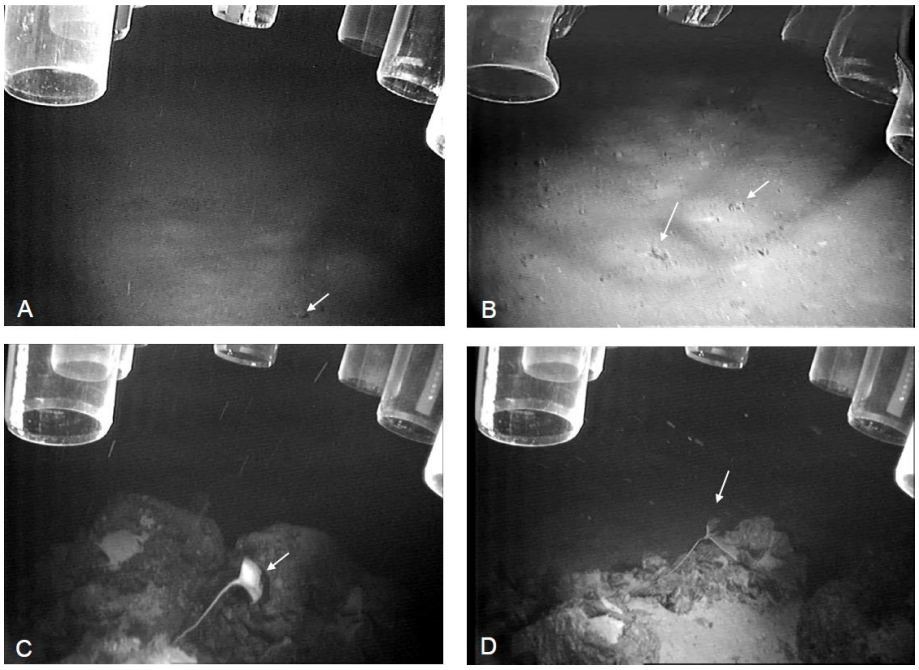

Fig. 5.13: Benthic megafauna observed by the TV-MUC. A&B: Mobile megafauna moving along the seafloor that might be decapods but are not clearly visible (Station 12). C&D Two examples for crinoids on rock substrate that might be *Bourgueticrinida* spp (Station 10).

On Station 10, the MUC hit a colony of siliceous sponges (demospongia, Fig. 5.14A-C). Microscopic needles of siliceous sponges were present in the >125 µm fraction of surface sediment samples from nearly every station. At several stations, smaller "fluffy" structures were visible and on Station 12, the MUC hit one larger colony of this structure (Fig. 5.14D). This colony likely belongs to a *Syringammina* sp., a large unicellular foraminifer species. A water sample was collected from this fluff layer using a Rhizon sampler.

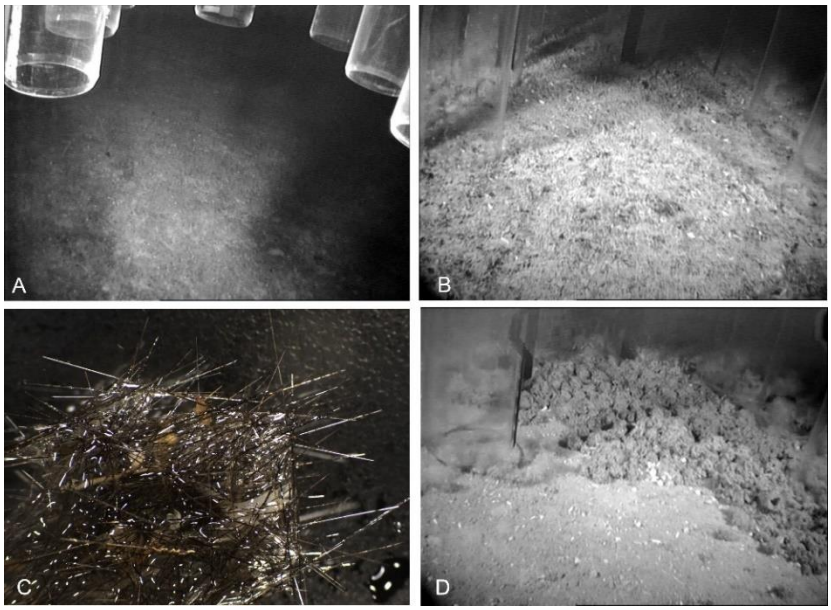

Fig. 5.14: Colonies of benthic megafauna observed by the TV-MUC. A&B: Large colonies of silicious sponges (demospongia) that have been hit at station 9. C: Microscope picture of material sampled from the siliceous sponge colony sampled at station 9. Silicious needles are clearly visible. D: Colony that likely belongs to *Syringammina* sp. (Station 12).

5.6.4 Description of the >125 µm fraction of surface sediments and living benthic foraminifera samples for intracellular nutrient analyses

(N. Glock[1])
[1] University of Hamburg

Surface sediments were wet sieved directly on-board using surface water over a 125 µm mesh. The >125 µm fraction was wet picked under the microscope within a few hours after sampling to identify and collect possible living specimens of benthic foraminifera for analyses of the intracellular nitrate and phosphate storage. Several benthic foraminiferal species from diverse habitats are known to store nitrate for denitrification (Pina-Ochoa et al. 2010) and the recent discovery of intracellular phosphate storage in benthic foraminifera from the Peruvian margin (Glock et al., 2020) gave additional evidence for the importance of these taxa to benthic nutrient cycling. Nevertheless, there are no data available, yet, about foraminiferal nutrient storage at hydrothermal vents or the bathyal Mid Atlantic Ridge.

The >125 µm fraction was composed mainly by planktic foraminifera (~99%) and in general very similar to sediments in the black smoker area of the East Pacific Rise described by Marchig et al. (1986). Benthic foraminifera were very rare. In total, 12 samples of monospecific benthic foraminifera have been collected with enough specimens for intracellular nutrient analyses. These were rinsed twice in nitrate and phosphate free artificial sea water, transported into 3 ml reverse osmosis water and crushed with a clean pipette tip. Afterwards, the samples were repeatedly frozen and thawed three times and finally sterile filtered according to the protocols by Glock et al. (2020).

Our general observations of the >125 µm fraction in the sediments indicate that the abundance of benthic foraminifera increases with distance from the vent site, in contrast to decreasing megafauna. Quantitative statements and conclusions can only be done after thorough analyses of the Rose Bengal samples to compare total abundances and biodiversity between the different stations. Agglutinated foraminifera were rare but apparently most abundant at stations 19 and 21. Siliceous sponge needles were present in traces in virtually every sample. Ostracodes were also present in traces. Foraminiferal tests were generally well preserved with no obvious signs of dissolution or strong diagenetic coating.

Most abundant benthic foraminifers belonged to *Cibicides spp.* with frequent appearances of *Cibicides robertsonianus* (Fig. 12.7A&B). Another frequent species was *Laticarinina pauperata* (Fig. 12.7C). In addition, we observed organic walled benthic foraminifera that inhabited shells of planktic foraminifera as described by Gooday et al. (2013) at most of the stations. Other observations of benthic meiofauna included a living nematode at station 14, and an unidentified, living invertebrate at station 19.

5.7 Aerosol sampling using high volume collector

(E. Achterberg[1])
[1] GEOMAR

We deployed one high volume aerosol collector (MCV CAV-A/Mb), which sampled the PM10 dry aerosol fraction during the cruise. The flowrate of the aerosol collectors was set to 60 m^3 h^{-1}. The collectors were placed on the monkey island of the vessel, and away from areas where personnel were smoking. The collectors switched off automatically during periods of unfavourable

wind directions, when stack contamination was a possibility. A windvane was attached to the collector to allow the directional sampling.

We employed Whatmann 41 filter (acid-cleaned, 203 mm x 254 mm) for trace elements and isotope sampling. Filters were changed every 48 h, and stored frozen (−20°C). A total of 10 filters each were collected during the cruise (with additional instrumental blanks). The sampling protocol followed the GEOTRACES recommendations.

5.8 Study of ammonium dynamics, pathways and its controlling factors

(J. Liu[1] and Q. Jia[1])

[1] GEOMAR

The aim in this study was to determine the ammonium dynamics, pathways and its controlling mechanism in North Atlantic Ocean by using a number of different techniques. Sampling of trace ammonium and in-situ incubation of ammonium uptake rate and nitrification rate were conducted to understand the ammonium dynamics and pathways. In addition, the role of trace metal (Fe) to ammonium pathways at DCM was assessed through Fe addition experiments to explore how N rate would response to different Fe conditions.

Sampling-Samples were collected at 17 stations during the cruise. Water samples were collected using trace-metal-clean Niskin-X bottles at six depths (ca. 10 m, 20 m, 30 m, 50 m, DCM, 120 m) from biology cast and at twelve depths from deep geochemical cast (Table 12.19-20. All the sampling for ammonium and ammonium-related incubations was conducted with ammonium-clean procedures.

Trace ammonium concentration- Sampling of trace ammonium was conducted for every depth at each station. All the ammonium samples measured on aboard. Sample were analysed using the fluorescence OPA batch method. The CTD cast details of sampling for ammonium at each station are summarized in Table 12.20.

Incubation for in-situ N rate- In-situ N rates were determined by the N15 labelling technique and conducted at 17 stations during the cruise (Table 12.19). N uptake rate was measured in 500 mL acid-cleaned Nalgene polycarbonate bottles. The bottles were rinsed with sample seawater 3 times and filled up to ca. 500 mL on deck. After addition of a N15-NH_4 or N15-NO_3 spike to final concentration of 50 nM, the bottle caps were tightly closed and all bottles quickly placed in a plastic bag into incubators with specific light levels. The filtration for N15-PN was conducted after 2-3 hours incubation and all GF/F filters were stored at -20℃ until the measurement with denitrification bacteria culture method and IRMS at Xiamen University (Table 12.19).

Nitrification rates were determined in 50 mL acid-cleaned Corning centrifuge tubes. Samples taken from surface and deep cast were spiked with 100 μL N15 enriched NH_4Cl to final concentration of 50 nM and incubated for 24 hours on deck with specific light levels and in the dark in a cooled room at 2℃, respectively. The filtration for N15-NO_3 was conducted with 60 mL syringe and 0.2 um filter unit after 24 hours incubation, and the filtrate was storage in -20℃ until the measurement with Gasbench-IRMS at GEOMAR (Table 12.19).

Fe/N limitation experiments at DCM-A total of 10 bioassay experiments at DCM were set up using acid-washed Nalgene polycarbonate bottles (1 L). Sampling was conducted directly from the Niskin bottles in the clean container and the bottles were placed in individual plastic bags and spiked in a laminar flow hood to prevent metal contamination.

Nutrient amendments were Fe, NO_3^-, and Fe+NO_3^-. The amended Fe and NO_3^- (chelexed and filter-sterilized) concentrations were 2 nM and 2 μM, respectively. Control bottles incubated with no nutrient addition were included with all experiments. All treatments were conducted in triplicate and incubated for 1~2 days in a screened on-deck incubator continuously flushed with underway surface seawater.

After nutrient amended incubation, uptake rates of ammonium, nitrate, and nitrification, and Chla, FRRf and flow cytometry were conducted in each treatment.

FRRf-As an indicator for Fe limitation of phytoplankton, a total of 256 FRRf samples from the shallow biology cast were measured on board (Table 12.19). 5ml samples were taken into measuring vials for FRRf measurements after at least half an hour in dark condition. For the blank correction, 5 mL filtered sample from each depth by using 5 mL syringe and 0.45 um filter unit was measured with Fast Ocean fluorescence detector.

6 Ship's Meteorological Station

(C. Rohleder[1])
[1] DWD

6.1 Weather for cruise M176/2

The research focus of expedition M176/2 was the investigation of the hydrothermal plume of a hot, submarine spring in the hydrothermal field called "Rainbow" on the Mid-Atlantic Ridge southwest of the Azores. The aim was to investigate the chemical and physical form in which trace metals from the source are transported and distributed in the water. For this purpose, mainly differently equipped CTDs were used. The use of CTDs is possible in almost any weather condition, therefore the mostly calm weather in the research area hardly played a role in the execution of the work.

6.2 Transit to the research area

On Wednesday, 01.09.2021 08:30, Research Vessel (RV) Meteor left the port of Emden and started its transit to the research area, which is about two thousand nautical miles away. An extensive high-pressure northwest of Scotland and its ridge extended south-eastward across the Alpine region while dominating the weather for the first days of the voyage. Under cloudy skies and rather weak northerly winds, RV Meteor passed Borkum and sailed towards the English Channel. The wind freshened noticeably for a short time.

While on its way through the English Channel, the ship found itself under the influence of the high now centred over Scotland and another, almost stationary high-pressure centre over the Iberian Peninsula. From the west, a low-pressure zone was approaching with several low centres. Leaving the English Channel during the 03.09.2021, RV Meteor slowly entered the above-mentioned area of low-pressure zone. Towards the evening of 04.09.2021, and in the following night, the wind increased noticeably (6-7 Bft), accompanied by several showers. The former high pressure over Scotland meanwhile moved to southern Sweden, forming a ridge extending over the British Isles and thus preventing the low-pressure area over the North Atlantic from moving rapidly eastward. At the same time, a depression instead moved slowly south-southeast to the coast of Portugal, and RV Meteor's track ran from the east side of this depression close to its core. This resulted in weak, variable winds on 05.09.2021 and for a short time there was even no wind.

Meanwhile, a high-pressure system west of the Azores weakened temporarily with the consequence of a low-pressure trough from an Iceland low crossing the archipelago with showers. RV Meteor reached the affected area in the night of 08.09.2021, light showers were experienced over the ship.

On the following night, RV Meteor reached the research area southwest of the Azores. A trough formed from a low over Ireland, which pushed south-eastward while weakening. An embedded, small-scale low brought RV Meteor light showers at the beginning of the research in the early morning hours of 09.09.2021.

6.3 Research work to the southwest of the Azores

The research area of this voyage was in the vicinity of 36.3N 33.8W. It was planned to work in for the next twenty days. At the beginning of the work, a low was located about 700 nautical miles north of the Azores, an associated trough line crossed the area from the north with showers on the rear site the research area got under the influence of a near stationary high to the west. This resulted in northerly, mostly moderate to fresh winds persisting for several days. Occasional showers occurred close to the ship.

In the following days, the high slowly moved eastward over the research area while weakening. At the same time, a low-pressure trough pushed north-eastward of the high, another one followed the night from 15.09. to 16.09.2021. The moist and unstable air brought within a north-westerly flow some showers into the working area. In the wake of these troughs a new high moved east-south-eastward from Nova Scotia and RV Meteor was at its southern flank on 17.09.2021. At the same time, an upper air feature embedded in the high approached the working area. It reached the ship in the night of 18.09.2021 and weather lightning was observed. Subsequently, the high pressure strengthened, with its core now north of the Azores. The winds shifted to southerly directions persisting for several days.

In addition, the high with its ridge reaching the southwest of the Azores blocked the displacement of the storm low "Ex-Odette", which has moved along the North American coast to Newfoundland. On 23.09.2021 its cold front slowly moved over the research area causing heavy rain (21.4 l/sqm in 6h). In the wake of the front, showers and thunderstorms intensified during the following night.

Meanwhile, another storm depression ("Ex-Rose") approached from the southwest which was embedded in the trough of "Ex-Odette". It slowly moved southeast of the research area. North of this low-pressure trough a ridge of a high extended southeast of Newfoundland into the sea area north of the Azores from September 26, 2021. Between these pressure areas, the wind freshened up quite strongly. On the last working day (27.09.2021), the ridge extended into the working area and developed an independent high northeast of the Azores during the beginning transit to Emden.

The precise positioning of the ship at the individual stations had to be carried out without the support of the defective bow thruster. The orientation of the ship was done by hand steering and was based on the wind direction. This often resulted in the swell hitting the ship from aside, causing the ship to roll violently despite the low significant wave heights - rarely more than one to two meters. This caused very difficult conditions for launching and recovering of the equipment.

6.4 Transit to Emden

During the first days of the transit of the Meteor to Emden, the ship passed through the high northeast of the Azores. For the transit an average speed of 10 knots was assumed. Due to heavy weather expected west of the British Isles into the Bay of Biscay the following weekend, it was decided on Sept. 28, 2021, to increase the speed to about 12 knots.

From 30.09.2021, Meteor gradually was influenced by the storm system located between the Irminger Sea and the British Isles. The centre of the low-pressure system was located about 300 nautical miles northwest of the Hebrides, and an associated low-pressure trough entered the area with clouds and some showers.

While the centre of the low moved to the sea area north of the British Isles, a secondary low developed on its southern flank, which passed the course of the Meteor on 02.10.2021. Heavy precipitation was experienced. Between 07 and 08 UTC the ship was close to the low, the wind had been blowing at 5 Bft from southerly directions, stopped almost completely for a short time while the core crossed and resumed up to 7 Bft from northerly directions later. Shortly thereafter, the heavy rain also subsided. According to the ship's rain gauge, 61.5 l/sqm of rain fell in the period from 06 to 12 UTC.

RV meteor continued through the English Channel, the secondary low moved northward to the Shetland Islands and later into the Norwegian Sea. On 04.10.2021, an associated trough extended southward over Ireland and slowly moved eastward. In this trough, a new low formed, RV Meteor was located at the eastern exit of the English Channel. The wind turned to southerly directions and persisted with strength (6-7 Bft, gusts up to 8 Bft) until reaching Borkum in the morning of 05.10.2021.

On the way down to Emden the wind decreased significantly. With wind from SW with 4-5 Bft RV Meteor reached the harbour on the 05th about 04 p.m. and ended the expedition M176-2.

7 Station List M176/2

7.1 Overall Station List

ISP= in situ pumps. CTD used: METEOR stainless steel CTD (METEOR CTD), GEOMAR Physical Oceanography Stainless steel CTD (CTD GEOMAR), and GEOMAR Ultra Clean Titanium CTD (CTD Ultra Clean).

Station	Date / Time UTC 2021	Device	Latitude N	Longitude W	Max Depth (m)	Comments
M176/2_1-1	04/09 07:23	Towfish	47° 32,685'	011° 51,631'	4644	Test Station,
M176/2_1-1	04/09 07:27	Towfish	47° 32,623'	011° 51,665'	4648	
M176/2_1-2	04/09 08:48	CTD Ultra Clean	47° 31,652'	011° 52,972'	4676	Test Station GEOMAR winch
M176/2_1-3	04/09 10:03	CTD METEOR	47° 31,587'	011° 53,381'	4679	Test Station
M176/2_1-4	04/09 10:44	CTD Ultra Clean	47° 31,782'	011° 53,987'	4679	Test Station, GEOMAR winch
M176/2_1-5	04/09 11:16	Towfish	47° 31,830'	011° 54,593'	4684	
M176/2_1-5	06/09 07:33	Towfish	43° 31,579'	021° 41,287'	3280	
M176/2_1-5	06/09 08:45	Towfish	43° 25,660'	021° 54,806'	3808	
M176/2_1-5	06/09 15:19	Towfish	42° 44,240'	023° 16,380'	3607	
M176/2_0_UW-3	04/09 13:15	P-70 Parasound	47° 22,197'	012° 17,136'	4744	
M176/2_0_UW-3	07/09 02:25	P-70 Parasound	41° 45,766'	025° 07,756'	3545	
M176/2_0_UW-3	08/09 21:32	P-70 Parasound	36° 33,135'	033° 27,038'	2530	
M176/2_0_UW-2	04/09 13:15	Multibeam	47° 22,192'	012° 17,154'	4744	
M176/2_0_UW-2	07/09 02:25	Multibeam	41° 45,751'	025° 07,780'	3545	
M176/2_0_UW-2	08/09 21:32	Multibeam	36° 33,145'	033° 27,023'	2416	
M176/2_0_UW-1	04/09 13:15	ADCP	47° 22,163'	012° 17,250'	4743	
M176/2_0_UW-1	07/09 02:25	ADCP	41° 45,742'	025° 07,794'	3545	
M176/2_0_UW-1	08/09 21:32	ADCP	36° 33,073'	033° 27,132'	2461	
M176/2_2-1	06/09 15:27	CTD Ultra Clean	42° 44,280'	023° 16,454'	3609	GEOMAR winch
M176/2_2-2	06/09 15:59	CTD METEOR	42° 44,272'	023° 16,568'	3606	W2,
M176/2_2-3	06/09 16:35	CTD Ultra Clean	42° 44,288'	023° 16,437'	3608	GEOMAR winch
M176/2_2-4	06/09 17:00	Towfish	42° 44,340'	023° 16,599'	3608	
M176/2_2-4	07/09 01:51	Towfish	41° 47,931'	025° 04,552'	3598	
M176/2_3-1	09/09 00:36	CTD GEOMAR Tow Yo	36° 14,383'	033° 53,362'	2174	W2, Posidonia
M176/2_3-2	09/09 01:45	Towfish	36° 14,332'	033° 53,593'	2306	
M176/2_3-2	09/09 01:52	Towfish	36° 14,226'	033° 53,682'	2303	Abbruch
M176/2_3-3	09/09 06:26	CTD Ultra Clean	36° 13,417'	033° 54,794'	2649	GEOMAR winch
M176/2_3-4	09/09 09:01	CTD GEOMAR isp	36° 13,454'	033° 54,826'	2679	W2, mit ISP
M176/2_3-5	09/09 14:08	Video Multi Corer	36° 13,450'	033° 54,735'	2609	W12
M176/2_3-6	09/09 16:53	CTD METEOR	36° 13,489'	033° 54,828'	2631	W3,
M176/2_3-8	09/09 17:58	CTD Ultra Clean	36° 13,475'	033° 55,077'	2659	GEOMAR winch

M176/2_3-9	09/09 18:32	Towfish	36° 13,883'	033° 55,193'	2786	
M176/2_3-9	09/09 21:32	Towfish	36° 18,440'	033° 50,933'	2885	
M176/2_4-1	09/09 22:15	CTD GEOMAR Tow Yo	36° 13,278'	033° 53,411'	2027	W2, Posidonia
M176/2_4-2	10/09 05:48	CTD Ultra Clean	36° 14,235'	033° 53,831'	2340	GEOMAR winch
M176/2_4-3	10/09 08:20	CTD GEOMAR isp	36° 14,249'	033° 53,912'	2380	W2, mit ISP
M176/2_4-4	10/09 13:26	Video Multi Corer	36° 14,194'	033° 53,866'	2502	W12
M176/2_4-5	10/09 17:43	CTD Ultra Clean	36° 14,211'	033° 53,848'	2353	GEOMAR winch
M176/2_4-6	10/09 18:17	Towfish	36° 14,319'	033° 54,040'	2494	
M176/2_4-6	10/09 23:22	Towfish	36° 14,436'	033° 54,717'	2614	
M176/2_5-1	10/09 23:45	CTD GEOMAR Tow Yo	36° 14,052'	033° 54,968'	2677	W2, Posidonia
M176/2_5-2	11/09 06:00	CTD Ultra Clean	36° 13,783'	033° 54,182'	2332	GEOMAR winch
M176/2_5-3	11/09 08:19	CTD GEOMAR isp	36° 13,808'	033° 54,399'	2427	W2, mit ISP
M176/2_5-4	11/09 13:12	CTD METEOR	36° 13,820'	033° 54,104'	2283	W3,
M176/2_5-5	11/09 14:44	CTD Ultra Clean	36° 13,763'	033° 54,174'	2308	GEOMAR winch
M176/2_5-6	11/09 15:32	Grab	36° 13,779'	033° 54,093'	2267	W3
M176/2_6-1	11/09 18:24	CTD GEOMAR Tow Yo	36° 13,428'	033° 53,235'	1989	W2, Posidonia
M176/2_6-2	12/09 02:07	Towfish	36° 16,895'	033° 55,494'	2224	
M176/2_6-2	12/09 05:13	Towfish	36° 14,927'	033° 52,809'	2220	
M176/2_6-3	12/09 05:48	CTD Ultra Clean	36° 15,065'	033° 52,968'	2339	GEOMAR winch
M176/2_6-4	12/09 08:33	CTD GEOMAR isp	36° 15,076'	033° 52,879'	2321	W2, mit ISP
M176/2_6-5	12/09 13:29	CTD METEOR	36° 15,020'	033° 52,943'	2419	W3,
M176/2_6-6	12/09 14:28	CTD Ultra Clean	36° 15,066'	033° 52,941'	2476	GEOMAR winch
M176/2_6-7	12/09 15:32	Video Multi Corer	36° 15,122'	033° 52,874'	2408	W12, Posidonia
M176/2_7-1	12/09 18:13	CTD GEOMAR Tow Yo	36° 12,733'	033° 53,736'	2186	W2, Posidonia
M176/2_7-2	13/09 05:32	CTD Ultra Clean	36° 13,836'	033° 54,159'	2337	GEOMAR winch
M176/2_7-3	13/09 08:26	CTD GEOMAR isp	36° 13,862'	033° 54,030'	2289	W2, ISP, Posidonia
M176/2_7-4	13/09 13:26	CTD METEOR	36° 13,827'	033° 54,135'	2299	W3, Posidonia
M176/2_7-5	13/09 15:54	CTD Ultra Clean	36° 13,825'	033° 54,113'	2300	GEOMAR winch
M176/2_7-6	13/09 16:36	Video Multi Corer	36° 13,913'	033° 54,176'	2357	W12, Posidonia
M176/2_8-1	13/09 19:33	CTD GEOMAR Tow YO	36° 14,652'	033° 52,272'	2053	W2, Posidonia
M176/2_8-2	14/09 01:21	Towfish	36° 16,368'	033° 54,882'	2541	
M176/2_8-2	14/09 05:18	Towfish	36° 14,065'	033° 54,180'	2436	
M176/2_8-3	14/09 05:43	CTD Ultra Clean	36° 14,076'	033° 53,979'	2271	GEOMAR winch
M176/2_8-4	14/09 08:25	CTD GEOMAR	36° 14,022'	033° 53,973'	2288	W2, Posidonia
M176/2_8-5	14/09 10:42	CTD METEOR	36° 14,093'	033° 53,954'	2293	W3, Posidonia
M176/2_8-6	14/09 14:18	CTD Ultra Clean	36° 14,078'	033° 53,966'	2358	GEOMAR winch
M176/2_8-7	14/09 14:59	Video Multi Corer	36° 14,069'	033° 53,967'	2283	W12, Posidonia

M176/2_8-8	14/09 17:07	CTD METEOR	36° 14,072'	033° 53,946'	2288	W3, Posidonia
M176/2_9-1	14/09 19:18	CTD GEOMAR Tow Yo	36° 13,818'	033° 53,026'	2063	W2, Posidonia
M176/2_9-2	15/09 05:41	CTD Ultra Clean	36° 16,556'	033° 53,710'	2512	GEOMAR winch
M176/2_9-3	15/09 08:28	CTD GEOMAR	36° 16,576'	033° 53,765'	2521	W2, Posidonia
M176/2_9-4	15/09 10:59	CTD METEOR	36° 16,450'	033° 53,825'	2497	W3, Posidonia
M176/2_9-5	15/09 13:09	Video Multi Corer	36° 16,559'	033° 53,696'	2507	W12, Posidonia
M176/2_9-6	15/09 15:42	CTD Ultra Clean	36° 16,559'	033° 53,701'	2509	GEOMAR winch
M176/2_9-7	15/09 16:18	CTD METEOR	36° 16,524'	033° 53,693'	2507	W3, Posidonia
M176/2_10-1	15/09 18:25	CTD GEOMAR Tow YO	36° 15,513'	033° 52,621'	2343	W2, Posidonia
M176/2_10-2	16/09 02:27	Towfish	36° 10,558'	033° 44,215'	1624	
M176/2_10-2	16/09 05:23	Towfish	36° 18,506'	033° 51,219'	2780	
M176/2_10-3	16/09 06:00	CTD Ultra Clean	36° 16,693'	033° 51,300'	2688	GEOMAR winch
M176/2_10-4	16/09 08:52	CTD GEOMAR	36° 16,676'	033° 51,261'	2663	W2, Posidonia
M176/2_10-5	16/09 11:11	CTD METEOR	36° 16,734'	033° 51,246'	2704	W3, Posidonia
M176/2_10-6	16/09 13:23	Video Multi Corer	36° 16,697'	033° 51,266'	2697	W12, Posidonia
M176/2_10-7	16/09 15:49	CTD Ultra Clean	36° 16,683'	033° 51,299'	2676	GEOMAR winch
M176/2_10-8	16/09 16:41	CTD METEOR	36° 16,676'	033° 51,313'	2659	W2, Posidonia
M176/2_11-1	16/09 19:09	CTD METEOR	36° 13,860'	033° 54,175'	2320	W3, Posidonia
M176/2_11-2	16/09 21:25	CTD GEOMAR To Yo	36° 14,244'	033° 54,873'	2655	W2, Posidonia
M176/2_11-3	17/09 02:54	CTD METEOR	36° 13,798'	033° 54,123'	2305	W2, Posidonia
M176/2_12-1	17/09 05:34	CTD Ultra Clean	36° 14,799'	033° 53,839'	2419	GEOMAR winch
M176/2_12-2	17/09 08:17	CTD GEOMAR	36° 14,832'	033° 53,858'	2419	W2, Posidonia
M176/2_12-3	17/09 10:17	CTD METEOR	36° 14,719'	033° 53,811'	2416	W3, Posidonia
M176/2_12-4	17/09 12:13	Video Multi Corer	36° 14,786'	033° 53,888'	2418	W12, Posidonia
M176/2_12-5	17/09 15:35	CTD Ultra Clean	36° 14,776'	033° 53,796'	2417	GEOMAR winch
M176/2_12-6	17/09 16:09	CTD METEOR	36° 14,780'	033° 53,864'	2419	W3, Posidonia
M176/2_13-1	17/09 18:25	CTD GEOMAR Tow Yo	36° 14,120'	033° 51,977'	2127	W2, Posidonia
M176/2_13-2	18/09 02:31	Towfish	36° 16,270'	033° 48,448'	2775	
M176/2_13-2	18/09 05:12	Towfish	36° 18,189'	033° 47,369'	2944	
M176/2_13-3	18/09 06:05	CTD Ultra Clean	36° 15,518'	033° 50,216'	2692	GEOMAR winch
M176/2_13-4	18/09 08:51	CTD GEOMAR	36° 15,490'	033° 50,183'	2654	W2, Posidonia
M176/2_13-5	18/09 10:56	CTD METEOR	36° 15,527'	033° 50,154'	2628	W3, Posidonia
M176/2_13-6	18/09 12:49	Video Multi Corer	36° 15,474'	033° 50,186'	2569	W12, Posidonia
M176/2_13-7	18/09 15:06	CTD METEOR	36° 15,516'	033° 50,157'	2641	W3, Posidonia
M176/2_13-8	18/09 16:48	CTD Ultra Clean	36° 15,495'	033° 50,181'	2618	GEOMAR winch
M176/2_14-1	18/09 18:05	CTD GEOMAR Tow Yo	36° 11,721'	033° 48,540'	2434	W2, Posidonia
M176/2_14-2	19/09 00:09	Towfish	36° 14,557'	033° 47,595'	2990	

M176/2_14-2	19/09 02:03	Towfish	36° 07,553'	033° 48,798'	1848	
M176/2_14-3	19/09 05:37	CTD Ultra Clean	36° 14,222'	033° 50,062'	2722	GEOMAR winch
M176/2_14-4	19/09 08:21	CTD GEOMAR	36° 14,212'	033° 50,026'	2665	W2, Posidonia
M176/2_14-5	19/09 10:27	CTD METEOR	36° 14,207'	033° 50,071'	2664	W3, Posidonia
M176/2_14-6	19/09 12:14	Video Multi Corer	36° 14,205'	033° 50,027'	2690	W12, Posidonia
M176/2_14-7	19/09 14:58	CTD Ultra Clean	36° 14,175'	033° 50,007'	2712	GEOMAR winch
M176/2_14-8	19/09 15:36	CTD METEOR	36° 14,190'	033° 50,081'	2666	W3, Posidonia
M176/2_15-1	19/09 17:58	CTD GEOMAR Tow Yo	36° 15,032'	033° 51,998'	2117	W2, Posidonia
M176/2_15-2	19/09 23:24	Towfish	36° 17,630'	033° 55,299'	2055	
M176/2_15-2	20/09 05:23	Towfish	36° 13,439'	033° 48,933'	2934	
M176/2_15-3	20/09 05:53	CTD Ultra Clean	36° 13,510'	033° 48,380'	2953	GEOMAR winch
M176/2_15-4	20/09 09:50	CTD METEOR	36° 13,345'	033° 48,254'	2905	W3, Posidonia
M176/2_15-5	20/09 12:15	Video Multi Corer	36° 13,374'	033° 48,469'	2900	W12, Posidonia
M176/2_15-6	20/09 14:43	CTD METEOR	36° 13,516'	033° 48,392'	3078	W3, Posidonia
M176/2_15-7	20/09 16:30	CTD Ultra Clean	36° 13,491'	033° 48,357'	3249	GEOMAR winch
M176/2_15-8	20/09 17:03	CTD METEOR	36° 13,527'	033° 48,353'	3236	W3, Posidonia
M176/2_16-1	21/09 05:48	CTD Ultra Clean	36° 13,189'	033° 47,159'	3065	GEOMAR winch
M176/2_16-2	21/09 08:27	CTD METEOR	36° 13,211'	033° 47,181'	3064	W3, Posidonia
M176/2_16-3	21/09 11:04	CTD METEOR	36° 13,169'	033° 47,165'	3040	W3, Posidonia
M176/2_16-4	21/09 12:53	Video Multi Corer	36° 13,204'	033° 47,145'	3065	W12, Posidonia
M176/2_16-5	21/09 15:14	CTD METEOR	36° 13,213'	033° 47,145'	3065	W3, Posidonia
M176/2_16-6	21/09 16:59	CTD Ultra Clean	36° 13,182'	033° 47,148'	3061	GEOMAR winch
M176/2_17-1	21/09 19:05	Towfish	36° 12,608'	033° 46,139'	2675	
M176/2_17-1	22/09 01:36	Towfish	36° 07,542'	033° 49,634'	2102	
M176/2_17-2	22/09 05:41	CTD Ultra Clean	36° 13,964'	033° 43,957'	2880	GEOMAR winch
M176/2_17-3	22/09 08:50	CTD GEOMAR	36° 14,032'	033° 43,891'	2814	W2, Posidonia
M176/2_17-4	22/09 11:02	CTD METEOR	36° 13,941'	033° 43,896'	2458	W3, Posidonia
M176/2_17-5	22/09 13:09	Video Multi Corer	36° 13,977'	033° 43,938'	2623	W12, Posidonia
M176/2_17-6	22/09 15:51	CTD Ultra Clean	36° 13,983'	033° 43,924'	2715	GEOMAR winch
M176/2_17-7	22/09 16:35	CTD METEOR	36° 13,987'	033° 43,859'	2778	W3, Posidonia
M176/2_17-8	22/09 19:24	Video Multi Corer	36° 14,064'	033° 43,812'	2941	W12, Posidonia
M176/2_18-1	23/09 05:41	CTD METEOR	36° 16,146'	033° 43,979'	2749	W3, Posidonia
M176/2_18-2	23/09 07:55	CTD Ultra Clean	36° 16,149'	033° 44,022'	2750	GEOMAR winch
M176/2_18-3	23/09 10:54	CTD METEOR	36° 16,184'	033° 43,973'	2750	W3, Posidonia
M176/2_18-4	23/09 12:44	Video Multi Corer	36° 16,236'	033° 44,098'	3052	W12, Posidonia
M176/2_18-5	23/09 13:37	CTD GEOMAR	36° 16,174'	033° 44,013'	2749	W2, Posidonia
M176/2_18-6	23/09 17:07	CTD Ultra Clean	36° 16,177'	033° 43,985'	2751	GEOMAR winch

M176/2_19-1	23/09 20:00	Towfish	36° 16,054'	033° 43,760'	2760	
M176/2_19-1	24/09 05:26	Towfish	36° 19,634'	033° 40,588'	2510	
M176/2_19-2	24/09 05:46	CTD Ultra Clean	36° 19,628'	033° 40,706'	2505	GEOMAR winch
M176/2_19-3	24/09 08:35	CTD GEOMAR	36° 19,616'	033° 40,636'	2509	W2, Posidonia
M176/2_19-4	24/09 10:44	CTD METEOR	36° 19,688'	033° 40,686'	2508	W3, Posidonia
M176/2_19-5	24/09 12:35	Video Multi Corer	36° 19,601'	033° 40,675'	2510	W12, Posidonia
M176/2_19-6	24/09 14:37	CTD Ultra Clean	36° 19,654'	033° 40,682'	2507	GEOMAR winch
M176/2_19-7	24/09 15:08	CTD METEOR	36° 19,728'	033° 40,757'	2506	W3, Posidonia
M176/2_20-1	24/09 17:01	Towfish	36° 19,616'	033° 40,631'	2509	
M176/2_20-1	24/09 18:15	Towfish	36° 14,345'	033° 53,246'	2167	
M176/2_20-2	24/09 18:34	CTD Ultra Clean	36° 13,871'	033° 54,158'	2319	GEOMAR winch
M176/2_21-1	24/09 23:29	CTD GEOMAR Tow Yo	36° 22,956'	033° 42,292'	2742	W2, Posidonia
M176/2_21-2	25/09 06:08	CTD Ultra Clean	36° 23,193'	033° 37,578'	2310	GEOMAR winch
M176/2_21-3	25/09 08:48	CTD GEOMAR	36° 23,258'	033° 37,639'	2306	W2, Posidonia
M176/2_21-4	25/09 10:46	CTD METEOR	36° 23,261'	033° 37,597'	2305	W3, Posidonia
M176/2_21-5	25/09 12:33	Video Multi Corer	36° 23,267'	033° 37,587'	2304	W12, Posidonia
M176/2_21-6	25/09 14:21	CTD Ultra Clean	36° 23,226'	033° 37,554'	2311	GEOMAR winch
M176/2_21-7	25/09 14:52	CTD METEOR	36° 23,235'	033° 37,536'	2310	W3, Posidonia
M176/2_22-1	25/09 18:35	CTD GEOMAR Tow YO	36° 12,781'	033° 43,223'	1911	W2, Posidonia
M176/2_22-2	26/09 02:20	Towfish	36° 15,418'	033° 45,920'	2678	
M176/2_22-2	26/09 05:09	Towfish	36° 28,619'	033° 35,255'	2320	
M176/2_23-1	26/09 05:33	CTD Ultra Clean	36° 29,486'	033° 34,734'	2179	GEOMAR winch
M176/2_23-2	26/09 08:01	CTD GEOMAR	36° 29,455'	033° 34,736'	2178	W2, Posidonia
M176/2_23-3	26/09 09:46	CTD METEOR	36° 29,425'	033° 34,755'	2201	W3, Posidonia
M176/2_23-4	26/09 11:26	Video Multi Corer	36° 29,438'	033° 34,651'	2184	W12, Posidonia
M176/2_23-5	26/09 13:30	CTD Ultra Clean	36° 29,519'	033° 34,778'	2178	GEOMAR winch
M176/2_23-6	26/09 14:04	CTD METEOR	36° 29,476'	033° 34,780'	2175	W3, Posidonia
M176/2_23-7	26/09 15:50	Towfish	36° 30,032'	033° 35,523'	2438	
M176/2_23-7	26/09 18:00	Towfish	36° 32,251'	033° 35,605'	2764	
M176/2_24-1	26/09 19:00	CTD GEOMAR Tow Yo	36° 33,429'	033° 31,408'	1806	W2, Posidonia
M176/2_24-2	27/09 06:01	CTD Ultra Clean	36° 33,390'	033° 34,643'	2940	GEOMAR winch
M176/2_24-3	27/09 09:13	CTD GEOMAR	36° 33,405'	033° 34,626'	2933	W2, Posidonia
M176/2_24-4	27/09 11:37	CTD METEOR	36° 33,316'	033° 34,649'	2933	W3, Posidonia
M176/2_24-5	27/09 13:37	Video Multi Corer	36° 33,351'	033° 34,672'	2937	W12, Posidonia
M176/2_24-6	27/09 16:08	CTD Ultra Clean	36° 33,430'	033° 34,882'	3017	GEOMAR winch
M176/2_24-7	27/09 17:02	CTD METEOR	36° 32,912'	033° 33,644'	2413	W3, Posidonia

8 Data and Sample Storage and Availability

A cruise summary report (CSR) has been compiled and submitted to DOD (Deutsches Ozeanographisches Datenzentrum), BSH, Hamburg, immediately after the cruise. The cruise was performed in international waters and therefore the CSR does not have to be submitted to any other country.
All hydrographic data acquired during the cruise are transferred to BSH, and also stored at the GEOTRACES data base at BODC, Liverpool, U.K., and will be made available to the PANGAEA data base. All trace metal and isotope data to be acquired will also be fed into these data bases and will be made publicly available within 3 years after cruise end (4rd quarter of 2024). All water and particulate and sediment samples are stored at the respective laboratories, where the measurements will be carried out. The Kiel Data Management Team (KDMT) provides an information and data archival system where metadata of the onboard DSHIP-System are collected and are made publicly available. This Ocean Science Information System (OSIS-Kiel) is accessible for all project participants and can be used to share and edit field information (https://portal.geomar.de/metadata/).
Availability of metadata in OSIS, 2 weeks after completion of the cruise and related experiments.
Availability of data in OSIS (https://portal.geomar.de/osis): 6 months after completion of the cruise and related experiments.

Table 8.1 lists the target data bases, tentative availability times and responsible scientists.

Hydrography - CTD and ADCP and multibeam data are held at DAM and GEOMAR Helmholtz Centre for Ocean Research Kiel and are publicly available immediately after cruise (responsible: Prof. E. Achterberg).
Dissolved trace metals - samples and data are held at GEOMAR, Kiel (responsible: Prof. E. Achterberg).
Particulate trace metals - samples and data are held at GEOMAR, Kiel (responsible: Prof. E. Achterberg).
Sediment and porewater - samples and data are held at GEOMAR, Kiel (responsible: Dr. Z Steiner).
Trace element and isotopes (REE, Ba) - samples and data are held at GEOMAR, Kiel (responsible: Prof. M. Frank).
Stable Fe isotopes - samples and data are held at GEOMAR, Kiel (responsible: Prof. E. Achterberg).
Radium isotopes - samples and data are held at the Institut für Geowissenschaften, Christian Albrechts Universität Kiel (responsible Dr. J. Scholten).
High Field Strength Elements and trace element speciation – samples and data are held at the Jacobs University Bremen (responsible Prof. A. Koschinsky).
Phytoplankton/productivity – samples and data are held at GEOMAR, Kiel (responsible Dr. T. Browning).
Nitrogen cycling and fixation - samples and data are held at GEOMAR (responsible Dr. T. Browning).
Nutrients, DOC, DOC, alkalinity, carbon cycle - samples and data are held at GEOMAR, Kiel (responsible Prof. E. Achterberg).

Table 8.1 Overview of data availability

Type	Database	Available	Contact
Hydrography	BODC/PANGAEA	Dec. 2021	eachterberg@geomar.de
Nutrients	BODC/PANGAEA	October 2024	eachterberg@geomar.de
Dissolved trace metals	BODC/PANGAEA	October 2024	eachterberg@geomar.de
Particulate trace metals	BODC/PANGAEA	October 2024	eachterberg@geomar.de
High field strength elements / metal speciation	BODC/PANGAEA	October 2024	a.koschinsky@jacobs-university.de
REEs and Ba isotopes	BODC/PANGAEA	October 2024	mfrank@geomar.de
Stable Fe isotopes	BODC/PANGAEA	October 2024	eachterberg@geomar.de
Radium isotopes	BODC/PANGAEA	October 2024	js@gpi.uni-kiel.de
Nitrogen cycing and fixation	BODC/PANGAEA	October 2024	tbrowning@geomar.de
Phytoplankton/productivity	BODC/PANGAEA	October 2024	tbrowning@geomar.de
Carbonate chemistry, DOC	BODC/PANGAEA	October 2024	eachterberg@geomar.de
Sediment and porewater	BODC/PANGAEA	October 2024	zsteiner@geomar.de

9 Acknowledgements

All the members of the RainbowPlume team are very grateful to the Deutsche Forschungs Gemeinschaft (DFG), the German Research Fleet Coordination Centre at the Universität Hamburg, the shipping company BRIESE RESEARCH and LPL Projects + Logistics GmbH for providing their outstanding support to science and ship logistics, which made this cruise possible. We thank DFG and GEOMAR for funding this cruise. The careful managing of the COVID situation by the Leitstelle and GEOMAR was outstanding, and allowed us to conduct our successful cruise. We also like to sincerely thank the captain, officers and crew on the METEOR who did a fantastic job at facilitating our research and making our life as pleasant as possible on board.

10 References

Bennett, S. A., Achterberg, E. P., Connelly, D. P. and German, C. R. (2008). The distribution and stabilisation of dissolved Fe in deep-sea hydrothermal plumes. Earth Planet. Sci. Lett. 270(3-4), 157-167.

Berner, R.A. (2004). A model for calcium, magnesium and sulfate in seawater over Phanerozoic time. Am. J. Sci. 304(5), 438-453.

Bowman, K. L., Hammerschmidt, C. R., Lamborg, C. H. and Swarr G., (2015). Mercury in the North Atlantic Ocean: The U.S. GEOTRACES zonal and meridional sections. Deep Sea Res. Part II Top. Stud. Oceanogr. 116, 251-261,

Broecker, W.S. and Peng, T.-H., (1982). Tracers in the sea. The Lamont-Doherty Geological Observatory, Palisades, NY.

Browning, T. J., Achterberg, E. P., Engel, A. and Mawji, E. (2021). Manganese co-limitation of phytoplankton growth and major nutrient drawdown in the Southern Ocean. Nat. Commun. 12, 1–9.

Browning, T.J., Achterberg, E.P., Rapp, I., Engel, A., Bertrand, E.M., Tagliabue, A. and Moore, C.M. (2017). Nutrient co-limitation at the boundary of an oceanic gyre. Nature 551, 242-246.

Buck, K.N., Moffet, J., Barbeau, K.A., Bundy, R.M., Kodo, Y., and Wu, J. (2012). The organic complexation of iron and copper: an intercomparison of competitive ligand exchange adsorptive cathodic stripping voltammetry (CLE-ACSV) techniques. Limnol. Oceanogr. Methods 10, 496-515.

Byrne, R. H. (2002). Inorganic speciation of dissolved elements in seawater: the influence of pH on concentration ratios. Geochem. Trans. 3, 11-16.

Cao, Z., Li, Y., Rao, X., Yu, Y., Hathorne, E. C., Siebert, C., et al. (2020). Constraining barium isotope fractionation in the upper water column of the South China Sea. Geochim. Cosmochim. Acta 288, 120–137.

Cave, R.R., German, C.R., Thomson, J. and Nesbitt, R.W. (2002). Fluxes to sediments underlying the Rainbow hydrothermal plume at 36°14′N on the Mid-Atlantic Ridge. Geochim. Cosmochim. Acta 66, 1905-1923.

Church, M. J., Jenkins, B. D., Karl, D. M. and Zehr, J. P. (2005a). Vertical distributions of nitrogen fixing phylotypes at Stn ALOHA in the oligotrophic North Pacific Ocean. Aquat. Microb. Ecol. 38, 3–14.

Church, M. J., Short, C. M., Jenkins, B. D., Karl, D. M. and Zehr, J. P. (2005b). Temporal patterns of nitrogenase gene (nifH) expression in the oligotrophic North Pacific Ocean. Appl. Environ. Microbiol. 71, 5362–5370.

Charlou, J. L., Donval, J. P., Jean-Baptiste, P. and Holm, N. (2002). Geochemistry of high H_2 and CH_4 vent fluids at the Rainbow hydrothermal field (36°14′N, MAR). Chem. Geol. 191, 345–359

Crowe, S. A., Døssing, L. N., Beukes, N. J., Bau, M., Kruger, S. J., Frei, R., and Canfield, D. E. (2013). Atmospheric oxygenation three billion years ago. Nature, 501(7468), 535–538.

Davis, A.C., Bickle, M.J., Teagle, D.A.H., 2003. Imbalance in the oceanic strontium budget. Earth Planet. Sci. Lett. 211, 173-187.

Delstanche, S., Opfergelt, S., Cardinal, D., Elsass, F., André, L. and Delvaux, B. (2009). Silicon isotopic fractionation during adsorption of aqueous monosilicic acid onto iron oxide, Geochim. Cosmochim. Acta 73, 923–934.

Dunn, R.; Eason, D.; Canales, J. and R. Sohn, (2016). Seafloor reflectivity of the Mid-Atlantic Ridge Rainbow region (35°45' - 36°35'N). IEDA.

Douville, E., Charlou, J. L., Oelkers, E. H., Bienvenu, P., Jove Colon, C. F., Donval, J. P., et al. (2002). The rainbow vent fluids (36°14′N, MAR): The influence of ultramafic rocks and phase separation on trace metal content in Mid- Atlantic Ridge hydrothermal fluids. Chem. Geol. 184, 37–48.

Edmonds, H. N. and German, C. R. (2004). Particle geochemistry in the Rainbow hydrothermal plume, Mid-Atlantic Ridge. Geochim. Cosmochim. Acta 68, 759–772.

Feng, X., Steiner, Z., Redfern, S.A.T., 2021. Fluorine incorporation into calcite, aragonite and vaterite $CaCO_3$: Computational chemistry insights and geochemistry implications. Geochim. Cosmochim. Acta 308, 384-392.

Fitzsimmons, J., John, S., Marsay, C. et al. Iron persistence in a distal hydrothermal plume supported by dissolved–particulate exchange. Nature Geosci 10, 195–201 (2017).

Frei, R., Gaucher, C., Døssing, L. N., & Sial, A. N. (2011). Chromium isotopes in carbonates—A tracer for climate change and for reconstructing the redox state of ancient seawater. Earth Planet. Sci. Lett., 312(1–2), 114–125.

Frei, R., Gaucher, C., Poulton, S. W., and Canfield, D. E. (2009). Fluctuations in Precambrian atmospheric oxygenation recorded by chromium isotopes. Nature, 461(7261), 250–253.

Geilert, S., Grasse, P., Doering, K., Wallmann, K., Ehlert, C., Scholz, F., Frank, M., Schmidt, M. and Hensen, C. (2020). Impact of ambient conditions on the Si isotope fractionation in marine pore fluids during early diagenesis. Biogeosciences, 17, 1745–1763.

German C. R., Campbell, A. C. and Edmond, J. M. (1991). Hydrothermal scavenging at the Mid-Atlantic Ridge: modification of trace element dissolved fluxes. Earth Planet. Sci. Lett. 107, 101–114.

German, C. R., Klinkhammer, G. P., and Rudnicki, M. D. (1996). The Rainbow Hydrothermal Plume, 36°15′N, MAR. Geophys. Res. Lett. 23, 2979–2982.

German, C. R., and Von Damm, K. L. (2003). "Hydrothermal Processes," (Elsevier Inc.), 181–222.

Gledhill, M., and Buck, K. N. (2012). The organic complexation of iron. Front. Microbiol. 3, 69.

Glock, N., Romero, D., Roy, A. S., Woehle, C., Dale, A. W. and Schönfeld, J., et al. (2020). A hidden sedimentary phosphate pool inside benthic foraminifera from the Peruvian upwelling region might nucleate phosphogenesis. Geochim. Cosmochim. Acta, 289, 14–32.

Gooday, A. J., Rothe, N., Pearce, R. B. (2013). New and poorly known benthic foraminifera (Protista, Rhizaria) inhabiting the shells of planktonic foraminifera on the bathyal Mid-Atlantic Ridge, Mar. Biol. Res., 9(5-6), 447-461.

Goring-Harford, H. J., Klar, J. K. K., Pearce, C. R., Connelly, D. P., Achterberg, E. P., & James, R. H. (2018). Behaviour of chromium isotopes in the eastern sub-tropical Atlantic Oxygen Minimum Zone. Geochim. Cosmochim. Acta, 236, 41–59.

Hathorne E. C., Haley B., Stichel T., Grasse P., Zieringer M. and Frank M. (2012). Online preconcentration ICP-MS analysis of rare earth elements in seawater. Geochem. Geophys. Geosyst. 13, Q01020.

Heimbürger, LE., Sonke, J., Cossa, D. et al. (2015). Shallow methylmercury production in the marginal sea ice zone of the central Arctic Ocean. Sci Rep 5, 10318.

Henderson, P.B., Morris, P.J., Moore, W.S. and Charette, M.A. (2013). Methodological advances for measuring low-level radium isotopes in seawater. J. Radioanal. Nucl. Chem. 296, 357–362.

Hodell, D.A., Mead, G.A. and Mueller, P.A. (1990). Variation in the strontium isotopic composition of seawater (8 Ma to present): Impications for chemical weathering rates and dissolved fluxes to the oceans. Chem. Geol. 80, 291-307.

Hoffman, C., Nicholas, S., Ohnemus, D., Fitzsimmons, J., Hoffman, C. L., Nicholas, S. L., et al. (2018). Near-field iron and carbon chemistry of non-buoyant hydrothermal plume particles, Southern East Pacific Rise 15°S. Mar. Chem. 201, 183–197.

Hopwood, M. J., Santana-González, C., Gallego-Urrea, J., Sanchez, N., Achterberg, E. P., et al. (2020). Fe(II) stability in coastal seawater during experiments in Patagonia, Svalbard, and Gran Canaria, Biogeosciences, 17, 1327–1342.

Horner, T. J., Kinsley, C. W., and Nielsen, S. G. (2015). Barium-isotopic fractionation in sea-water mediated by barite cycling and ocean circulation. Earth Planet Sci. Lett. 430, 511–522.

Hsieh, Y. Te, Bridgestock, L., and Henderson, G. M. (2021). Barium isotopes in mid-ocean ridge hydrothermal vent fluids. Geochim. Cosmochim. Acta 292, 348–363.

Humphris, S.E., Thompson, G., 1978. Hydrothermal alteration of oceanic basalts by seawater. Geochim. Cosmochim. Acta 42, 107-125.

IOC, SCOR, IAPSO, 2010. The international thermodynamic equation of seawater – 2010: Calculation and use of thermodynamic properties, Intergovernmental Oceanographic Commission, Manuals and Guides No. 56, www.TEOS-10.org, p. 196.

Kadko, D. (1993). An assessment of the effect of chemical scavenging within submarine hydrothermal plumes upon ocean geochemistry. Earth Planet. Sci. Lett. 120, 361–374.

Kadko, D., (1996). Radioisotopic studies of submarine hydrothermal vents. Rev. Geophys. 34, 349–366.

Kadko, D. and Moore, W. (1988). Radiochemical constraints on the crustal residence time of submarine hydrothermal fluids: Endeavour Ridge. Geochim. Cosmochim. Acta 52, 659–668.

Kim, T., Obata, H., Kondo, Y., Ogawa, H. and Gamo, T. (2015). Distribution and speciation of dissolved zinc in the western North Pacific and its adjacent seas. Mar. Chem. 173, 330–341.

Kleint, C., Hawkes, J. A., Sander, S. G. and Koschinsky, A. (2016): Voltammetric investigation of hydrothermal iron speciation. Front. Mar. Sci. 3, 75.

Kremling, K., (1999). Determination of the major constituents, in: K. Grasshoff, K.K.a.M.E. (Ed.), Methods of Seawater Analysis. WILEY-VCH Verlag GmbH, Weinheim, pp. 229-251.

Ku, T. L. and Luo, S., (2008). Ocean Circulation/Mixing Studies with Decay-Series Isotopes, in: Krishnaswami, S., Cochran, J. K. (Eds), Radioactivity in the Environment, vol. 13, Elsevier, Amsterdam, 307–344 pp.

Janssen, D. J., Rickli, J., Quay, P. D., White, A. E., Nasemann, P., and Jaccard, S. L. (2020). Biological Control of Chromium Redox and Stable Isotope Composition in the Surface Ocean. Glob. Biogeochem. Cycle 34(1).

Lecuyer, C., 2016. Seawater residence times of some elements of geochemical interest and the salinity of the oceans. Bulletin De La Societe Geologique De France 187, 245-259.

Lee, J. M., Heller, M. I., and Lam, P. J. (2018). Size distribution of particulate trace elements in the U.S. GEOTRACES Eastern Pacific Zonal Transect (GP16). Mar. Chem. 201, 108–123.

Mandernack, K. W., and Tebo, B. (1993). Manganese scavenging and oxidation at hydrothermal vents and in vent plumes. Geochim. Cosmochim. Acta 57, 3907–3923.

Marchig, V., Erzinger, J., and Heinze, P.-H. (1986). Sediment in the black smoker area of the East Pacific Rise (18.5°S). Earth Planet. Sci. Lett., 79, 93–106.

Millero, F.J., Feistel, R., Wright, D.G. and McDougall, T.J. (2008). The composition of Standard Seawater and the definition of the Reference-Composition Salinity Scale. Deep Sea Res. Part I Oceanogr. Res. Pap. 55, 50-72.

Millero, F. J., Sotolongo, S. and Izaguire, M. (1987). The oxidation kinetics of Fe (II) in seawater. Geochim. Cosmochim. Acta 51, 793–802.

Milliman, J.D. (1993). Production and accumulation of calcium-carbonate in the ocean - budget of a non steady state. Glob. Biogeochem. Cycle 7, 927-957.

Milne, A., Schlosser, C., Wake, B. D., Achterberg, E. P., Chance, R., et al. (2017), Particulate phases are key in controlling dissolved iron concentrations in the (sub)tropical North Atlantic, Geophys. Res. Lett., 44, 2377– 2387

Mohr, W., Großkopf, T., Wallace, D. W. and LaRoche, J. (2010). Methodological underestimation of oceanic nitrogen fixation rates. PLoS One 5, e12583.

Moisander, P. H., Beinart, R. A., Voss, M. and Zehr, J. P. (2008). Diversity and abundance of diazotrophic microorganisms in the South China Sea during intermonsoon. ISME J 2, 954–967.

Monperrus, M., Tessier, E., Veschambre, S. et al. (2005). Simultaneous speciation of mercury and butyltin compounds in natural waters and snow by propylation and species-specific isotope dilution mass spectrometry analysis. Anal Bioanal Chem 381, 854–862.

Moore, W.S. and Arnold, R. (1996). Measurement of 223Ra and 224Ra in coastal waters using a delayed coincidence counter. J. Geophys. Res. 101, 1321–1329.

Moore, C. M., Mills, M. M., Arrigo, K. R., Berman-Frank, I., Bopp, L., Boyd, P. W., et al. (2013). Processes and patterns of oceanic nutrient limitation. Nat. Geosci. 6, 701–710.

Murray, J. W., Spell, B. and Paul, B. (1983). The Contrasting Geochemistry of Manganese and Chromium in the Eastern Tropical Pacific Ocean. In Trace Metals in Sea Water (pp. 643–669). Springer US.

Nealson, K. H., Tebo, B. M. and Rosson, R. A. (1988). Occurrence and Mechanisms of Microbial Oxidation of Manganese. Adv. Appl. Microbiol. 33, 279–318.

Nishioka, J., Obata, H. and Tsumune, D. (2013). Evidence of an extensive spread of hydrothermal dissolved iron in the Indian Ocean. Earth Planet. Sci. Lett. 361, 26–33.

Piña-Ochoa, E., Høgslund, S., Geslin, E., Cedhagen, T., Revsbech, N. P., Nielsen, L. P., et al. (2010). Widespread occurrence of nitrate storage and denitrification among Foraminifera and Gromiida. Proc. Natl. Acad. Sci. U.S.A., 107(3), 1148–1153.

Ren, J. L., Zhang, J., Luo, J. Q., Pei, X. K. and Jiang, Z. X. (2001). Improved fluorimetric determination of dissolved aluminium by micelle-enhanced lumogallion complex in natural waters. Analyst 126(5), 698-702.

Resing, J. A., Sedwick, P. N., German, C. R., Jenkins, W. J., Moffett, J. W., Sohst, B. M., et al. (2015). Basin-scale transport of hydrothermal dissolved metals across the S Pacific. Nature 523, 200–203.

Richter, F.M. and Turekian, K.K. (1993). Simple models for the geochemical response of the ocean to climatic and tectonic forcing. Earth Planet. Sci. Lett. 119, 121-131.

Rickli, J., Janssen, D. J., Hassler, C., Ellwood, M. J. and Jaccard, S. L. (2019). Chromium biogeochemistry and stable isotope distribution in the Southern Ocean. Geochim. Cosmochim. Acta, 262, 188–206.

Rude, P.D. and Aller, R.C. (1991). Fluorine mobility during early diagenesis of carbonate sediment: An indicator of mineral transformations. Geochim. Cosmochim. Acta 55, 2491-2509.

Rudnicki, M. D. and Elderfield, H. (1993). A chemical model of the buoyant and neutrally buoyant plume above the TAG vent field, 26 degrees N, MAR. Geochim. Cosmochim. Acta 57, 2939–2957.

Sander, S. and Koschinsky, A. (2000). Onboard-ship redox speciation of chromium in diffuse hydrothermal fluids from the North Fiji Basin, Mar. Chem., 71(1–2), 83–102.

Saito, M., Noble, A., Tagliabue, A. et al. (2013). Slow-spreading submarine ridges in the South Atlantic as a significant oceanic iron source. Nature Geosci 6, 775–779.

Scheiderich, K., Amini, M., Holmden, C., and Francois, R. (2015). Global variability of chromium isotopes in seawater demonstrated by Pacific, Atlantic, and Arctic Ocean samples. Earth Planet. Sci. Lett. 423, 87–97.

Schönfeld, J. (2012). History and development of methods in Recent benthic foraminiferal studies. J. Micropalaeontol. 31(1), 53–72.

Sherrell, R. M., Field, M. P. and Ravizza, G. (1999). Uptake and fractionation of rare earth elements on hydrothermal plume particles at 9°45'N, East Pacific Rise. Geochim. Cosmochim. Acta 63, 1709–1722.

Statham, P. J., German, C. R. and Connelly, D. P. (2005). Iron (II) distribution and oxidation kinetics in hydrothermal plumes at the Kairei and Edmond vent sites. Earth Planet. Sci. Lett. 236, 588–596.

Steiner, Z., Sarkar, A., Prakash, S., Vinayachandran, P.N., Turchyn, A.V., 2020. Dissolved strontium, Sr/Ca ratios, and the abundance of Acantharia in the Indian and Southern Oceans. ACS Earth Space Chem. 4, 802-811.

Tagliabue, A., Bopp, L., Dutay, J.-C., Bowie, A. R., Chever, F., Jean-Baptiste, P., et al. (2010). Hydrothermal contribution to the oceanic dissolved iron inventory. Nat. Geosci 3, 252–256.

Talley, L., Pickard, D., Emery, W., and Swift, J. H. (2011). Descriptive physical oceanography Academic Press.

Thompson, A. W., Carter, B. J., Turk-Kubo, K., Malfatti, F., Azam, F. and Zehr, J. P. (2014). Genetic diversity of the unicellular nitrogen-fixing cyanobacteria UCYN-A and its prymnesiophyte host. Environ. Microbiol. 16, 3238–3249.

Tipper, E.T., Gaillardet, J., Galy, A., Louvat, P., Bickle, M.J., Capmas, F. (2010). Calcium isotope ratios in the world's largest rivers: A constraint on the maximum imbalance of oceanic calcium fluxes. Glob. Biogeochem. Cycle 24, 13.

Toner, B. M., Fakra, S. C., Manganini, S. J., Santelli, C. M., Marcus, M. A., Moffett, J. W., et al. (2009). Preservation of iron(II) by carbon-rich matrices in a hydrothermal plume. Nat. Geosci. 2, 197–201.

US Environmental Protection Agency (EPA) method 1631.

Ustick, L. J., Larkin, A. A., Garcia, C. A., Garcia, N. S., Brock, M. L., Lee, J. A., Wiseman N. A., Moore, J. K. and Martiny, A. C. (2021). Metagenomic analysis reveals global-scale patterns of ocean nutrient limitation. Science 372, 287- 91.

Wang, W., Geilert, S., Wie, H. Z., and Jiang, S. Y. (2021). Competition of equilibrium and kinetic silicon isotope fractionation during silica precipitation from acidic to alkaline pH solutions in geothermal systems, Geochim. Cosmochim. Acta 306, 44-62.

Winkler, L. W. (1888). The determination of dissolved oxygen in water. Berlin DeutChem Gas 21, 2843-2855.

Wu, J. F., Boyle, E., Sunda, W. and Wen, L. S. (2001). Soluble and colloidal iron in the olgotrophic North Atlantic and North Pacific. Science 293(5531), 847–849.

Yu, Y. (2021). Stable Barium Isotopes: Biogeochemical Cycling and Palaeoceanographic Applications. Doctoral thesis, Christian-Albrechts-Universität, Kiel, 147 pp.

Yucel, M., Gartman, A., Chan, C. S. and Luther, G. W. (2011). Hydrothermal vents as a kinetically stable source of iron-sulphide-bearing nanoparticles to the ocean. Nat. Geosci 4, 367–371.

Zheng, X., Beard, B. L., Reddy, T. R., Roden, E. E., and Johnson, C. M. (2016). Abiologic silicon isotope fractionation between aqueous Si and Fe(III)-Si gel in simulated Archean seawater?: Implications for Si isotope records in Precambrian sedimentary rocks, Geochim. Cosmochim. Acta 187, 102–122.

11 Abbreviations

ADCP	Acoustic Doppler Current Profiler
AMAR	American Mid-Atlantic Ridge
BATS	Bermuda Atlantic Time-series Study
BIF	Banded Iron Formation
Chl	Chlorophyll
CRM	Certified Reference Material
CTD	Conductivity, Temperature and Depth
CVAFS	Cold Vapor Automatic Fluorescence Spectrometry
DCM	Deep Chlorophyll Maximum
DGM	Dissolved Gaseous Mercury
DI	Deionised water
DIC	Dissolved Inorganic Carbon
DOC	Dissolved Organic Carbon
DON	Dissolved Organic Nitrogen
EDTA	Ethylenediaminetetraacetic acid
EEZ	Exclusive Economic Zone
EPR	East Pacific Rise
FTU	Formazin Turbidity Unit
GF/F	Glass Fibre Filter
HFSE	High-Field Strength Elements
HgT	Total mercury
HPLC	High Performance Liquid Chromatography
ICP-MS	Inductively Coupled Plasma Mass Spectrometry
ICP-OES	Inductively Coupled Plasma Optical Emission Spectroscopy
KDMT	Kiel Data Management Team
LADCP	Lowered Acoustic Doppler Current Profiler
LCW	Labrador Sea Water
LDPE	Low-density Polyethylene
MAR	Mid-Atlantic Ridge
MC-ICP-MS	Multi-Collector Inductively Coupled Plasma Mass Spectrometry
MeHg	Methylmercury
MUC	Multi-corer
MW	Mediterranean Water
MWCO	Molecular Weight Cut-Off
NACW	North Atlantic Central Water
NADW	North Atlantic Deep Water
NIST	National Institute of Standards and Technology
PC	Polycarbonate
PES	Polyethersulfone
PET	Polyethylene terephthalate

POC	Particulate Organic Carbon
PON	Particulate Organic Nitrogen
PVDF	Polyvinylidene fluoride
RaDeCC	Radium Delayed Coincidence Counting
REE	Rare Earth Elements
ROS	Reactive Oxygen Species
SOD	Superoxide Dismutase
SRP	Soluble Reactive Phosphorous
SS	Stainless Steel
TA	Total Alkalinity
TDN	Total Dissolved Nitrogen
TE	Trace elements
TEI	Trace elements and their isotopes
TM	Trace Metals
TOC	Total Organic Carbon
TON	Total Oxidised Nitrogen (nitrate + nitrite)
TSG	Thrmosalinograph

12 Appendices

12.1 Turbidity profiles measured during the Tow-Yo casts

Chris Galley and Lukas Klose

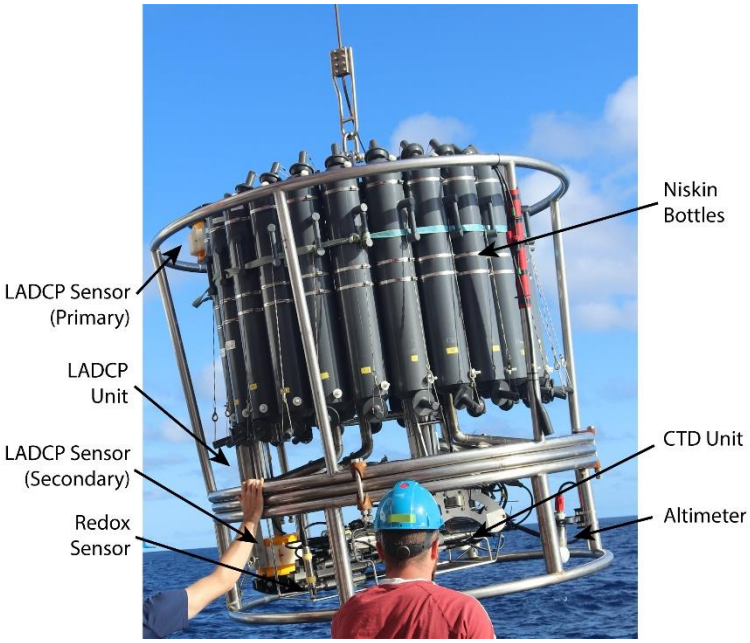

Fig. 12.1. The stainless-steel CTD frame and sensors used to map out Rainbow's hydrothermal plume.

- 08.09. to 09.09.2021: Line T12. Started NE of the vent field and surveyed in SW direction to map the southern extent of the plume. However, a proper background value was not reached.

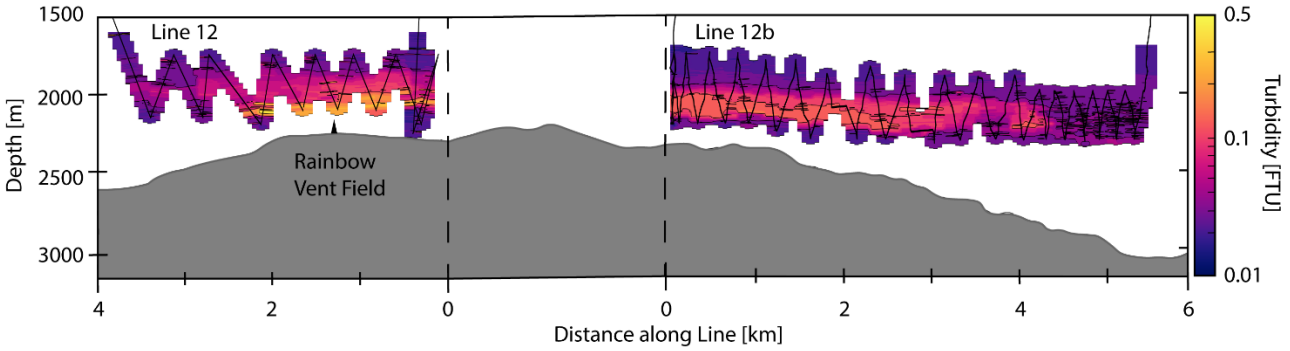

- 09.09. go 10.09.2021: Line T3. The survey started on top of Rainbow ridge and followed a SE to NW direction over the vent field

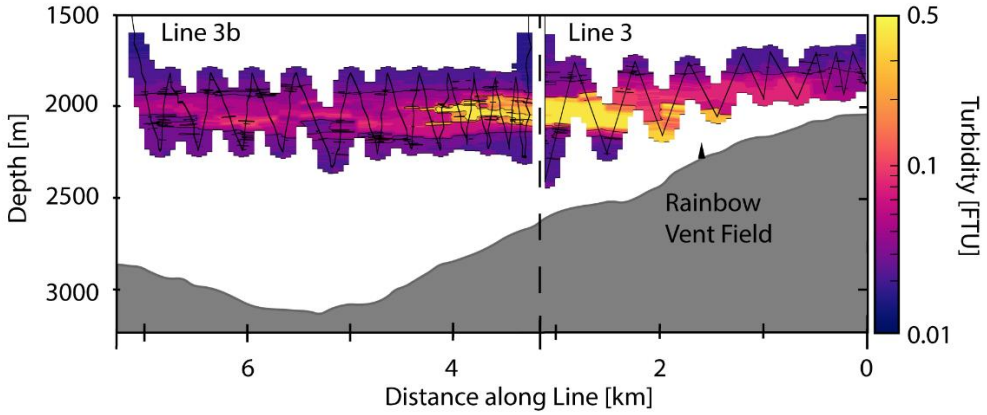

- 10.09. to 11.09.2021: Line T2. It was planned as NW to SE profile but had been stopped due to bad weather as the ship could not follow course.

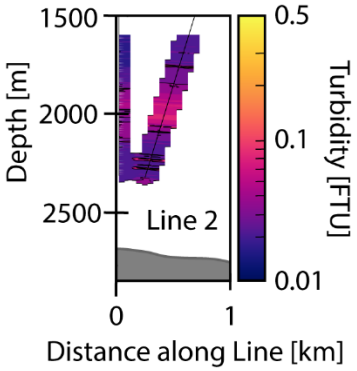

- 11.09. to 12.09.2021: Line 4-10. The survey line was planned as profile in S-N direction. However, ship had problems holding the course.

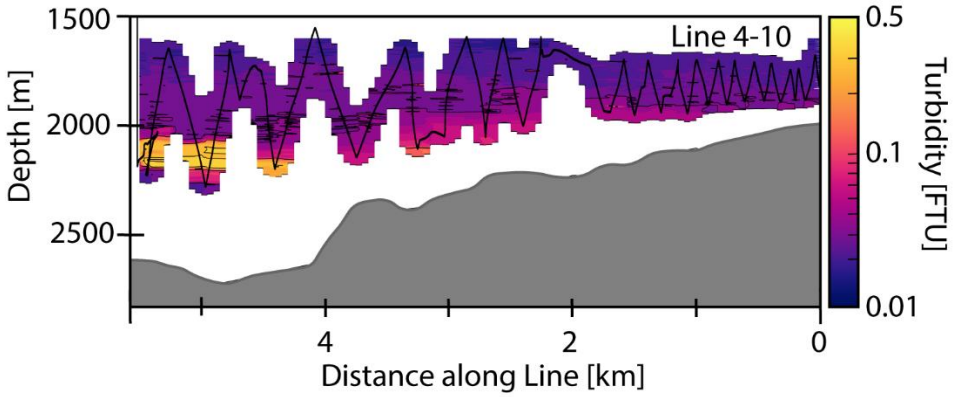

- 12.09. to 13.09.2021: Line T1-6. The profile started on top of Rainbow ridge and was oriented in a SE-NW direction, crossing over the Rainbow vent field.

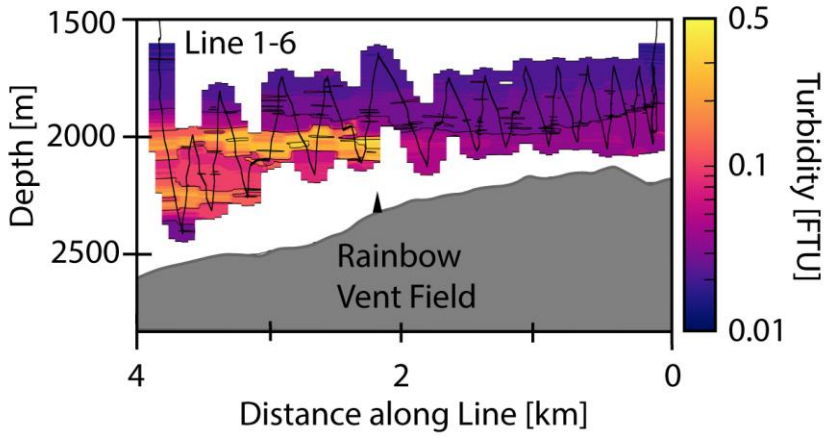

- 13.09. to 14.09.2021: Line T8. The profile started on top of Rainbow ridge and was oriented in a SW-NW direction parallel to T3.

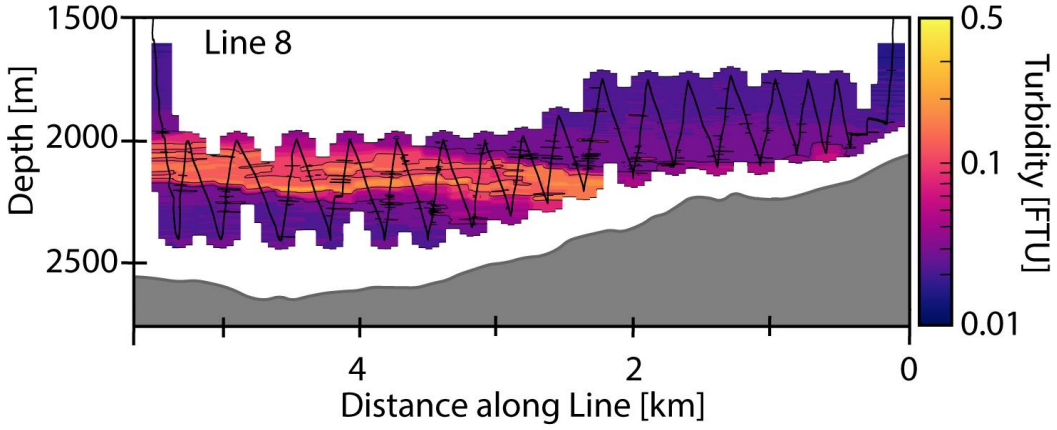

- 14.09. to 15.09.2021: Line T7. The profile started on top of Rainbow vent field in SW-NW direction parallel to T3 and T8 between those two survey lines.

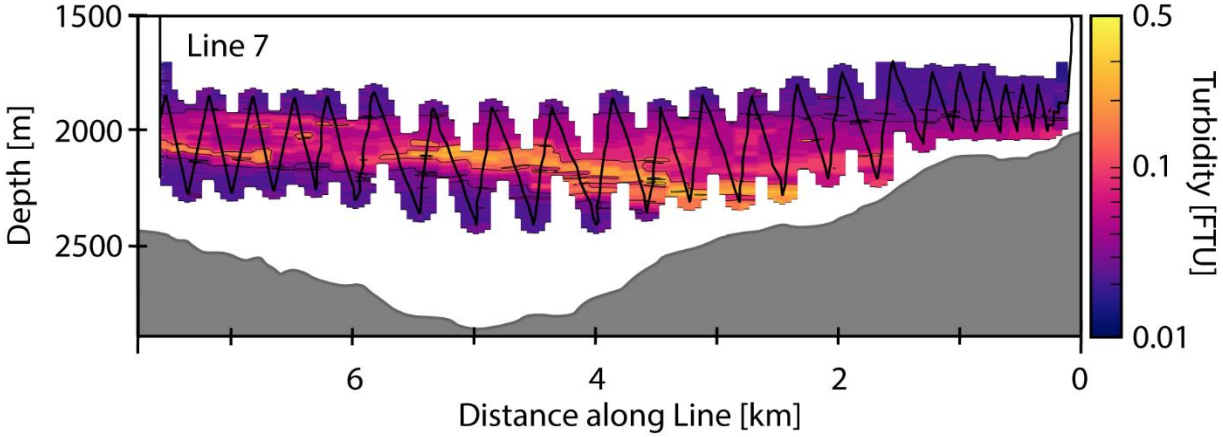

- 15.09. to 16.09.2021: Line T12b. The line started on the northern section of Rainbow ridge and extended in NE direction along the line extending from T12.

- 16.09 to 17.09.2021: Line T3b. The line started at the NW end of line T3 and extended further to the NW.

- 17.09 to 18.09.2021: Line T10. The profile started on eastern side of Rainbow ridge and extended to the NE, perpendicular to the anticipated flow direction of the plume.

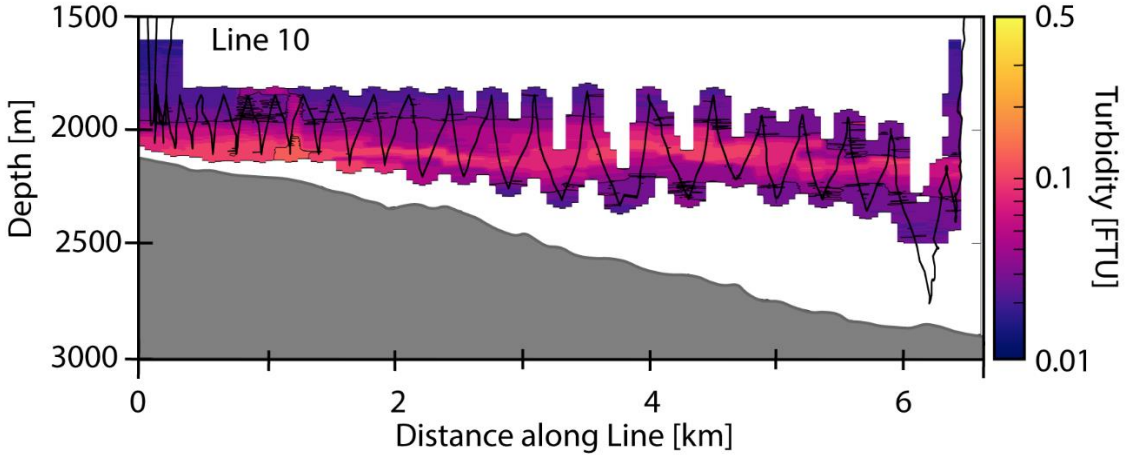

- 18.09.2021 to 19.09.2021: T11. The profile was conducted further east, downstream of T10, and was orientated in a SSW to NNE direction.

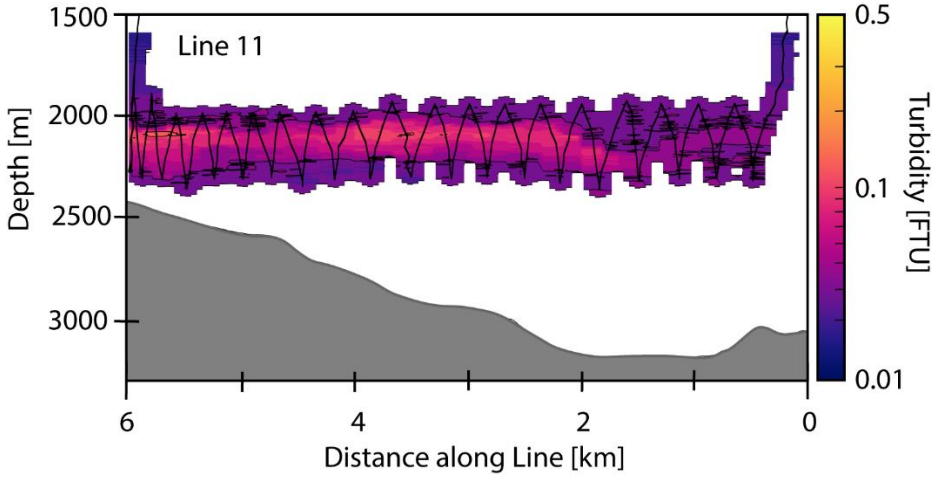

- 19.09.2021 to 20.09.2021: T13. The survey line of T8 running parallel to T3, T7 and T8 orientated in a SE to NW direction.

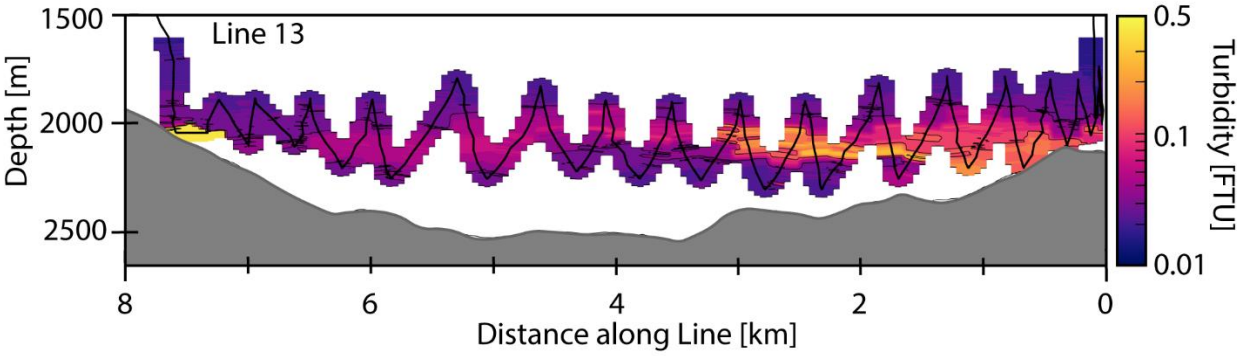

- 24.09. to 25.09.2021: T14. The survey line was conducted approx. 32 km downstream of the plume in NW to SE direction. The profile was cut short because of weather.

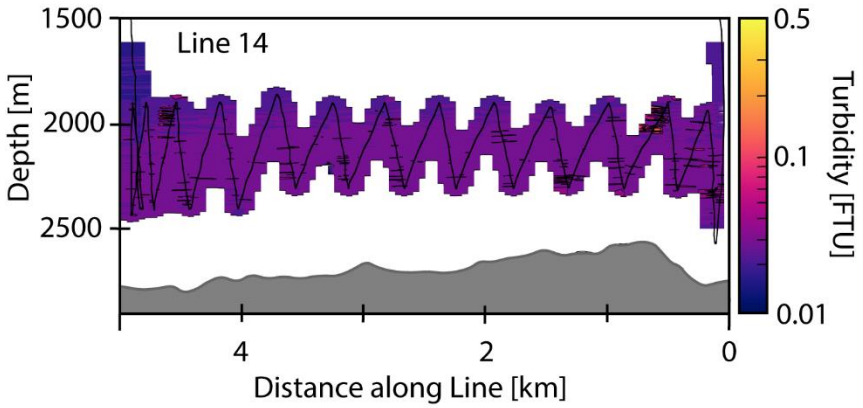

- 25.09. to 26.09.2021: T15. The survey line started between T11 and T14 an began in SE to NW direction but then had to switch to a northern followed by a western direction because of the weather conditions.

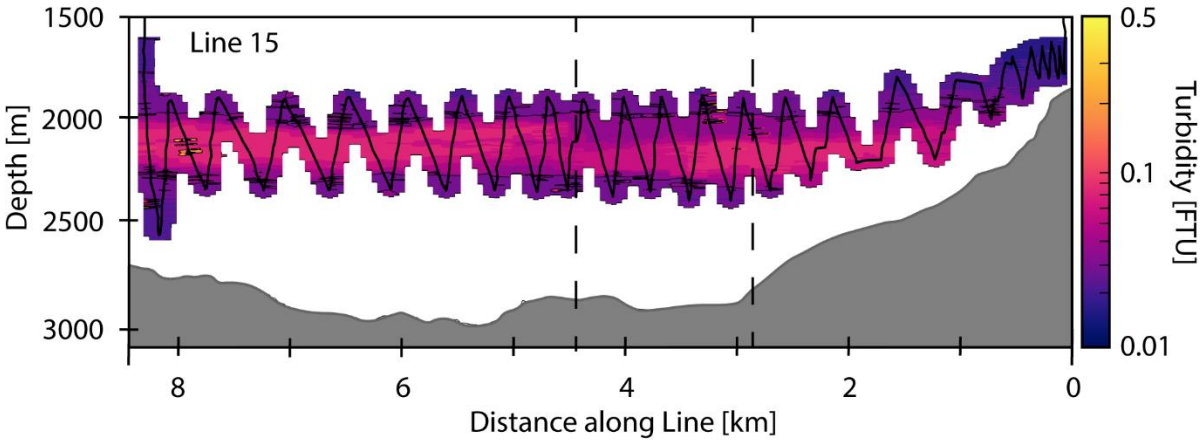

- 26.09. to 27.09. 2021: Line T16. The survey line following the plume approx. 60 km downstream was conducted in a E to W direction, perpendicular to the expected flow direction. However, due to unfavorable weather conditions the ship's speed was too high leading to survey bad resolution.

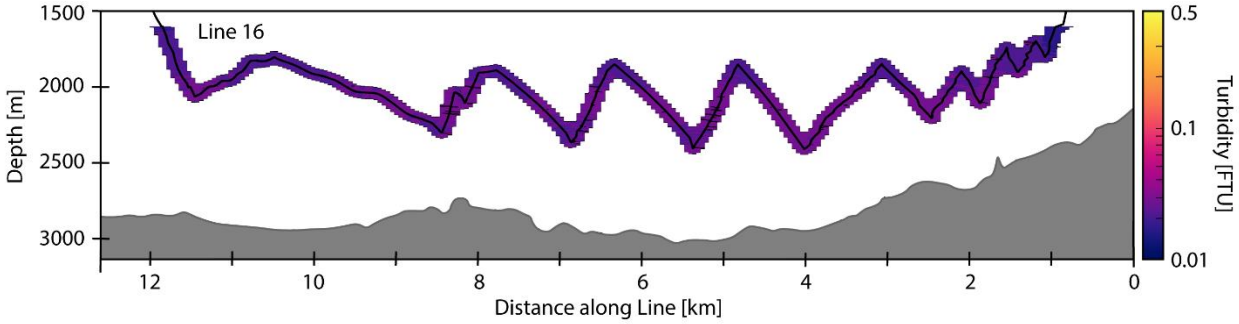

12.2 Vertical CTD LADCP Measurements

Chris Galley and Lukas Klose

At most of the vertical CTD stations, and during the lateral CTD surveys, a LADCP sensor was equipped to the CTD frame and collected data on the water column's current vectors. The LADCP device was composed of two sensors, an upward facing primary sensor and a downward facing secondary second. By combining the doppler current data from both sensors a more accurate distribution of the lateral ocean current vectors could be calculated.

The following plots display both horizontal components of the measured ocean currents at each station, as well as the current vectors' magnitude and turbidity.

- Station 3:

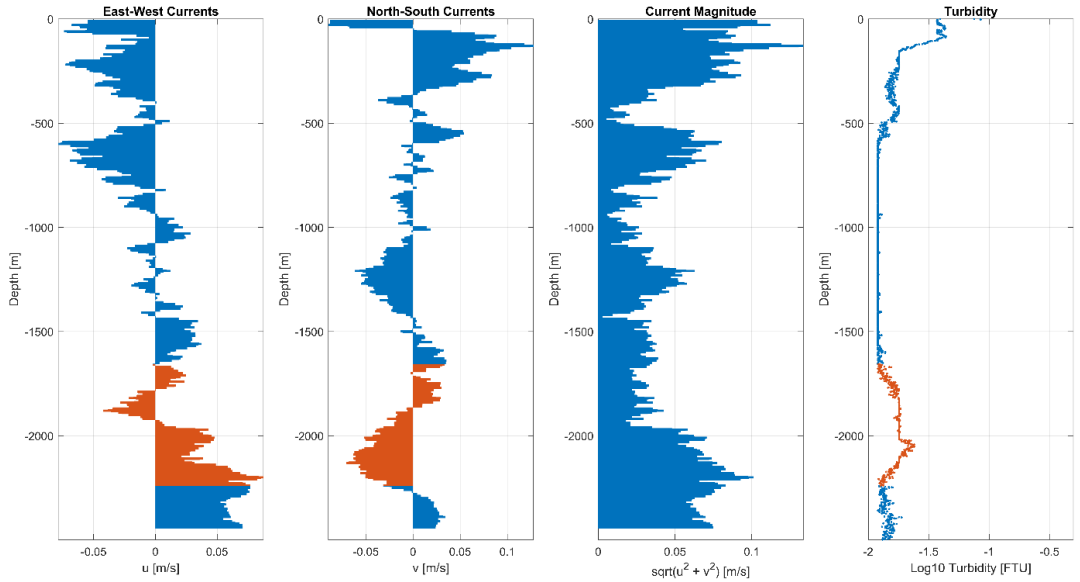

- Station 4:

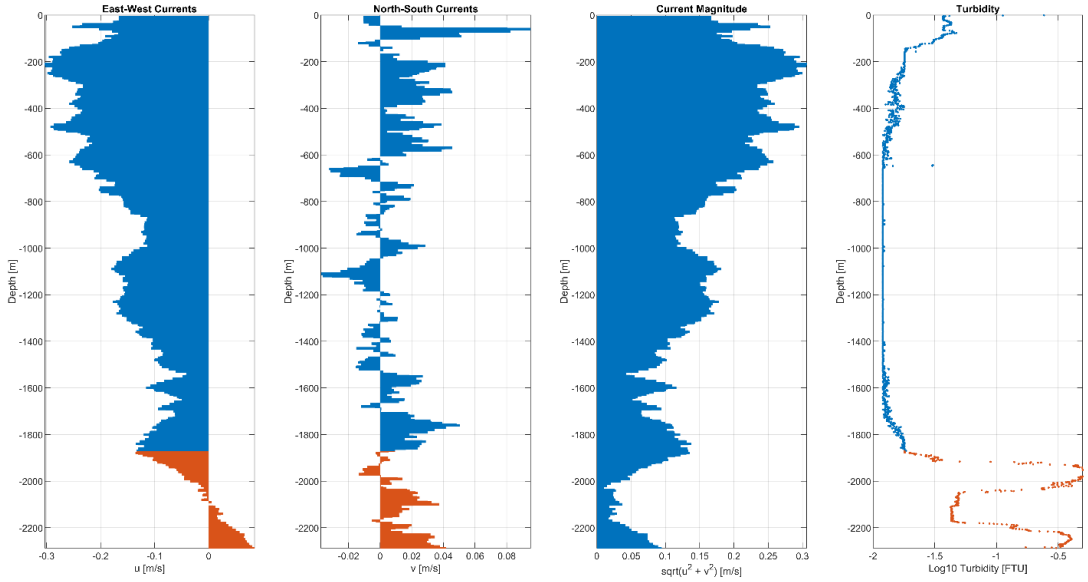

- Station 5:

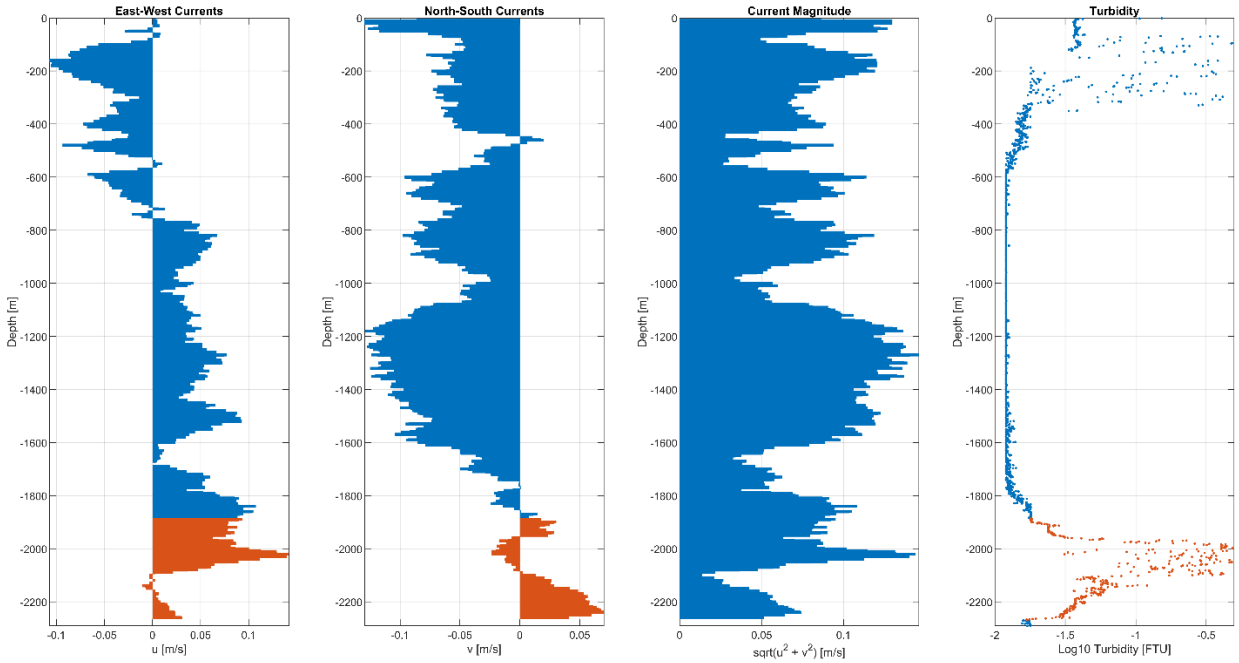

- Station 6:

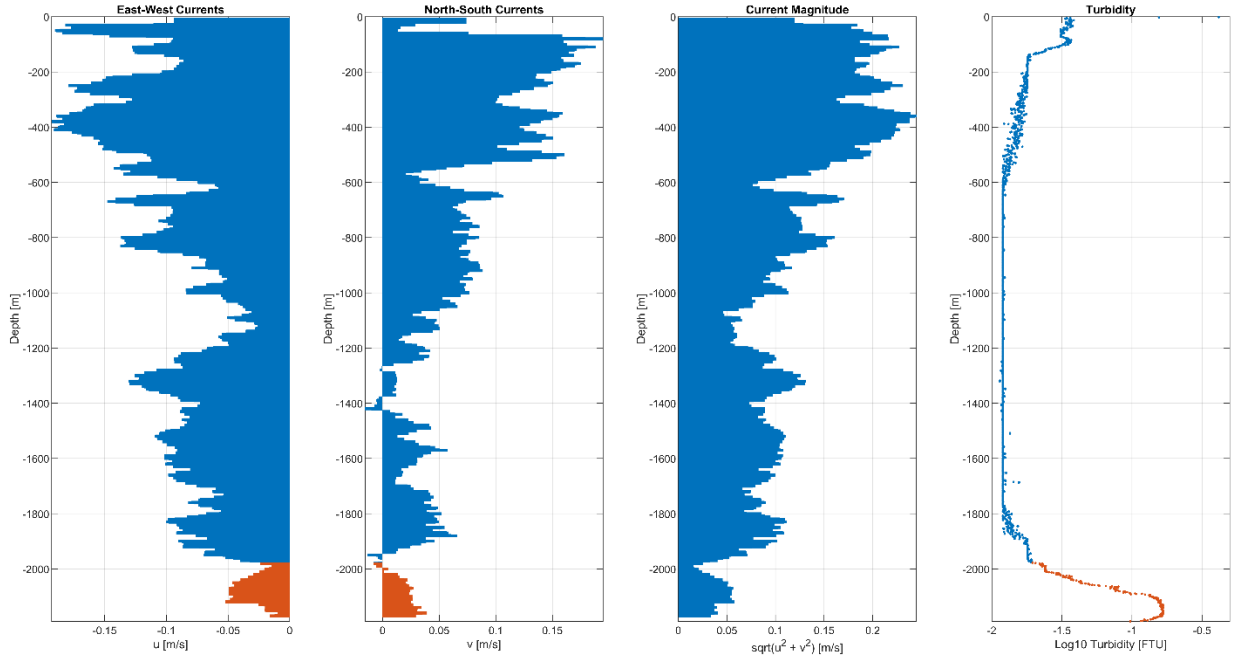

- Station 7:

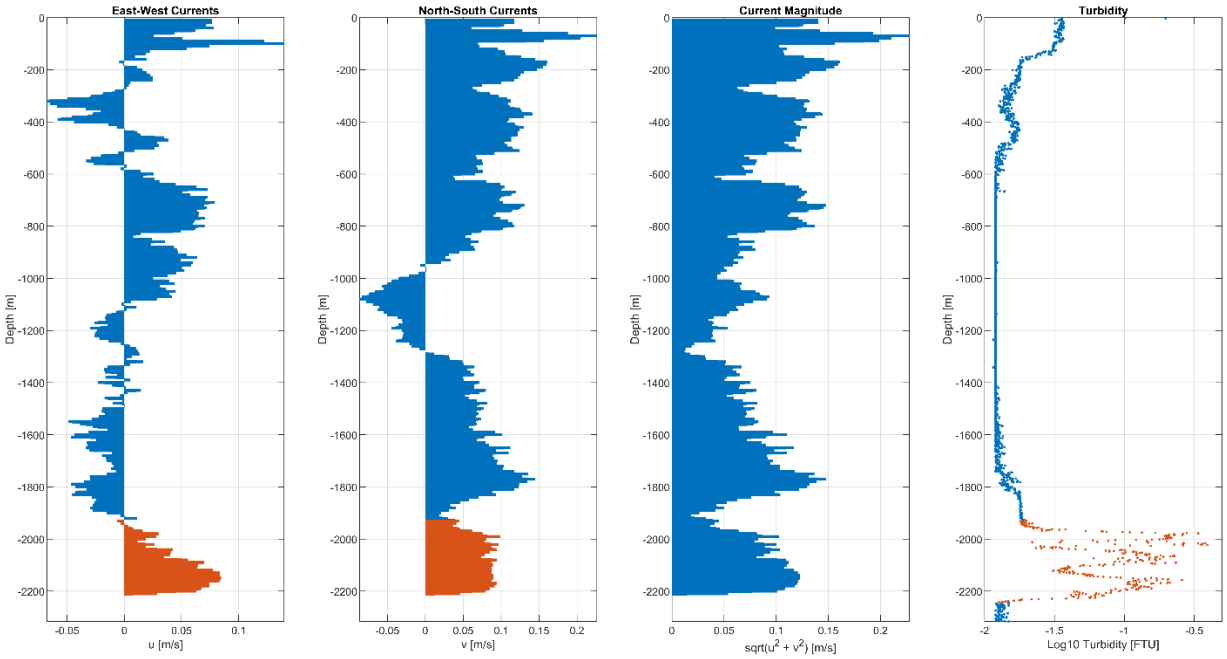

- Station 8:

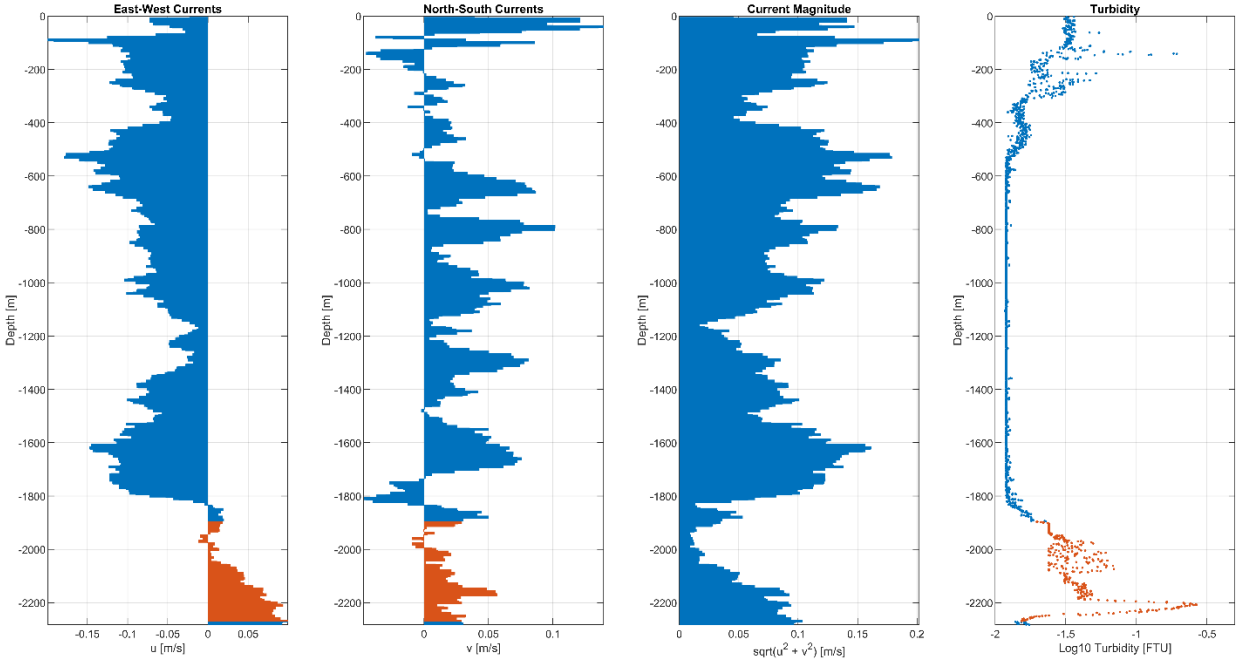

- Station 9:

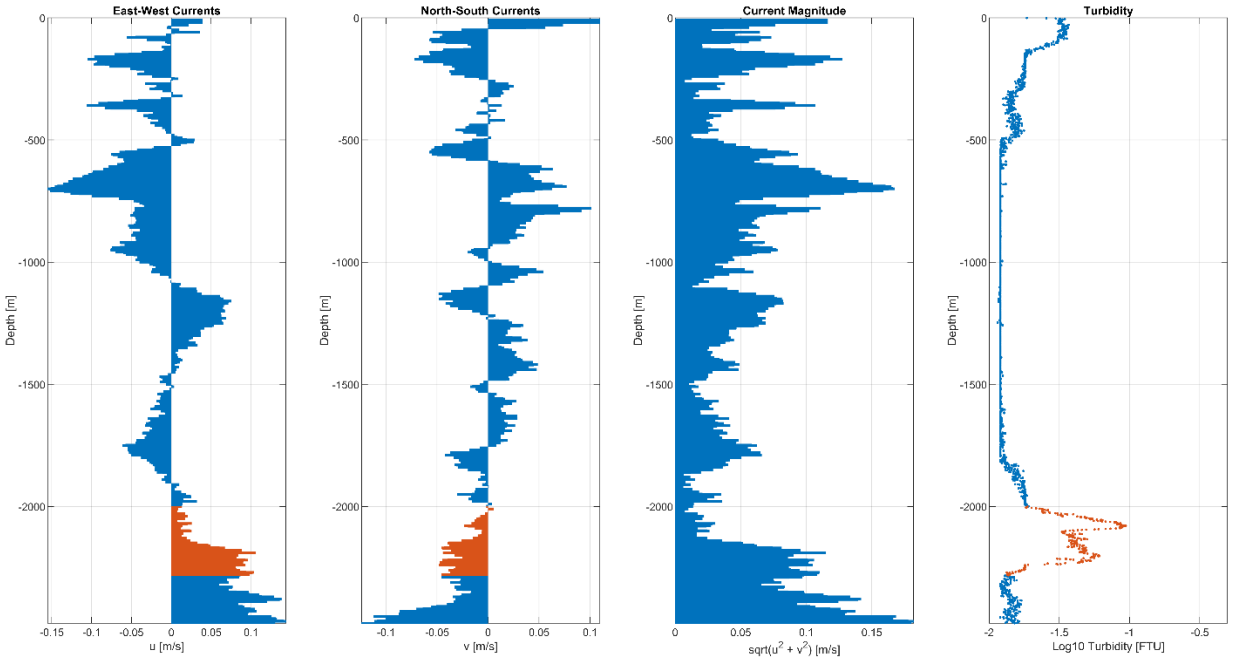

- Station 10:

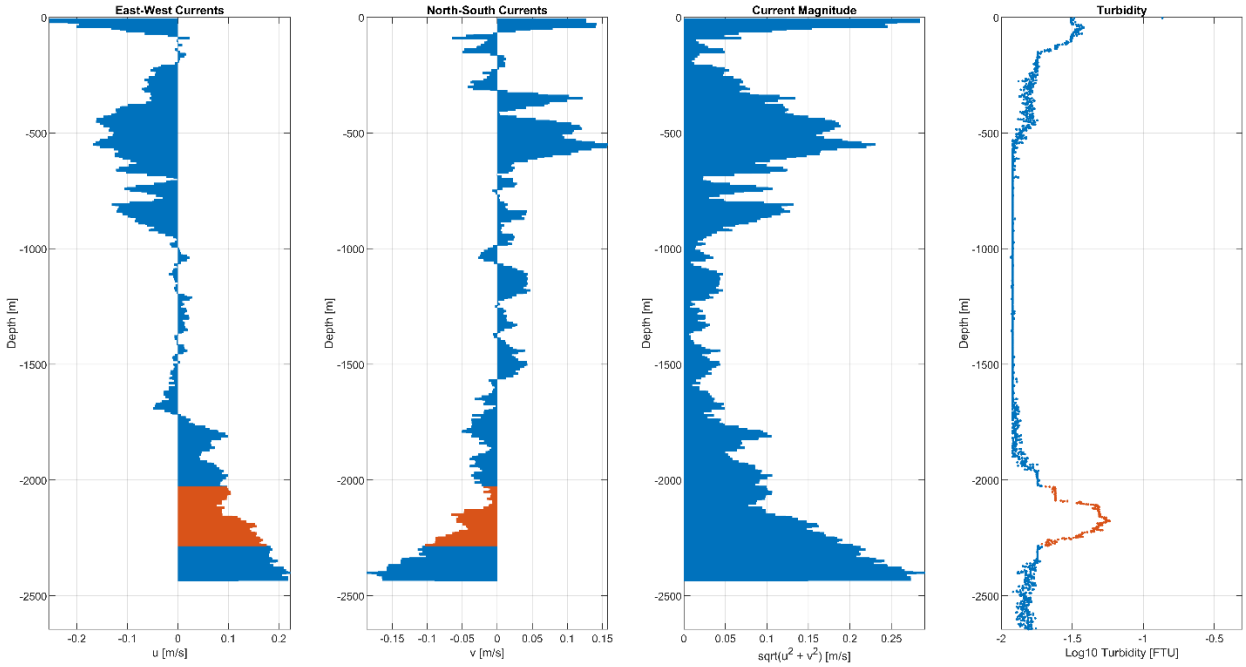

- Difficulties were met processing Station 13's LADCP data, and as such the current data is not yet available.

- Station 14:

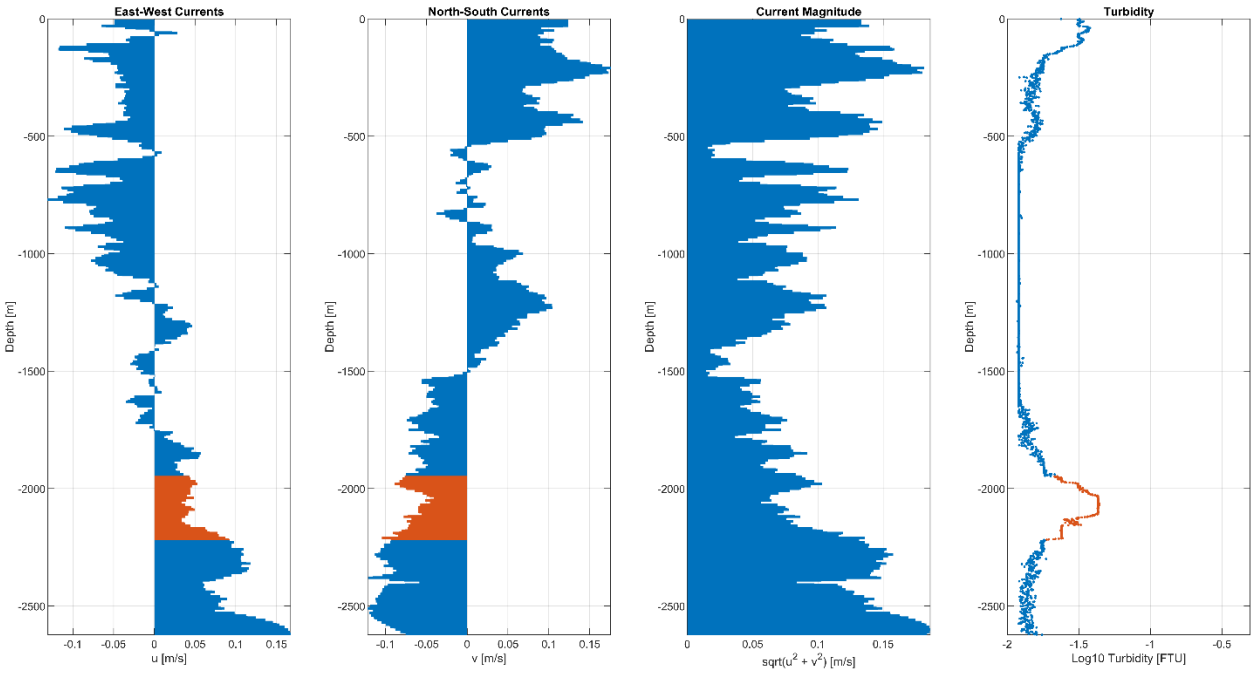

- At Station 15 and 16 the LADCP was under repair and not attached to the CTD frame. Therefore, current vector data is not available at these two stations

- Station 17:

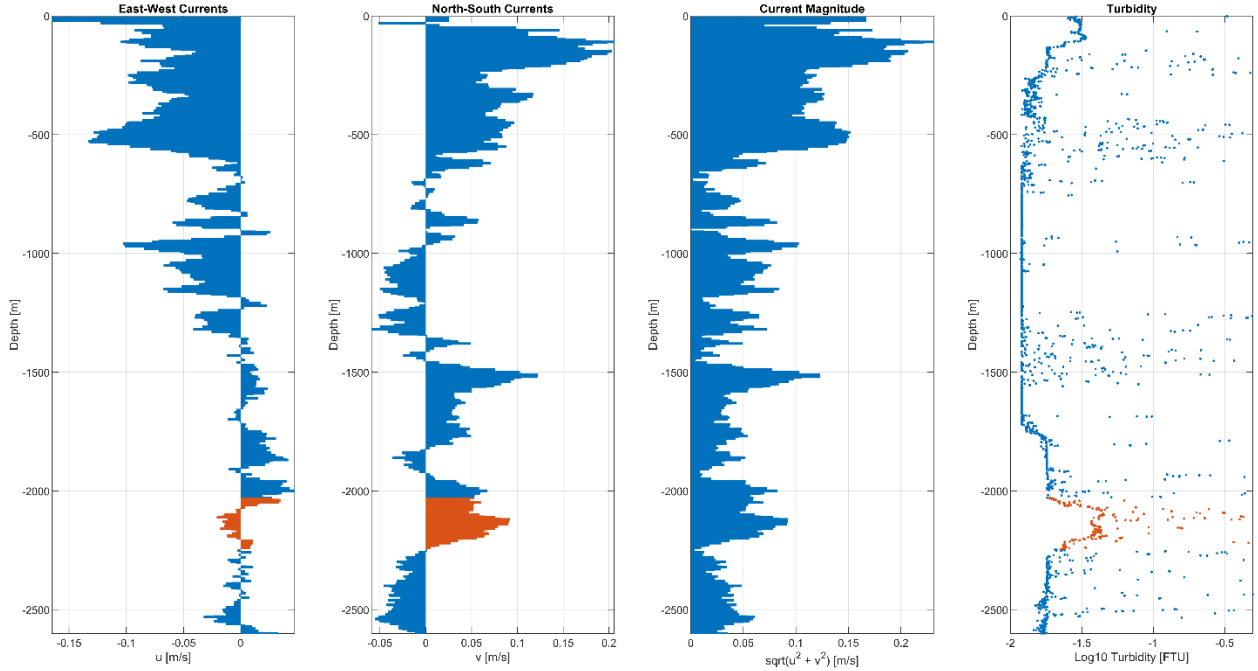

- Station 18:

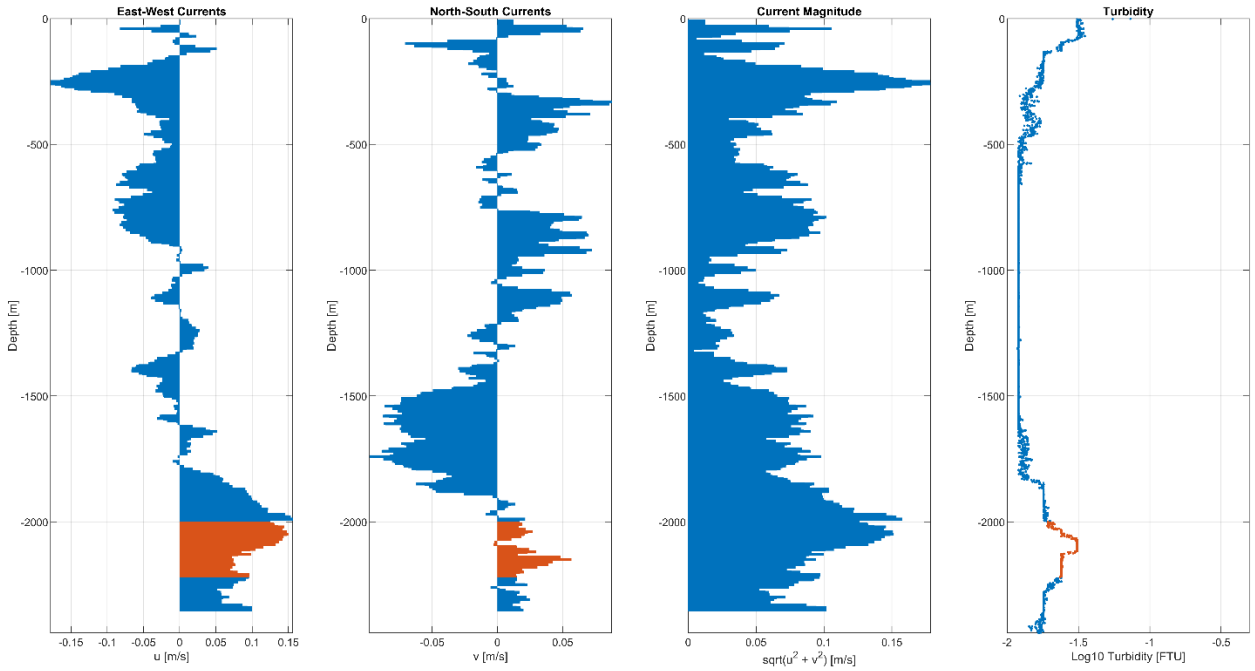

- Station 19:

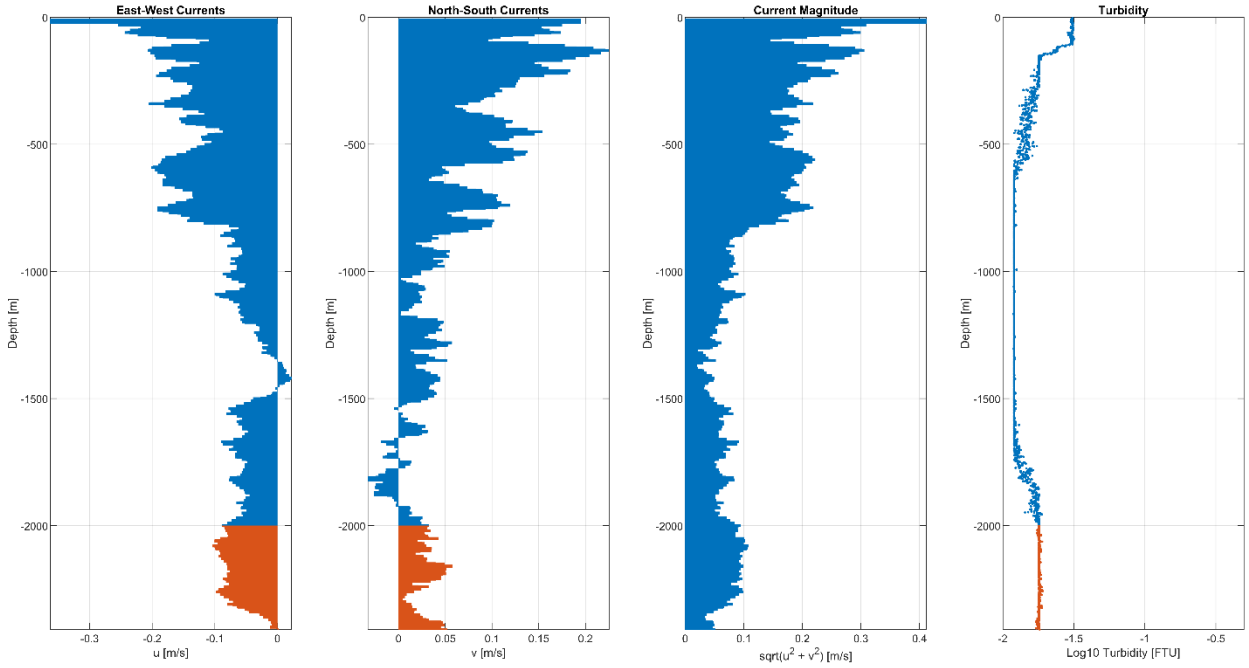

- Station 21:

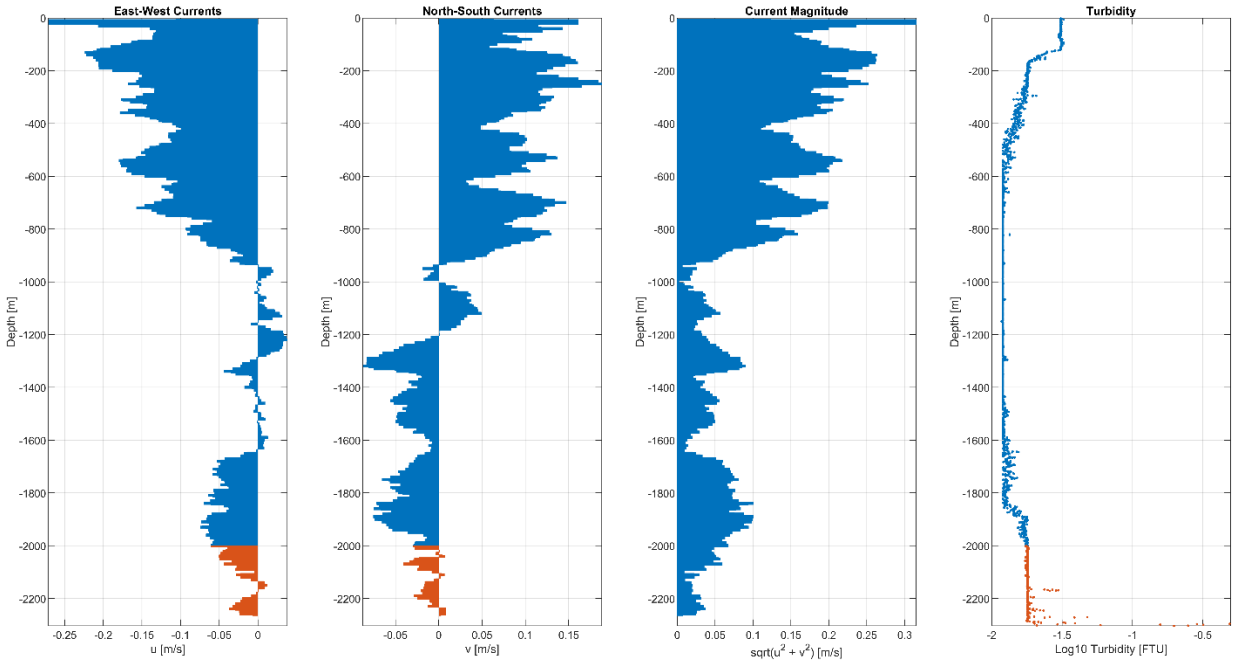

- Station 23:

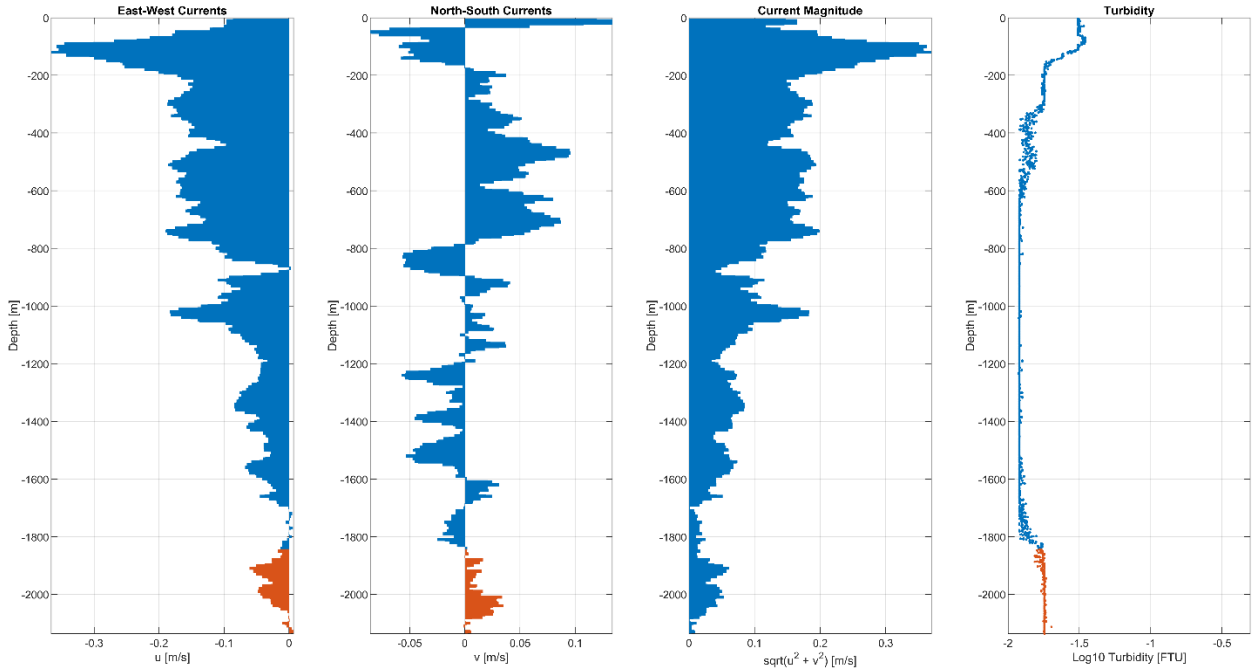

- Station 24:

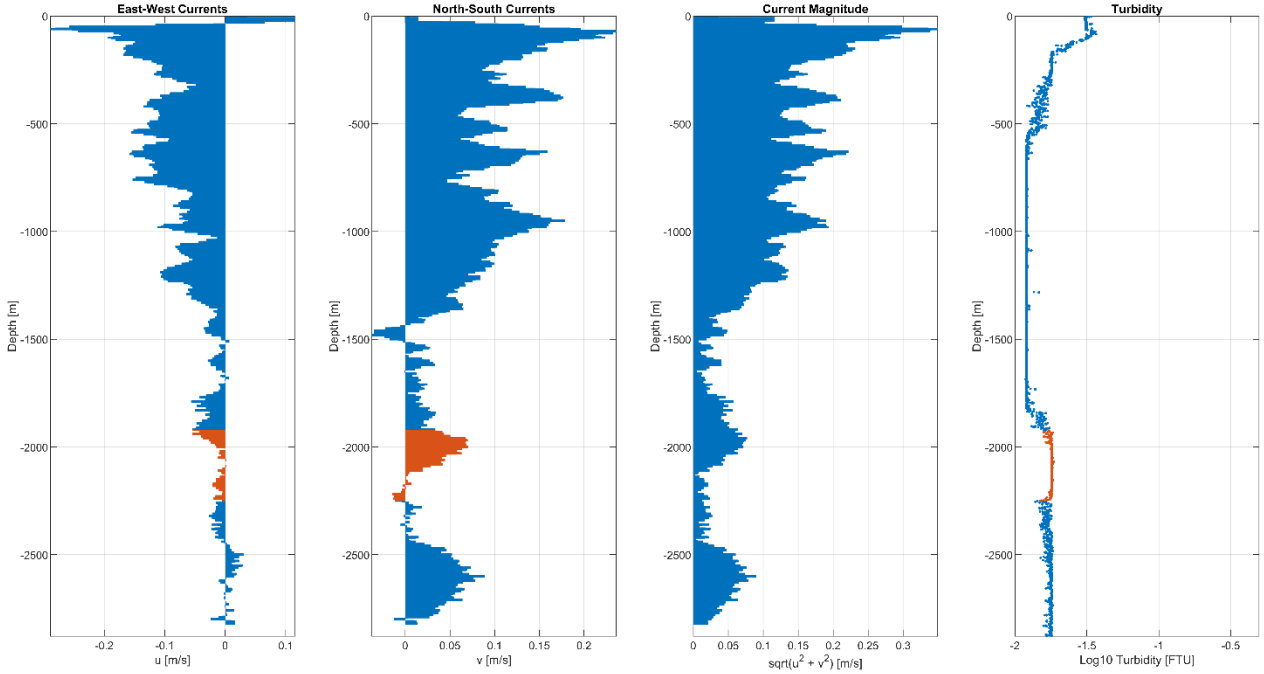

12.3 Biological nitrogen fixation

(Z. Wen)

Table 12.1 Sampling information by Biology_CTD

Sample No.	Station	Date (UTC)	Time (UTC)	Latitude _North	Longitude _West
1#	M176_2_3	2021-09-09	18:14	36° 13.487’	33° 55.046’
2#	M176_2_4	2021-09-10	18:00	36° 14.213’	33° 53.851’
3#	M176_2_5	2021-09-11	15:15	36° 13.762’	33° 54.137’
4#	M176_2_6	2021-09-12	14:28	36° 15.014’	33° 52.930’
5#	M176_2_7	2021-09-13	16:15	36° 13.824’	33° 54.114’
6#	M176_2_8	2021-09-14	14:41	36° 14.077’	33° 53.971’
7#	M176_2_9	2021-09-15	16:02	36° 16.582’	33° 53.768’
8#	M176_2_10	2021-09-16	16:11	36° 16.710’	33° 51.353’
9#	M176_2_12	2021-09-17	15:55	36° 14.776’	33° 53.796’
10#	M176_2_13	2021-09-18	17:07	36° 15.489’	33° 50.148’
11#	M176_2_14	2021-09-19	15:19	36° 14.240’	33° 49.994’
12#	M176_2_15	2021-09-20	16:50	36° 13.494’	33° 48.354’
13#	M176_2_16	2021-09-21	16:57	36° 13.190’	33° 47.135’
14#	M176_2_17	2021-09-22	16:05	36° 13.997’	33° 44.030’
15#	No sample	No sample	No sample	36° 16.149’	33° 44.012’
16#	M176_2_19	2021-09-24	14:58	36° 19.644’	33° 40.717’
17#	M176_2_21	2021-09-25	14:42	36° 23.278’	33° 37.576’
18#	M176_2_23	2021-09-26	14:30	36° 29.491’	33° 34.764’
19#	M176_2_24	2021-09-27	16:15	36° 33.264’	33° 34.823’

Table 12.2 Experiment information of bioassay incubations

Experiment No.	Date (UTC)	Time (UTC)	Latitude _North	Longitude _West	Incubation period (h)
1#	2021-09-05	12:50	45° 21’	17° 37’	49.67
2#	2021-09-12	03:40	36° 18.100’	33° 57.272’	51.50
3#	2021-09-16	03:00	36° 16.582’	33° 53.768’	52.00
4#	2021-09-19	02:20	36° 13.763’	33° 47.680’	53.17
5#	2021-09-22	23:10	36° 13.091’	33° 45.770’	54.83
6#	2021-09-24	19:30	36° 19.664’	33° 40.717’	60.67

(Zhongwei Yuan)

Table 12.3 Regular tow-fish sampling information

No.	UTC Date	UTC Time	Longitude [W]	Latitude [N]
100001	05/09/2021	12:50	17°37‘	45°21’
100002	06/09/2021	9:50	22°07‘	43°19’
100003	06/09/2021	18:20	23°32.078‘	42°35.901’
100004	06/09/2021	22:09	24°20.186‘	42°10.685’

Table 12.4 CTD sampling information

Station	UTC Date	UTC Time	Longitude [W]	Latitude [N]	Sample No.	Bottle	Depth (m)
Stn 3	09/09/2021	18:14	33°55.046‘	36°13.487’	30004	4	120
Stn 3	09/09/2021	18:14	33°55.046‘	36°13.487’	30010	10	80
Stn 3	09/09/2021	18:14	33°55.046‘	36°13.487’	30018	18	30
Stn 3	09/09/2021	18:14	33°55.046‘	36°13.487’	30020	20	20
Stn 3	09/09/2021	18:14	33°55.046‘	36°13.487’	30024	24	10
Stn 4	10/9/2021	18:00	33°53.851‘	36°14.213‘	30028	4	120
Stn 4	10/9/2021	18:00	33°53.851‘	36°14.213‘	30034	10	80
Stn 4	10/9/2021	18:00	33°53.851‘	36°14.213‘	30038	14	50
Stn 4	10/9/2021	18:00	33°53.851‘	36°14.213‘	30042	18	30
Stn 4	10/9/2021	18:00	33°53.851‘	36°14.213‘	30045	21	20
Stn 4	10/9/2021	18:00	33°53.851‘	36°14.213‘	30048	24	10
Stn 5	11/9/2021	15:15	33°54.137’	36°13.762'	30052	4	120
Stn 5	11/9/2021	15:15	33°54.137’	36°13.762'	30058	10	90
Stn 5	11/9/2021	15:15	33°54.137’	36°13.762'	30062	14	50
Stn 5	11/9/2021	15:15	33°54.137’	36°13.762'	30066	18	30
Stn 5	11/9/2021	15:15	33°54.137’	36°13.762'	30069	21	20
Stn 5	11/9/2021	15:15	33°54.137’	36°13.762'	30072	24	10
Stn 6	12/9/2021	14:28	33°52.930’	36°15.014'	30076	4	120
Stn 6	12/9/2021	14:28	33°52.930’	36°15.014'	30082	10	90
Stn 6	12/9/2021	14:28	33°52.930’	36°15.014'	30086	14	50
Stn 6	12/9/2021	14:28	33°52.930’	36°15.014'	30090	18	30
Stn 6	12/9/2021	14:28	33°52.930’	36°15.014'	30093	21	20
Stn 6	12/9/2021	14:28	33°52.930’	36°15.014'	30096	24	10
Stn 7	13/9/2021	16:15	33°54.114‘	36°13.824’	30100	4	120
Stn 7	13/9/2021	16:15	33°54.114‘	36°13.824’	30106	10	75
Stn 7	13/9/2021	16:15	33°54.114‘	36°13.824’	30110	14	50
Stn 7	13/9/2021	16:15	33°54.114‘	36°13.824’	30114	18	30
Stn 7	13/9/2021	16:15	33°54.114‘	36°13.824’	30117	21	20
Stn 7	13/9/2021	16:15	33°54.114‘	36°13.824’	30120	24	10
Stn 8	14/9/2021	14:41	33°53.971‘	36°14.077’	30124	4	120

Stn 8	14/9/2021	14:41	33°53.971‘	36°14.077’	30130	10	90
Stn 8	14/9/2021	14:41	33°53.971‘	36°14.077’	30134	14	50
Stn 8	14/9/2021	14:41	33°53.971‘	36°14.077’	30138	18	30
Stn 8	14/9/2021	14:41	33°53.971‘	36°14.077’	30141	21	20
Stn 8	14/9/2021	14:41	33°53.971‘	36°14.077’	30144	24	10
Stn 9	15/9/2021	16:02	33°53.768‘	36°16.582‘	30148	4	120
Stn 9	15/9/2021	16:02	33°53.768‘	36°16.582‘	30154	10	75
Stn 9	15/9/2021	16:02	33°53.768‘	36°16.582‘	30158	14	50
Stn 9	15/9/2021	16:02	33°53.768‘	36°16.582‘	30162	18	30
Stn 9	15/9/2021	16:02	33°53.768‘	36°16.582‘	30165	21	20
Stn 9	15/9/2021	16:02	33°53.768‘	36°16.582‘	30168	24	10
Stn 10	16/9/2021	16:11	33°51.353‘	36°16.710‘	30172	4	120
Stn 10	16/9/2021	16:11	33°51.353‘	36°16.710‘	30178	10	80
Stn 10	16/9/2021	16:11	33°51.353‘	36°16.710‘	30182	14	50
Stn 10	16/9/2021	16:11	33°51.353‘	36°16.710‘	30186	18	30
Stn 10	16/9/2021	16:11	33°51.353‘	36°16.710‘	30189	21	20
Stn 10	16/9/2021	16:11	33°51.353‘	36°16.710‘	30192	24	10
Stn 11	17/9/2021	15:55	33°53.796‘	36°14.776‘	30196	4	120
Stn 11	17/9/2021	15:55	33°53.796‘	36°14.776‘	30202	10	90
Stn 11	17/9/2021	15:55	33°53.796‘	36°14.776‘	30206	14	50
Stn 11	17/9/2021	15:55	33°53.796‘	36°14.776‘	30210	18	30
Stn 11	17/9/2021	15:55	33°53.796‘	36°14.776‘	30213	21	20
Stn 11	17/9/2021	15:55	33°53.796‘	36°14.776‘	30216	24	10
Stn 12	18/9/2021	17:07	33°50.184‘	36°15.489‘	30220	4	120
Stn 12	18/9/2021	17:07	33°50.184‘	36°15.489‘	30226	10	90
Stn 12	18/9/2021	17:07	33°50.184‘	36°15.489‘	30230	14	50
Stn 12	18/9/2021	17:07	33°50.184‘	36°15.489‘	30234	18	30
Stn 12	18/9/2021	17:07	33°50.184‘	36°15.489‘	30237	21	20
Stn 12	18/9/2021	17:07	33°50.184‘	36°15.489‘	30240	24	10
Stn 13	19/9/2020	15:19	33°49.994‘	36°14.240‘	30244	4	120
Stn 13	19/9/2021	15:19	33°49.994‘	36°14.240‘	30250	10	90
Stn 13	19/9/2021	15:19	33°49.994‘	36°14.240‘	30254	14	50
Stn 13	19/9/2021	15:19	33°49.994‘	36°14.240‘	30258	18	30
Stn 13	19/9/2021	15:19	33°49.994‘	36°14.240‘	30261	21	20
Stn 13	19/9/2021	15:19	33°49.994‘	36°14.240‘	30264	24	10
Stn 14	20/9/2020	16:50	33°48.354‘	36°13.494‘	30268	4	120
Stn 14	20/9/2021	16:50	33°48.354‘	36°13.494‘	30274	10	90
Stn 14	20/9/2021	16:50	33°48.354‘	36°13.494‘	30278	14	50
Stn 14	20/9/2021	16:50	33°48.354‘	36°13.494‘	30282	18	30
Stn 14	20/9/2021	16:50	33°48.354‘	36°13.494‘	30285	21	20
Stn 14	20/9/2021	16:50	33°48.354‘	36°13.494‘	30288	24	10
Stn 15	21/9/2021	17:22	33°47.135‘	36°13.190‘	30292	4	120
Stn 15	21/9/2021	17:22	33°47.135‘	36°13.190‘	30298	10	80
Stn 15	21/9/2021	17:22	33°47.135‘	36°13.190‘	30302	14	50
Stn 15	21/9/2021	17:22	33°47.135‘	36°13.190‘	30306	18	30
Stn 15	21/9/2021	17:22	33°47.135‘	36°13.190‘	30309	21	20
Stn 15	21/9/2021	17:22	33°47.135‘	36°13.190‘	30312	24	10
Stn 16	22/9/2021	16:05	33°44.030‘	36°13.997‘	30316	4	120
Stn 16	22/9/2021	16:05	33°44.030‘	36°13.997‘	30322	10	75
Stn 16	22/9/2021	16:05	33°44.030‘	36°13.997‘	30326	14	50

Stn 16	22/9/2021	16:05	33°44.030‘	36°13.997‘	30330	18	30
Stn 16	22/9/2021	16:05	33°44.030‘	36°13.997‘	30333	21	20
Stn 16	22/9/2021	16:05	33°44.030‘	36°13.997‘	30336	24	10
Stn 18	24/9/2021	14:58	33°40.717’	36°19.644‘	30364	4	120
Stn 18	24/9/2022	14:58	33°40.717’	36°19.644‘	30370	10	80
Stn 18	24/9/2023	14:58	33°40.717’	36°19.644‘	30374	14	50
Stn 18	24/9/2024	14:58	33°40.717’	36°19.644‘	30378	18	30
Stn 18	24/9/2025	14:58	33°40.717’	36°19.644‘	30381	21	20
Stn 18	24/9/2026	14:58	33°40.717’	36°19.644‘	30384	24	10
Stn 19	25/9/2021	14:42	33°37.576’	36°23.278‘	30388	4	120
Stn 19	25/9/2022	14:42	33°37.576’	36°23.278‘	30394	10	65
Stn 19	25/9/2023	14:42	33°37.576’	36°23.278‘	30398	14	50
Stn 19	25/9/2024	14:42	33°37.576’	36°23.278‘	30402	18	30
Stn 19	25/9/2025	14:42	33°37.576’	36°23.278‘	30405	21	20
Stn 19	25/9/2026	14:42	33°37.576’	36°23.278‘	30408	24	10
Stn 20	26/9/2021	13:53	33°34.764’	36°29.491‘	30412	4	120
Stn 20	26/9/2021	13:53	33°34.764’	36°29.491‘	30418	10	70
Stn 20	26/9/2021	13:53	33°34.764’	36°29.491‘	30422	14	50
Stn 20	26/9/2021	13:53	33°34.764’	36°29.491‘	30426	18	30
Stn 20	26/9/2021	13:53	33°34.764’	36°29.491‘	30429	21	20
Stn 20	26/9/2021	13:53	33°34.764’	36°29.491‘	30432	24	10
Stn 21	27/9/2021	16:29	33°34.823’	36°33.264‘	30434	2	120
Stn 21	27/9/2021	16:29	33°34.823’	36°33.264‘	30442	10	70
Stn 21	27/9/2021	16:29	33°34.823’	36°33.264‘	30446	14	50
Stn 21	27/9/2021	16:29	33°34.823’	36°33.264‘	30450	18	30
Stn 21	27/9/2021	16:29	33°34.823’	36°33.264‘	30453	21	20
Stn 21	27/9/2021	16:29	33°34.823’	36°33.264‘	30456	24	10

Table 12.5 Dilution experiment information

No.	UTC Date	UTC Time	Longitude [W]	Latitude [N]
1	12/09/2021	5:00	33°53.232‘	36°15.076’
2	14/09/2021	4:50	33°55.625‘	36°15.950’
3	20/09/2021	5:20	33°48.834‘	36°13.272
4	22/09/2021	0:10	33°45.770‘	36°03.091’
5	24/09/2021	0:40	33°47.182‘	36°11.233’
6	26/09/2022	5:01	33°35.620‘	36°28.336’

Table 12.6 Uptake experiment information

No.	UTC Date	UTC Time	Longitude [W]	Latitude [N]
1	16/09/2021	5:30	33°51.496‘	36°18.274’
2	26/09/2021	16:55	33°40.879‘	36°34.173’

12.4 Plume titanium CTD casts

(S. Poehle, K. Gosnell, L. Zhou, D. Jasinski)

Table 12.6 Parameters collected the plume casts of the trace metal clean rosette

Group of analytes	Detailed information	Responsible person
Mercury	DGM: Dissolved gaseous mercury MeHg: Methyl-mercury Hg-total (unfiltered sample aliquots)	Kathleen Gosnell Natalia Torres
Dissolved TM - GEOTRACES	Fe, Zn, Cd, Ni, Mn, Pb, Co (0.2 µm AcroPak filtered)	Eric Achterberg
Soluble TM	Fe, Zn, Cd, Ni, Mn, Pb, Co (0.2 µm AcroPak filtered)	Eric Achterberg
Fe isotopes	(0.2 µm AcroPak filtered)	Eric Achterberg
Ba isotopes and REE	REE: rare earth elements (0.2 µm AcroPak filtered)	Zhouling Zhang
Major elements	Mg, Ca, Sr, Li, K, Na, F (0.2 µm AcroPak filtered)	Zvi Steiner
Dissolved Al	(0.2 µm AcroPak filtered)	Linbin Zhou
Nutrients	(0.2 µm AcroPak filtered)	André Mutzberg
Particulate matter – TM	Fe, Zn, Cd, Ni, Mn, Pb, Co (0.2 µm PES filtered)	Linbin Zhou
Particulate matter - Fe	For Fe analysis via Synchroton (0.2 µm PES filtered)	Eric Achterberg
SQF	Sequential filtration (0.8 µm, 0.2 µm, 0.015 µm) for Pt, Zr, Nb, Ta, Hf, TM and ligands (unfiltered sample aliquots)	Andrea Koschinksy
UF	Ultrafiltration (10 kDa membrane) for Pt, Zr, Nb, Ta, Hf, TM and ligands (0.2 µm AcroPak filtered)	Andrea Koschinsky
Dissolved TM	Fe, Zn, Cu (0.2 µm AcroPak filtered)	Andrea Koschinsky
HFSE	High field strength elements: Zr, Hf, Nb, Ta (0.2 µm AcroPak filtered)	Andrea Koschinsky
Pt	(0.2 µm AcroPak filtered)	Andrea Koschinsky
Cr redox species	Cr^{3+}, Cr^{6+} and Cr(total) (0.2 µm AcroPak filtered)	Andrea Koschinsky
V redox species	V^{5+} and V^{4+} (0.2 µm AcroPak filtered)	Andrea Koschinksy
Fe ligands	(0.2 µm AcroPak filtered)	Andrea Koschinsky
Zn ligands	(0.2 µm AcroPak filtered)	Andrea Koschinsky
Cu ligands	(0.2 µm AcroPak filtered)	Andrea Koschinsky
Cr-total and δ53Cr	Isotope measurements and total concentration of Cr (0.2 µm AcroPak filtered)	Delphine Gilliard

Cr speciation_Cr^{3+}	Determination of Cr^{3+}(0.2 µm AcroPak filtered)	Delphine Gilliard

During transit between two stations a towed fish (device to sample surface seawater from approx. 3 m water depth under trace metal clean conditions) was operated at the starboard side of the ship in approx. 7 m distance and provided surface seawater into the clean laboratory container via a membrane pump. Samples taken were acidified with HCl according to the acidification described above under the laminar flow bench.

12.5 On-deck sampling of the trace metal Niskin bottles

(L. Blum)

Table 12.7 Stations along the plume and the parameters that were taken.

Station	Helium	oxygen	DIC	ammonia	DOC	salinity	nutrients	siderophores
M176/2-3 09.09.2021 36° 13,417' N 33° 54,794' W	x	x	x		x	x	x	x
M176/2-4 10.09.2021 36° 14,235' N 33° 53,831' W	x	x	x		x	x	x	x
M176/2-5 11.09.2021 36° 13,783' N 33° 54,182' W	x	x	x		x	x	x	x
M176/2-6 12.09.2021 36° 15,065' N 33° 52,968' W	x	x	x		x	x	x	
M176/2-7 13.09.2021 36° 13,836' N 33° 54,159' W	x	x	x		x	x	x	x
M176/2-8 14.09.2021 36° 14,076' N 33° 53,979' W	x	x	x		x	x	x	x
M176/2-9 15.09.2021 36° 16,556' N 33° 53,710' W	x	x	x		x	x	x	x
M176/2-10 16.09.2021 36° 16,693' N 33° 51,300' W	x	x	x		x	x	x	

Station	Helium	oxygen	DIC	ammonia	DOC	salinity	nutrients	siderophores
M176/2-12 17.09.2021 36° 14,799' N 33° 53,839' W	x	x	x		x	x	x	x
M176/2-13 18.09.2021 36° 15,518' N 33° 50,216' W	x	x	x		x	x	x	
M176/2-14 19.09.2021 36° 15,518' N 33° 50,216' W	x	x	x		x	x	x	x
M176/2-15 20.09.2021 36° 13,510' N 33° 48,380' W	x	x	x		x	x	x	
M176/2-16 21.09.2021 36° 13,189' N 33° 47,159' W	x	x	x		x	x	x	
M176/2-17 22.09.201 36° 13,964' N 33° 43,957' W	x	x	x		x	x	x	x
M176/2-18 23.09.201 36° 13,964' N 33° 43,957' W	x	x	x		x	x	x	
M176/2-19 24.09.201 36° 19,628' N 33° 40,706' W	x	x	x		x	x	x	
M176/2-21 25.09.201 36° 23,193' N 33° 37,578' W	x	x	x		x	x	x	x
M176/2-23 26.09.201 36° 29,486' N 33° 34,734' W	x	x	x		x	x	x	
M176/2-24 27.09.201 36° 33,390' N 33° 34,643' W	x	x	x		x	x	x	

Station	Helium	oxygen	DIC	ammonia	DOC	salinity	nutrients	siderophores

Table 12.8 Calculated dissolved oxygen concentrations and sample depths.

Date	Station No.	Depth [m]	Bedford No.	Bottle No.	Bottle factor	Factor Sodium thiosulphate	titr. mL Sodium thiosulphate	O2 [µmol/L]
9/9/2021	3		20002	151	46.579	0.993798696	5.777	267.42
9/9/2021	3		20024	156	46.584	0.993798696	5.612	259.81
9/9/2021	3		30004	165	50.485	0.993798696	4.593	230.44
9/9/2021	3		30024	167	49.989	0.993798696	4.420	219.58
9/10/2021	4		20026	104	46.358	0.993798696	5.458	251.45
9/10/2021	4		20048	172	49.739	0.993798696	5.015	247.90
9/10/2021	4		30028	194	50.064	0.993798696	4.688	233.25
9/10/2021	4		30038	233	47.099	0.993798696	4.628	216.62
9/11/2021	5		20052	165	50.485	0.993798696	5.347	268.27
9/11/2021	5		20066	167	49.989	0.993798696	5.322	264.39
9/11/2021	5		30052	156	46.584	0.993798696	5.060	234.25
9/11/2021	5		30072	151	46.579	0.993798696	4.715	218.26
9/11/2021	5		70009	104	46.358	0.993798696	5.175	238.41
9/11/2021	5		70010	172	49.739	0.993798696	4.623	228.52
9/11/2021	5		70011	194	50.064	0.993798696	4.248	211.35
9/11/2021	5		70012	233	47.099	0.993798696	4.165	194.95
9/11/2021	5		70013	180	49.879	0.993798696	5.577	276.45
9/12/2021	6		20074	187	49.631	0.993798696	5.395	266.10
9/12/2021	6		20096	234	46.627	0.993798696	5.638	261.25
9/12/2021	6		30076	190	49.710	0.993798696	4.695	231.94
9/12/2021	6		30096	232	46.432	0.993798696	4.697	216.74
9/12/2021	6		70014	190	49.710	0.993798696	5.360	264.79
9/12/2021	6		70015	165	50.485	0.993798696	5.100	255.88
9/12/2021	6		70016	151	46.579	0.993798696	4.982	230.62
9/12/2021	6		70018	194	50.064	0.993798696	4.138	205.88
9/13/2021	7		20098	233	47.099	0.993798696	5.705	267.03
9/13/2021	7		20120	172	49.739	0.993798696	5.300	261.98
9/13/2021	7		30100	167	49.989	0.993798696	4.715	234.24
9/13/2021	7		30120	156	46.584	0.993798696	4.718	218.42
9/13/2021	7		70019	165	50.485	0.993798696	5.293	265.56
9/13/2021	7		70020	172	49.739	0.993798696	5.183	256.20

9/13/2021	7		70023	151	46.579	0.993798696	4.250	196.73
9/14/2021	8		20122	167	49.989	0.993798696	5.367	266.63
9/14/2021	8		20144	194	50.064	0.993798696	5.310	264.19
9/14/2021	8		30124	233	47.099	0.993798696	4.850	227.01
9/14/2021	8		30144	190	49.710	0.993798696	4.423	218.50
9/14/2021	8		70024	180	49.879	0.993798696	5.405	267.92
9/14/2021	8		70025	190	49.710	0.993798696	5.200	256.89
9/14/2021	8		70026	172	49.739	0.993798696	4.643	229.51
9/14/2021	8		70027	104	46.358	0.993798696	3.643	167.84
9/14/2021	8		70028	187	49.631	0.993798696	4.277	210.95
9/15/2021	9		30148	151	46.579	0.993798696	4.768	220.71
9/15/2021	9		30168	232	46.432	0.993798696	5.768	266.16
9/15/2021	9		70029	165	50.485	0.993798696	5.270	264.41
9/15/2021	9		70030	234	46.627	0.993798696	5.505	255.09
9/15/2021	9		70031	167	49.989	0.993798696	4.548	225.94
9/15/2021	9		70032	233	47.099	0.993798696	3.712	173.75
9/15/2021	9		70033	194	50.064	0.993798696	4.188	208.37
9/16/2021	10		20170	187	49.631	0.993798696	5.808	286.47
9/16/2021	10		20192	104	46.358	0.993798696	5.333	245.70
9/16/2021	10		30172	172	49.739	0.993798696	4.805	237.52
9/16/2021	10		30192	190	49.710	0.993798696	4.500	222.31
9/17/2021	12		20194	232	46.432	0.993798696	5.782	266.80
9/17/2021	12		20216	180	49.879	0.993798696	5.335	264.45
9/17/2021	12		30196	151	46.579	0.993798696	4.982	230.62
9/17/2021	12		30216	104	46.358	0.993798696	4.737	218.24
9/17/2021	12		70034	156	46.584	0.993798696	5.702	263.97
9/17/2021	12		70035	187	49.631	0.993798696	5.152	254.11
9/17/2021	12		70036	167	49.989	0.993798696	4.713	234.14
9/17/2021	12		70037	165	50.485	0.993798696	3.933	197.33
9/17/2021	12		70038	234	46.627	0.993798696	4.527	209.77
9/18/2021	13		20218	194	50.064	0.993798696	5.370	267.18
9/18/2021	13		20240	233	47.099	0.993798696	5.648	264.36
9/18/2021	13		30220	194	50.064	0.993798696	4.673	232.50
9/18/2021	13		30240	233	47.099	0.993798696	4.800	224.67
9/19/2021	14		20242	234	46.627	0.993798696	5.338	247.35
9/19/2021	14		20264	165	50.485	0.993798696	4.883	244.99
9/19/2021	14		30264	232	46.432	0.993798696	4.728	218.17
9/19/2021	14		70039	190	49.710	0.993798696	5.365	265.04
9/19/2021	14		70040	167	49.989	0.993798696	5.138	255.25
9/19/2021	14		70041	172	49.739	0.993798696	4.688	231.73

9/19/2021	14		70042	187	49.631	0.993798696	3.925	193.59
9/19/2021	14		70043	156	46.584	0.993798696	4.518	209.16
9/20/2021	15		20266	165	50.485	0.993798696	5.325	267.17
9/20/2021	15		20288	104	46.358	0.993798696	5.782	266.38
9/20/2021	15		30268	151	46.579	0.993798696	5.040	233.30
9/20/2021	15		30288	232	46.432	0.993798696	4.695	216.65
9/21/2021	16		20290	167	49.989	0.993798696	5.465	271.50
9/21/2021	16		20310	180	49.879	0.993798696	5.383	266.83
9/21/2021	16		30295	165	50.485	0.993798696	4.588	230.19
9/21/2021	16		30312	104	46.358	0.993798696	4.830	222.52
9/22/2021	17		20314	180	49.879	0.993798696	5.388	267.08
9/22/2021	17		20336	167	49.989	0.993798696	5.303	263.45
9/22/2021	17		30316	232	46.432	0.993798696	4.925	227.26
9/22/2021	17		30336	151	46.579	0.993798696	4.688	217.01
9/23/2021	18		20338	156	46.584	0.993798696	5.768	267.03
9/23/2021	18		20360	233	47.099	0.993798696	5.571	260.76
9/24/2021	19		20362	104	46.358	0.993798696	5.800	267.21
9/24/2021	19		20384	165	50.485	0.993798696	5.305	266.16
9/24/2021	19		30364	180	49.879	0.993798696	4.690	232.48
9/24/2021	19		30384	167	49.989	0.993798696	4.480	222.56
9/25/2021	21		20386	167	49.989	0.993798696	5.380	267.27
9/25/2021	21		20408	180	49.879	0.993798696	5.315	263.46
9/25/2021	21		30388	104	46.358	0.993798696	4.895	225.52
9/25/2021	21		30406	165	50.485	0.993798696	4.370	219.25
9/25/2021	21		70044	194	50.064	0.993798696	5.325	264.94
9/25/2021	21		70045	190	49.710	0.993798696	5.225	258.12
9/25/2021	21		70046	234	46.627	0.993798696	4.958	229.74
9/25/2021	21		70047	172	49.739	0.993798696	3.995	197.48
9/25/2021	21		70048	187	49.631	0.993798696	4.175	205.92
9/26/2021	23		20410	232	46.432	0.993798696	5.770	266.25
9/26/2021	23		20432	233	47.099	0.993798696	5.553	259.92
9/26/2021	23		30412	151	46.579	0.993798696	4.845	224.28
9/26/2021	23		30432	156	46.584	0.993798696	4.715	218.28
9/27/2021	23		70054	187	49.631	0.993798696	5.365	264.62
9/27/2021	23		70055	190	49.710	0.993798696	5.173	255.55
9/27/2021	23		70056	167	49.989	0.993798696	4.648	230.91
9/27/2021	23		70057	234	46.627	0.993798696	4.225	195.78
9/27/2021	23		70058	194	50.064	0.993798696	4.242	211.06
9/27/2021	24		20434	180	49.879	0.993798696	5.395	267.43
9/27/2021	24		20456	172	49.739	0.993798696	5.305	262.23

9/27/2021	24		30436	156	46.584	0.993798696	4.740	219.44
9/27/2021	24		30456	151	46.579	0.993798696	4.923	227.89

Table 12.9 Sample volume and depths of particulate and dissolved Siderophores.

Date	Station No.	Bedford No.	depths in m	volume in L
09.09.21	M176-2-3	20002		2
09.09.21	M176-2-3	20008		2
09.09.21	M176-2-3	20010		1
09.09.21	M176-2-3	20014		2
09.09.21	M176-2-3	20018		2
09.09.21	M176-2-3	20024		2
09.09.21	M176-2-3	30006		2
09.09.21	M176-2-3	30011		2
10.09.21	M176-2-4	20026		2
10.09.21	M176-2-4	20030		2
10.09.21	M176-2-4	20034		2
10.09.21	M176-2-4	20038		2
10.09.21	M176-2-4	20042		2
10.09.21	M176-2-4	20048		2
10.09.21	M176-2-4	30029		2
10.09.21	M176-2-4	30034		2
10.09.21	M176-2-4	30035		2
11.09.21	M176-2-5	20058		2
11.09.21	M176-2-5	20060		2
11.09.21	M176-2-5	20062		2
11.09.21	M176-2-5	20064		1
11.09.21	M176-2-5	20066		1
11.09.21	M176-2-5	20070		2
11.09.21	M176-2-5	30053		2
11.09.21	M176-2-5	30058		2
11.09.21	M176-2-5	30059		2
13.09.21	M176-2-7	20104		2
13.09.21	M176-2-7	20106		2
13.09.21	M176-2-7	20108		2
13.09.21	M176-2-7	20110		2
13.09.21	M176-2-7	20112		2
13.09.21	M176-2-7	20114		2
13.09.21	M176-2-7	30101		1.5

13.09.21	M176-2-7	30106		2
13.09.21	M176-2-7	30107		2
14.09.21	M176-2-8	20126		2
14.09.21	M176-2-8	20128		2
14.09.21	M176-2-8	20130		1.7
14.09.21	M176-2-8	20134		2
14.09.21	M176-2-8	20136		2
14.09.21	M176-2-8	20138		2
14.09.21	M176-2-8	30125		2
14.09.21	M176-2-8	20130		2
14.09.21	M176-2-8	30131		2
15.09.21	M176-2-9	20152		2
15.09.21	M176-2-9	20152		2
15.09.21	M176-2-9	20154		2
15.09.21	M176-2-9	20156		2
15.09.21	M176-2-9	20158		2
15.09.21	M176-2-9	20160		2
15.09.21	M176-2-9	20162		2
15.09.21	M176-2-9	30149		2
15.09.21	M176-2-9	30154		2
15.09.21	M176-2-9	30155		2
17.09.21	M176-2-12	20198		2
17.09.21	M176-2-12	20202		2
17.09.21	M176-2-12	20204		1.8
17.09.21	M176-2-12	20206		1.8
17.09.21	M176-2-12	20208		1.8
17.09.21	M176-2-12	20212		1.6
17.09.21	M176-2-12	30197		2
17.09.21	M176-2-12	30202		2
17.09.21	M176-2-12	30203		2
19.09.21	M176-2-14	20252		2
19.09.21	M176-2-14	20254		2
19.09.21	M176-2-14	20256		2
19.09.21	M176-2-14	20258		2
19.09.21	M176-2-14	20260		2
19.09.21	M176-2-14	20262		2
20.09.21	M176-2-17	20318		2
20.09.21	M176-2-17	20322		2
20.09.21	M176-2-17	20324		2
20.09.21	M176-2-17	20326		2

20.09.21	M176-2-17	20328		2
20.09.21	M176-2-17	20330		2
20.09.21	M176-2-17	30317		2
20.09.21	M176-2-17	30322		1.8
20.09.21	M176-2-17	30323		2
25.09.21	M176-2-21	20386		2
25.09.21	M176-2-21	20390		2
25.09.21	M176-2-21	20394		2
25.09.21	M176-2-21	20396		2
25.09.21	M176-2-21	20400		2
25.09.21	M176-2-21	20404		1
25.09.21	M176-2-21	30389		2
25.09.21	M176-2-21	30394		2
25.09.21	M176-2-21	30398		2

12.6 Chromium samples

(D. Gilliard)

Table 12.10 Stations for Cr samples ([Cr], Cr isotopes, and Cr speciation) and their respective labels and depths. Refer to the porewater and sediments tables for the corresponding Cr samples.

Station ID	**Depth (m)**	**Samples (1L)**	**Samples (3x15mL)**
		[Cr] and δ53Cr	Cr speciation
M176/2_3	2489	20001	20001
36°13418 °N	2195	20005	
33°54794 °W	2147	20007	
	2097	20009	20009
	2049	20011	
	1999	20013	
	1599	20023	20023
M176/2_4	2286	20025	20025
36°53235 °N	2246	20027	
33°55831 °W	2196	20029	20029
	2145	20031	
	2095	20033	20033
	2045	20035	
	1996	20037	
	1897	20041	20041
	1697	20045	
	1598	20047	20047
M176/2_5	2289	20049	20049

36°13782 °N	2187	20053	20053
33°54153 °W	2140	20055	
	2092	20057	20057
	2041	20059	
	1990	20061	
	1939	20063	20063
	1890	20065	
	1695	20069	
	1593	20071	20071
M176/2_7	2312	20097	20097
36°13837 °N	2236	20101	20101
33°54165 °W	2203	20103	
	2173	20105	20105
	2160	20107	
	2122	20109	
	2094	20111	20111
	2040	20113	
	1878	20117	
	1778	20119	20019
M176/2_9	2475	20145	20145
36°16583 °N	2297	20149	20149
33°53694 °W	2198	20151	
	2173	20153	20153
	2150	20155	
	2125	20157	
	2099	20159	20159
	2074	20161	
	2023	20165	
	1899	20167	20167
M176/2_15	3034	20265	20265
36°13509 °N	2592	20269	
33°48380 °W	2196	20273	
	2096	20277	20277
	2044	20281	20281
	1894	20287	20287
M176/2_16	2389		20289
36°13189 °N	2120		20297
33°47159 °W	2070		20301
	1897		20311

M176/2_18	2388	20337	20337
36°16149 °N	2249	20341	
33°44022 °W	2171	20345	20345
	2120	20349	
	2093	20351	20351
	1984	20357	20357
	1783	20359	20359
M176/2_23	2135	20409	20409
36°29486 °N	2020	20417	20417
33°34734 °W	1971	20421	20421
	1898	20427	20427
	1697	20431	20431

12.7 In-situ pumps

(Z. Zhang)

Table 12.11 Sample ID of filter samples from in-situ pumps.

Pump ID	Depth (m)	Filter type	Volume pumped (L)	Sample ID	Comment
9-Sep	*M176/2_3*				
C1	2250	Quartz	98	50001	
C2	2150	PES	-3	50002	Pump didn’t work, sampled as Blank
C3	2100	Quartz	686	50003	
C4	2050	PES	0	50004	Pump didn’t work, sampled as Blank
C5	2000	Quartz	597	50005	
C6	1900	PES	826	50006	
10-Sep	*M176/2_4*				
C1	2250	Quartz	353	50007	
C2	2150	PES	-4	50009	Pump didn’t work, sampled as Blank
C3	2100	Quartz	543	50008	
C6	1900	PES	464	50010	
11-Sep	*M176/2_5*				
C1	2250	Quartz	404	50011	
C3	2150	Quartz	547	50012	
C5	2050	Quartz	706	50013	
C6	1900	PES	313	50014	
12-Sep	*M176/2_6*				
C1	2150	Quartz	42	50015	
C2	2100	PES	302	50016	
C3	2050	Quartz	96	50017	
C4	2000	PES	65	50018	
C5	1950	Quartz	448	50019	
13-Sep	*M176/2_7*				

C5	1900	Quartz	1063	50020	

Table 12.12 Sample ID of PES filters (25mm punch) from in-situ pumps taken for Metal mineralogy analysis.

Station	Sta.03	Sta.04	Sta.05	Sta.06
Date	9/9	9/10	9/11	9/12
Sample ID	50002	50009	50014	50016
	50004	50010		50018
	50006			

Table 12.13 Sample ID of PES filters (25mm) from Niskin bottles taken for Metal speciation analysis.

Station	**Sta.07**	**Sta.08**	**Sta.09**	**Sta.10**	**Sta.12**	**Sta.13**	**Sta.14**	**Sta.15**
Date	*9/13*	*9/14*	*9/15*	*9/16*	*9/17*	*9/18*	*9/19*	*9/20*
Sample ID	20098	20121	20147	20169	20196	20222	20242	20268
	20104	20123	20151	20181	20204	20230	20254	20278
	20106	20127	20155	20183	20206	20232	20256	20280
	20112	20137	20157	20185	20208	20234	20258	20282
	20116	20139	20165	20191	20214	20240	20264	20288
Station	**Sta.16**	**Sta.17**	**Sta.18**	**Sta.19**	**Sta.21**	**Sta.23**	**Sta.24**	
Date	*9/21*	*9/22*	*9/23*	*9/24*	*9/25*	*9/26*	*9/27*	
Sample ID	20290	20316	20338	20362	20386	20410	20434	
	20300	20326	20348	20368	20390	20414	20440	
	20302	20328	20350	20372	20394	20418	20446	
	20304	20330	20352	20376	20400	20422	20450	
	20312	20336	20354	20384	20408	20430	20456	
			20360					

12.8 Radium

(L. Viera and P. Battermann)

Table 12.14 Stations for Ra isotope samples, type of samples collected and their respective depths. ISP (in-situ pump) refers to samples collected from the in-situ pumps using Mn-cartridges, and CTD refers to the seawater samples collected from the CTD bottles and filtered through Mn-fibers.

Station ID	**Sample type**	**Depth**
M176/2_3	Mn-cartridge, ISP	2100 m and 1900 m
M176/2_4	Mn-cartridge, ISP Pore water Overlying water	2250 m, 2100 m, and 1900 m 1 cm, 3 cm, 6 cm, 9 cm, 12 cm, 15 cm, 18 cm, and 21 cm
M176/2_5	Mn-cartridge, ISP	2250 m, 2150 m, 2050 m, and 1900 m
M176/2_6	Mn-cartridge, ISP Pore water Overlying water	2100 and 1800 m 1 cm, 3 cm, 6 cm, 9 cm, 12 cm, 15 cm, 18 cm, and 21 cm
M176/2_7	Mn-cartridge, ISP	1900 m

	Mn-fiber, CTD Pore water Overlying water	2275m and 2190 m 1 cm, 3 cm, 6 cm, 9 cm, 12 cm, 15 cm, 18 cm, 21 cm, and 24 cm
M176/2_8	Mn-fiber, CTD Pore water Overlying water	2296 m, 2250 m, 2200 m, 2156 m, and 1687 m 1 cm, 3 cm, 6 cm, 9 cm, 12 cm, 15 cm, and 18 cm
M176/2_9	Mn-fiber, CTD	2366 m, 2269 m, 2158 m, 2129 m, 2120 m and 1946 m
M176/2_10	Mn-fiber, CTD Pore water Overlying water	2371m, 2273m, 2370 m, 2199m, 2076m, 1682 m 1 cm, 3 cm, 6 cm, and 9 cm
M176/2_11	Mn-fiber, CTD	2238 m, 2195 m, 2126 m, and 2049 m
M176/2_12	Mn-fiber, CTD Pore water Overlying water	2173 m, 2125 m, 2114 m, 2062 m, 2017 m, and 1697 m 3 cm, 6 cm, 9 cm, 12 cm, 15 cm, 18 cm, 21 cm, 24 cm and 27 cm
M176/2_13	Mn-fiber, CTD	2371 m, 2270 m, 2185 m, 2092 m, 2036 m, and 1689 m
M176/2_14	Mn-fiber, CTD	2470 m, 2224 m, 2099 m, 2039 m, and 1697 m
M176/2_15	Mn-fiber, CTD	2397 m, 2299 m, 2068 m, 1993 m, and 1678 m
M176/2_16	Mn-fiber, CTD	2499 m, 2398 m, 2188 m, 2076 m, and 1497 m
M176/2_17	Mn-fiber, CTD	2571 m, 2471 m, 2198 m, 2097 m, and 1699 m
M176/2_18	Mn-fiber, CTD	2500 m, 2400 m, 2148 m, 2183 m, and 1485 m
M176/2_19	Mn-fiber, CTD Overlying water	2422 m, 2269 m, 2299 m, 2148 m, and 1597 m
M176/2_20	Mn-fiber, CTD	2200 m
M176/2_21	Mn-fiber, CTD	2223 m, 2123 m, 2055 m, 1897 m, and 1697 m
M176/2_23	Mn-fiber, CTD Overlying water	2077 m, 1977 m, 1947 m, 1847 m, and 1698 m
M176/2_24	Mn-fiber, CTD Overlying water	2665 m, 2467 m, 2167 m, 1587 m, 1497 m

12.8 Thorium

(D. Gilliard[)]

Table 12.15 Stations for ^{234}Th, ^{238}U, and ^{230}Th samples

Station ID	Date	^{234}Th, ^{238}U	^{230}Th
M176/2_3	09.09.21	2250m, 2150m, 2100m, 2050m, 2000m, 1900m	2250m, 2150m, 2100m, 2050m, 2000m, 1900m
M176/2_4	10.09.21	2250m, 2150m, 2100m, 2050m, 1900m	2250m, 2150m, 2100m, 2050m, 1900m
M176/2_5	11.09.21	2250 m, 2200 m, 2100 m, 2050m, 1900m	2250m, 2200 m, 2125m, 2100m, 2050m, 1900m
M176/2_6	12.09.21	2150m, 2100m, 2000m, 1950m, 1800m	2150m, 2100m, 2050m, 2000m, 1950m, 1800m
M176/2_7	13.09.21	2150m, 2100m, 2050m, 1950m, 1750m	2150m, 2100m, 2050m, 1950m, 1750m

M176/2_8	14.09.21	2296 m, 2250 m, 2200 m, 2156 m, 1687m	2296 m, 2250 m, 2200 m, 2156 m, 1687m
M176/2_9	15.09.21	2366m, 2269m, 2158m, 2129m, 2120m, 1946 m	2366m, 2269m, 2158m, 2129m, 2120m, 1946 m
M176/2_10	16.09.21	2371m, 2273m, 2370m, 2199m, 2076m, 1682m	2371m, 2273m, 2370m, 2199m, 2076m, 1682m
M176/2_12	17.09.21	2173m, 2125m, 2114m, 2062m, 2017m, 1697m	2173m, 2125m, 2114m, 2062m, 2017m, 1697m
M176/2_13	18.09.21	2371m, 2270m, 2185m, 2092m, 1689m	2371m, 2270m, 2185m, 2092m, 2036m, 1689m
M176/2_14	19.09.21	2470m, 2224m, 2099m, 2039m, 1697m	2470m, 2224m, 2099m, 2039m, 1697m
M176/2_15	20.09.21	2397m, 2299m, 2068m, 1993m, 1678m	2397m, 2299m, 2068m, 1993m, 1678m
M176/2_16	21.09.21	2499 m, 2398 m, 2188 m, 2076 m, 1497 m	2499 m, 2398 m, 2188 m, 2076 m, and 1497 m
M176/2_17	22.09.21	2571m, 2471m, 2198m, 2097m, 1699m	2571m, 2471m, 2198m, 2097m, 1699m
M176/2_18	23.09.21	2500m, 2400m, 2148m, 2183 m, 1485m	2500m, 2400m, 2148m, 2183 m, 1485m
M176/2_19	24.09.21	2422m, 2269m, 2299m, 2148m, 1597m	2422m, 2269m, 2299m, 2148m, 1597m
M176/2_21	25.09.21	2223m, 2123m, 2055m, 1897m, 1697m	2223m, 2123m, 2055m, 1897m, 1697m
M176/2_23	26.09.21	2077m, 1977m, 1947m, 1847m, 1698m	2077m, 1977m, 1947m, 1847m, 1698m
M176/2_24	27.09.21	2665m, 2467m, 2167m, 1587m, 1497m	2665m, 2467m, 2167m, 1587m, 1497m

Fig. 12.2 Particulate ^{234}Th from station M176/2_11, above the Rainbow vent.

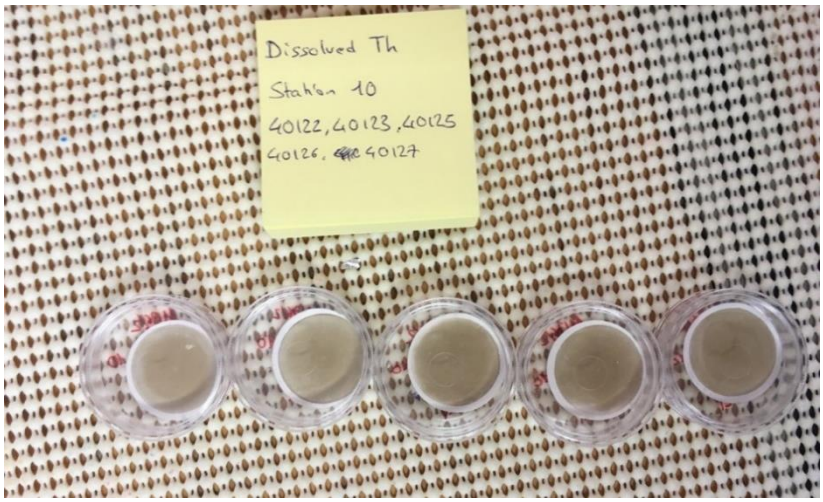

Fig. 12.3 Dissolve ^{234}Th from station M176/2_10.

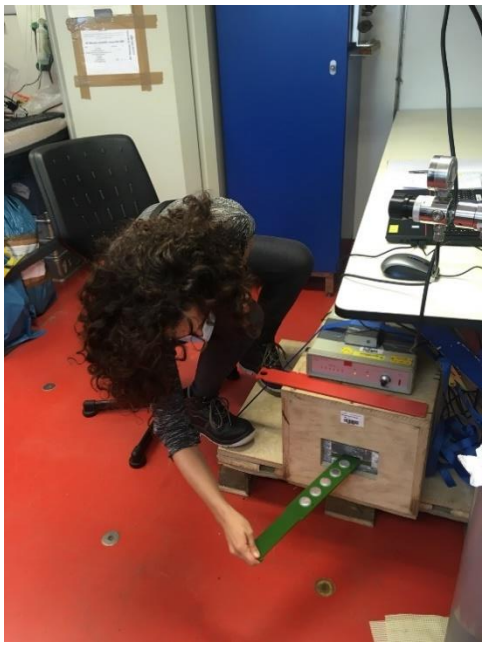

Fig. 12.4 Measurements of dissolve or particulate Th234 on the Risø low-level beta GM multicounter.

Fig. 12.5 Sampling of ^{230}Th and ^{234}Th

12.10 Sediment and porewater

(Z. Steiner, N. Glock, Z. Zhang, S. Krüger)

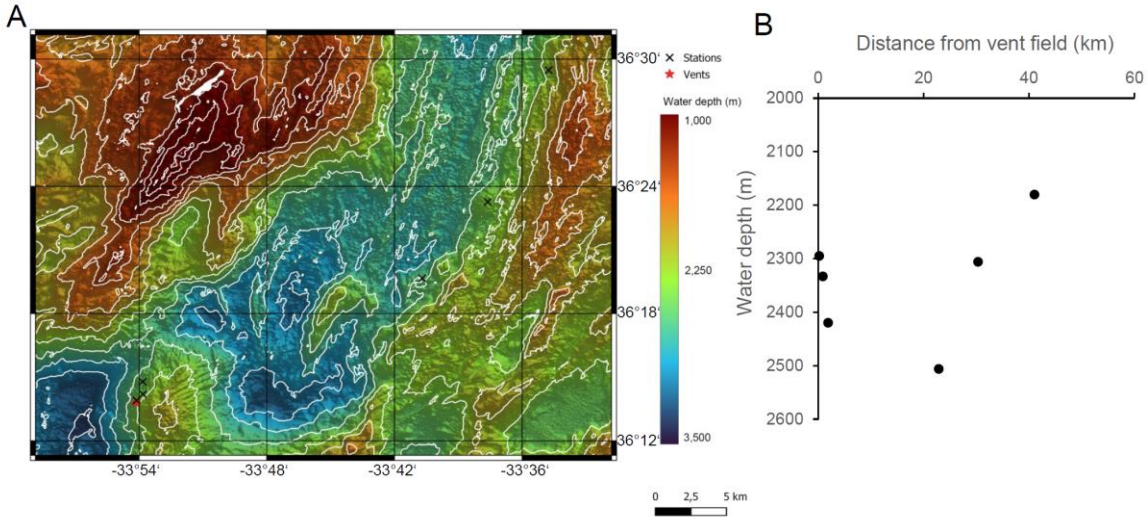

Fig. 12.6 A: Map of the sampling area. MUC sampling locations for Rose Bengal staining are marked with a black x. Rainbow vent site is marked with a red star. B: Distance of sampling locations for Rose Bengal staining from the Rainbow vent site.

Table 12.16 Porewater and sediment samples taken for stable barium isotopes and silicon isotopes.

Station	Date	Sediment core	Only surface sediment	Porewater samples	Rose Bengal samples
M176/2_3	9/9		√		
M176/2_4	9/10	√		√	√
M176/2_5	9/11		√		

M176/2_6	9/12	√		√	
M176/2_7	9/13	√		√	√
M176/2_8	9/14	√		√	
M176/2_9	9/15		√		
M176/2_10	9/16	√		√	
M176/2_12	9/17	√		√	√
M176/2_13	9/18		√		
M176/2_14	9/19		√		
M176/2_15	9/20		√		
M176/2_16	9/21		√		
M176/2_17	9/22		√		
M176/2_19	9/24	√		√	√
M176/2_21	9/25	√			√
M176/2_23	9/26	√		√	√
M176/2_24	9/27	√		√	

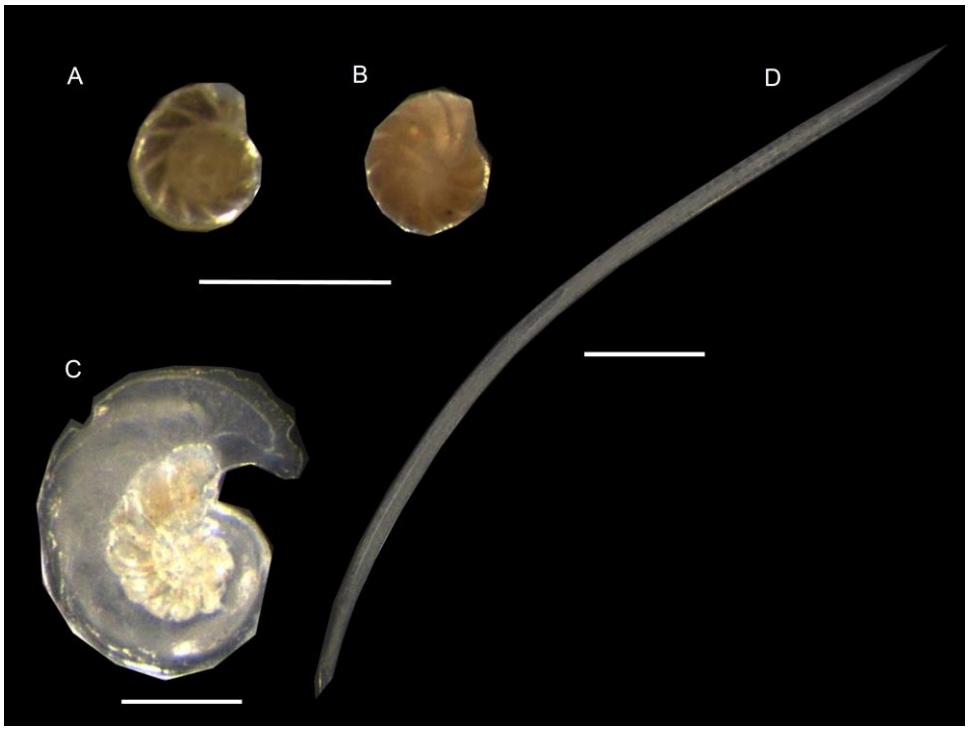

Fig. 12.7 Examples of meiofauna observed in the >125 µm fraction of surface sediments. A&B: Cibicides robertsonianus (A = spiral side; B = umbilical side); C: *Laticarinina pauperata*; D: Nematode; Scale bar: 500 µm.

12.11 Aerosols

(E. Achterberg)

Table 12.17 Aerosol samples collected during the cruise

Filter	Number on filter	Rate (m3/h)	start	end	Volume pumped (m3)	Accumulated volume	Comment
1	B15	60	05.09 1740 h	07.09 17:40 h	2692.3	4078	
2	R13	60	07.09 20:09 h	09.09 20:09 h	2863	6941	

3	43	60	10.09 1943 h	13.09 07:10 h	73.1	7014	Flow alarm Pump stopped
4	44	60	13.09 07:13 h	15.09 07:13 h	2548.3		
5	R16	60	15.09 15:37 H	17.09 10.15 H	2030	11504	NOT QUITE 48 h
6	45	60	17.09 10:19 H	19.09 10:19 H	2297.5	13800	Finished cycle
7	R3	60	20.09 19:43 H	22.09 18:57 H	1641.6	15441	Flow alarm. Pump stopped
8	43	60	22.09 18:57 H	24.09 19:58 H	724.9		Flow alarm pump stopped
9	R15	60	24.09 19:58 H	26.09 20:19 H	2067.2	18233	Finished cycle
10	R6	60	26.09 20:20 H	27.09 18:38 H	1300		Stopped after ca. 22 h as we had reached the EEZ oft he Azores
11	48	60	01.10 12:12 H	04.10 06:13 H	446.4		Sampled in intern. Waters north of Azores. Hope to sample aerosols from La Palma volcano outbreak. Wind was mostly from behind the vessel and pump was hence switched off.
Instru mental blank 1	48	0	01.10				Filter placed in aerosol collector and removed again
Instr bl 2	81	0	01.10				See above
Instr bl 3	R1	0	01.10				See above

All times are UTC
Flow duration set for 48 h for aerosol collection

12.12 Nutrients

Fig. 12.8 Typical nutrient measurement setup with SEAL-Analytical-Quaatro39 Segmented flow analyser on ship

12.13 Ammonium dynamics samples

(J. Liu and Q. Jia)

Table 12.19 Summary for all the collected sample and measurment method

Collected sample	Total number	Measuring method/ equipment	Institution
Trace ammonium	340	Carry Eclipse Fluorescence detector	GEOMAR
N15-NOx	850	NaN2 method and IRMS	GEOMAR
N15-PN	930	Denitrification bacteria method and IRMS	Xiamen University
Flow cytometry	288	FACS Calibur flow cytometer	GEOMAR
FRRf	256	Fast Ocean fluorescence detector	GEOMAR

Table 12.20 Sampling CTD details of NH_4^+ and nitrification rate

Station	Date	CTD Cast	Time (UTC)	Latitude (N)	Longitude (W)	NH_4^+	Nitrification Rate
M176/2_3	09/09/2021	deep	06:26	36° 13,417'	33° 54.794'	✓	✓
		shallow	17:58	36° 13.475'	33° 55.077'	✓	
M176/2_4	10/09/2021	deep	05:48	36° 14.235'	33° 53.831'	✓	
		shallow	17:43	36° 14.211'	33° 53.848'	✓	
M176/2_5	11/09/2021	deep	06:00	36° 13.783'	33° 54.182'	✓	✓
		shallow	14:44	36° 13.763'	33° 54.174'	✓	✓
M176/2_7	13/09/2021	deep	05:32	36° 13.836'	33° 54.159'	✓	
		shallow	15:54	36° 13.825'	33° 54.113'	✓	✓
M176/2_8	14/09/2021	deep	05:43	36° 14.076'	33° 53.979'	✓	
		shallow	14:18	36° 14.078'	33° 53.966	✓	✓
M176/2_9	15/09/2021	deep	05:41	36° 16.556'	33° 53.710'	✓	
		shallow	15:42	36° 16.559'	33° 53.701'	✓	✓
M176/2_10	16/09/2021	deep	06:00	36° 16.693'	33° 51.300'	✓	
		shallow	15:49	36° 16.683'	33° 51.299'	✓	✓
M176/2_11	17/09/2021	deep	05:34	36° 14.799'	33° 53.839'	✓	
		shallow	15:35	36° 14.776'	33° 53.796'	✓	✓
M176/2_12	18/09/2021	deep	06:05	36° 15.518'	33° 50.216'	✓	
		shallow	16:48	36° 15.495'	33° 50.181'	✓	✓
M176/2_13	19/09/2021	deep	05:37	36° 14.222'	33° 50.062'	✓	
		shallow	14:58	36° 14.175'	33° 50.007'	✓	
M176/2_14	20/09/2021	deep	05:53	36° 13.510'	33° 48.380'	✓	
		shallow	16:30	36° 13.491'	33° 48.357'	✓	✓
M176/2_17	22/09/2021	deep	05:41	36° 13.964'	33° 43.957'	✓	✓
		shallow	15:51	36° 13.983'	33° 43.924'	✓	✓
M176/2_18	23/09/2021	deep	07:55	36° 16.149'	33° 44.022'	✓	
		shallow	17:07	36° 16.177'	33° 43.985'	✓	
M176/2_19	24/09/2021	deep	05:46	36° 19.628'	33° 40.706'	✓	
		shallow	14:37	36° 19.654'	33° 40.682'	✓	✓
M176/2_21	25/09/2021	deep	06:08	36° 23.193'	33° 37.578'	✓	
		shallow	14:21	36° 23.226'	33° 37.554'	✓	
M176/2_22	26/09/2021	deep	05:33	36° 29.486'	33° 34.734'	✓	
		shallow	13:30	36° 29.519'	33° 34.778'	✓	✓
M176/2_24	27/09/2021	deep	06:01	36° 33.390'	33° 34.643'	✓	
		shallow	16:08	36° 33.430'	33° 34.882'	✓	✓

12.14 Jacobs University Bremen samples

(L. Klose, S. Pöhle, V. Menon)

Table 12.21 List of all sampled stations and the respective sampling program.

Date	Station ID	Latitude	Longitude	superstation	normal station
09.09.2021	M176/2_3	36° 13,418 'N	33° 54,794 'W	x	
10.09.2021	M176/2_4	36° 14.235 'N	33° 53.831 'W		x
11.09.2021	M176/2_5	36° 13.732 'N	33° 54.153 'W	x	
12.09.2021	M176/2_6	36° 15,097 'N	33° 53.033 'W		x
13.09.2021	M176/2_7	36° 13.847 'N	33° 54.165 'W	x	
14.09.2021	M176/2_8	36° 14.076 'N	33° 53.979 'W		x
15.09.2021	M176/2_9	36° 16.583 'N	33° 53.694 'W	x	
16.09.2021	M176/2_10	36 °16.693 'N	33° 51.300 'W		x
17.09.2021	M176/2_11	36° 14.806 'N	33° 53.844 'W	x	
18.09.2021	M176/2_13	36° 15.517 'N	33° 50.216 'W		x
19.09.2021	M176/2_14	36° 14.178 'N	33° 50.100 'W		x
20.09.2021	M176/2_15	36° 13.509 'N	33° 48.380 'W	x	
22.09.2021	M176/2_17	36° 13.966 'N	33° 43.988 'W		x
23.09.2021	M176/2_18	36° 16.149 'N	33° 44.022 'W	x	
25.09.2021	M176/2_21	36° 23.248 'N	33° 37.599 'W		x
27.09.2021	M176/2_24	36° 33.426 'N	33° 34.686 'W	x	

Table 12.22 Overview of all collected subsamples in their respective size fractions.

	Clean lab	Sequential Filtration			Ultrafiltration	
size fraction	**0.2 µm**	**0.8 µm**	**0.2 µm**	**0.015 µm**	**<10 kDa**	**>10 kDa**
TM	151	29	29	29	13	12
HFSE	151	29	29	29	13	10
Pt	91	29	29	29	13	9
Cr	81	-	-	-	-	-
V	81	-	-	-	-	-
FeL	64	28	28	28	13	4
ZnL	28	-	-	-	-	-
CuL	28	-	-	-	-	-
Filter	-	29	29	29	-	-

Table 12.24 Sampling CTD details of Fe/N limitation experiment at DCM layer

Station	Date	CTD Cast	Time (UTC)	Latitude (N)	Longitude (W)	Depth	NH4 uptake rate	NO3 uptake Rate	Nitrification Rate	Chla	Flow Cytometry	FRRF
M176/2_3	09/09/2021	shallow	17:58	36° 13.475'	33° 55.077'	DCM	✓	✓	✓	✓	✓	✓
M176/2_7	13/09/2021	shallow	15:54	36° 13.825'	33° 54.113'	DCM	✓	✓	✓	✓	✓	✓
M176/2_8	14/09/2021	shallow	14:18	36° 14.078'	33° 53.966	DCM	✓	✓	✓	✓	✓	✓
M176/2_9	15/09/2021	shallow	15:42	36° 16.559'	33° 53.701'	DCM	✓	✓	✓	✓	✓	✓
M176/2_10	16/09/2021	shallow	15:49	36° 16.683'	33° 51.299'	DCM	✓	✓	✓	✓	✓	✓
M176/2_11	17/09/2021	shallow	15:35	36° 14.776'	33° 53.796'	DCM	✓	✓	✓	✓	✓	✓
M176/2_12	18/09/2021	shallow	16:48	36° 15.495'	33° 50.181'	DCM	✓	✓	✓	✓	✓	✓
M176/2_17	22/09/2021	shallow	15:51	36° 13.983'	33° 43.924'	DCM	✓	✓	✓	✓	✓	✓
M176/2_18	23/09/2021	shallow	17:07	36° 16.177'	33° 43.985'	DCM	✓	✓	✓	✓	✓	✓
M176/2_21	25/09/2021	shallow	14:21	36° 23.226'	33° 37.554'	DCM	✓	✓	✓	✓	✓	✓
M176/2_22	26/09/2021	shallow	13:30	36° 29.519'	33° 34.778'	DCM	✓	✓	✓	✓	✓	✓

Table 12.25 Overview of stations sampled with TM clean CTD and the parameters for which aliquots were collected in the clean laboratory container. This table includes all parameters related to workgroups from GEOMAR.

Parameter / Station	DGM	Me-Hg	Hg-total	Diss TM – GEOTRACES	Diss TM – GEOTRACES Storage	Soluble TM	Fe isotopes	Ba isotopes and REE	Dissolved Al	Major elements	Nutrients	Particulate matter - TM	Particulate matter - Fe analysis
M176/2-3 09.09.2021 36° 13,417' N 33° 54,794' W	x	X	x	x		x	x	x	x		x		

Parameter / Station	DGM	Me-Hg	Hg-total	Diss TM – GEO-TRACES	Diss TM – GEO-TRACES Storage	Soluble TM	Fe isotopes	Ba isotopes and REE	Dissolved Al	Major elements	Nutrients	Particulate matter - TM	Particulate matter - Fe analysis
M176/2-4 10.09.2021 36° 14,235' N 33° 53,831' W	x	X	x	x		x	x	x	x	x	x	x	
M176/2-5 11.09.2021 36° 13,783' N 33° 54,182' W	x	X	x	x		x	x	x	x	x	x	x	
M176/2-6 12.09.2021 36° 15,065' N 33° 52,968' W	x	X	x	x	x		x	x	x	x	x	x	
M176/2-7 13.09.2021 36° 13,836' N 33° 54,159' W	x	X	x	x	x	x	x	x	x	x	x	x	x
M176/2-8 14.09.2021 36° 14,076' N 33° 53,979' W	x	X	x	x	x	x	x	x	x	x	x	x	x
M176/2-9 15.09.2021 36° 16,556' N 33° 53,710' W	x	X	x	x	x	x	x	x	x	x	x	x	x
M176/2-10 16.09.2021	x	X	x	x	x	x	x	x	x	x	x	x	x

Parameter / Station	DGM	Me-Hg	Hg-total	Diss TM – GEOTRACES	Diss TM – GEOTRACES Storage	Soluble TM	Fe isotopes	Ba isotopes and REE	Dissolved Al	Major elements	Nutrients	Particulate matter - TM	Particulate matter - Fe analysis
36° 16,693' N 33° 51,300' W													
M176/2-12 17.09.2021 36° 14,799' N 33° 53,839' W	x	x	x	x	x	x	x	x	x	x	x	x	x
M176/2-13 18.09.2021 36° 15,518' N 33° 50,216' W	x	x	x	x	x	x	x	x	x	x	x	x	x
M176/2-14 19.09.2021 36° 15,518' N 33° 50,216' W	x	x	x	x	x	x	x	x	x	x	x	x	x
M176/2-15 20.09.2021 36° 13,510' N 33° 48,380' W	x	x	x	x	x	x	x	x	x	x	x	x	x
M176/2-16 21.09.2021 36° 13,189' N 33° 47,159' W	x	x	x	x	x	x	x	x	x	x	x	x	X
M176/2-17 22.09.201 36° 13,964' N 33° 43,957' W	x	x	x	x	x	x	x	x	x	x	x	x	x

Parameter / Station	DGM	Me-Hg	Hg-total	Diss TM – GEO-TRACES	Diss TM – GEO-TRACES Storage	Soluble TM	Fe isotopes	Ba isotopes and REE	Dissolved Al	Major elements	Nutrients	Parti-culate matter - TM	Parti-culate matter - Fe analysis
M176/2-18 23.09.201 36° 13,964' N 33° 43,957' W	x	x	X[a]	x	x	x	x	x	x	x	x	x	x
M176/2-19 24.09.201 36° 19,628' N 33° 40,706' W	x	x	x	x	x	x	x	x	x		x	x	x
M176/2-21 25.09.201 36° 23,193' N 33° 37,578' W				x	x	x	x	x	x		x	x	x
M176/2-23 26.09.201 36° 29,486' N 33° 34,734' W	x	x	x	x	x	x	x	x	x		x	x	x
M176/2-24 27.09.201 36° 33,390' N 33° 34,643' W	x	x	x	x	x	x	x	x	x	x	x	x	x

[b] Samples for intercomparison of Hg were collected in 500 ml glass bottles but at station 18 only.

Table 12.26 Overview of stations sampled with TM clean CTD and the parameters for which aliquots were collected in the clean laboratory container. This table includes all parameters related to the workgroups of the University of Lausanne and Jacobs University Bremen.

	Jacobs University Bremen										University of Lausanne	
Parameter / Station	**SQF**	**UF**	**Diss TM**	**HFSE**	**Pt**	**Cr redox species_Cr^{3+} and Cr^{6+}**	**V redox species**	**Fe ligands**	**Zn ligands**	**Cu ligands**	**Cr-total and δ^{53}Cr**	**Cr speciation_Cr^{3+}**
M176/2-3 09.09.2021 36° 13,417' N 33° 54,794' W	x		x	x	x	x	x	x	x	x	x	x
M176/2-4 10.09.2021 36° 14,235' N 33° 53,831' W			x	x							x	x
M176/2-5 11.09.2021 36° 13,783' N 33° 54,182' W	x		x	x	x	x	x	x	x	x	x	x
M176/2-6 12.09.2021 36° 15,065' N 33° 52,968' W	x		x	x	x							
M176/2-8 14.09.2021 36° 14,076' N 33° 53,979' W			x	x								
M176/2-9 15.09.2021 36° 16,556' N	x	x	x	x	x	x	x	x	x	x	x	x

	Jacobs University Bremen										**University of Lausanne**	
Parameter / Station	**SQF**	**UF**	**Diss TM**	**HFSE**	**Pt**	**Cr redox species_Cr^{3+} and Cr^{6+}**	**V redox species**	**Fe ligands**	**Zn ligands**	**Cu ligands**	**Cr-total and $\delta^{53}Cr$**	**Cr speciation_Cr^{3+}**
33° 53,710' W												
M176/2-10 16.09.2021 36° 16,693' N 33° 51,300' W			x	x							x	
M176/2-12 17.09.2021 36° 14,799' N 33° 53,839' W	x	x	x	x	x	x	x	x	x	x		
M176/2-13 18.09.2021 36° 15,518' N 33° 50,216' W			x	x								
M176/2-14 19.09.2021 36° 15,518' N 33° 50,216' W			x	x								
M176/2-15 20.09.2021 36° 13,510' N 33° 48,380' W	x	x	x	x	x	x	x	x	x	x	x	x
M176/2-16 21.09.2021 36° 13,189' N 33° 47,159' W											x	x

	Jacobs University Bremen										University of Lausanne	
Parameter / Station	**SQF**	**UF**	**Diss TM**	**HFSE**	**Pt**	**Cr redox species_Cr^{3+} and Cr^{6+}**	**V redox species**	**Fe ligands**	**Zn ligands**	**Cu ligands**	**Cr-total and $\delta^{53}Cr$**	**Cr speciation_Cr^{3+}**
M176/2-17 22.09.201 36° 13,964' N 33° 43,957' W			x	x								
M176/2-18 23.09.201 36° 13,964' N 33° 43,957' W	x	x	x	x	x	x	x	x			x	x
M176/2-21 25.09.201 36° 23,193' N 33° 37,578' W			x	x								
M176/2-23 26.09.201 36° 29,486' N 33° 34,734' W											x	x
M176/2-24 27.09.201 36° 33,390' N 33° 34,643' W	x	x	x	x	x	x	x	x	x	x		

Table 12.27 Summary of samples collected by Jacobs University Bremen.

clean lab container															
Date	**Sampling Time [UTC]**	**Station ID**	**Bedford Number**	**Niskin Bottle**	**Depth [m]**	**Latitude [N]**	**Longitude [W]**	**FeL**	**ZnL**	**CuL**	**Pt**	**Cr-Spec. 0.2 µm**	**V-Spec.**	**HFSE**	**TM**
09.09.2021	07:30	M176/2_3	20001	1	2498	36° 13,418	33° 54,794	x	x	x	x	x	x	x	x
	07:30	M176/2_3	20003	3	2498	36° 13,418	33° 54,794				x	x	x	x	x
	07:36	M176/2_3	20005	5	2196	36° 13,418	33° 54,794	x			x	x	x	x	x
	07:37	M176/2_3	20007	7	2147	36° 13,418	33° 54,794	x			x	x	x	x	x
	07:39	M176/2_3	20009	9	2098	36° 13,418	33° 54,794	x	x	x	x	x	x	x	x
	07:41	M176/2_3	20011	11	2049	36° 13,418	33° 54,794	x			x	x	x	x	x
	07:43	M176/2_3	20013	13	2000	36° 13,418	33° 54,794	x	x	x	x	x	x	x	x
	07:45	M176/2_3	20015	15	1902	36° 13,418	33° 54,794	x			x	x	x	x	x
	07:47	M176/2_3	20017	17	1851	36° 13,418	33° 54,794				x	x	x	x	x
	07:51	M176/2_3	20019	19	1703	36° 13,418	33° 54,794							x	x
	07:55	M176/2_3	20023	23	1600	36° 13,418	33° 54,794	x	x	x	x	x	x		
10.09.2021	06:41	M176/2_4	20025	1	2286	36° 14.235	33° 53.831							x	x
	06:48	M176/2_4	20033	9	2095	36° 14.235	33° 53.831							x	x
	06:54	M176/2_4	20037	13	1996	36° 14.235	33° 53.831							x	x
	06:57	M176/2_4	20041	17	1898	36° 14.235	33° 53.831							x	x
	07:05	M176/2_4	20047	23	1598	36° 14.235	33° 53.831							x	x
11.09.2021	07:04	M176/2_5	20049	1	2289	36° 13.732	33° 54.153	x	x	x	x	x	x	x	x
	07:06	M176/2_5	20051	3	2237	36° 13.732	33° 54.153				x	x	x	x	x
	07:08	M176/2_5	20053	5	2187	36° 13.732	33° 54.153	x			x	x	x	x	x
	07:10	M176/2_5	20055	7	2140	36° 13.732	33° 54.153	x			x	x	x	x	x
	07:12	M176/2_5	20057	9	2092	36° 13.732	33° 54.153	x	x	x	x	x	x	x	x
	07:14	M176/2_5	20059	11	2042	36° 13.732	33° 54.153	x			x	x	x	x	x
	07:16	M176/2_5	20061	13	1990	36° 13.732	33° 54.153	x	x	x	x	x	x	x	x
	07:18	M176/2_5	20063	15	1939	36° 13.732	33° 54.153	x			x	x	x	x	x
	07:20	M176/2_5	20065	17	1891	36° 13.732	33° 54.153				x	x	x	x	x
	07:30	M176/2_5	20071	23	1594	36° 13.732	33° 54.153	x	x	x	x	x	x	x	x

clean lab container																
Date	Sampling Time [UTC]	Station ID	Bedford Number	Niskin Bottle	Depth [m]	Latitude [N]	Longitude [W]	FeL	ZnL	CuL	Pt	Cr-Spec. 0.2 µm	V-Spec.	HFSE	TM
12.09.2021	06:48	M176/2_6	20073	1	2188	36° 15,097	33° 53.033				x			x	x
12.09.2021	06:42	M176/2_6	20075	3	2139	36° 15,097	33° 53.033				x			x	x
	06:53	M176/2_6	20077	5	2113	36° 15,097	33° 53.033				x			x	x
	06:55	M176/2_6	20079	7	2090	36° 15,097	33° 53.033				x			x	x
	06:58	M176/2_6	20081	9	2068	36° 15,097	33° 53.033				x			x	x
	07:00	M176/2_6	20083	11	2043	36° 15,097	33° 53.033				x			x	x
	07:03	M176/2_6	20085	13	1993	36° 15,097	33° 53.033				x			x	x
	07:05	M176/2_6	20087	15	1943	36° 15,097	33° 53.033				x			x	x
	07:07	M176/2_6	20089	17	1892	36° 15,097	33° 53.033				x			x	x
	07:15	M176/2_6	20095	23	1694	36° 15,097	33° 53.033				x			x	x
13.09.2021	06:36	M176/2_7	20097	1	2312	36° 13.847	33° 54.165	x	x	x	x	x	x	x	x
	06:39	M176/2_7	20099	3	2269	36° 13.847	33° 54.165				x	x	x	x	x
	06:42	M176/2_7	20101	5	2236	36° 13.847	33° 54.165	x			x	x	x	x	x
	06:45	M176/2_7	20103	7	2203	36° 13.847	33° 54.165	x			x	x	x	x	x
	06:48	M176/2_7	20105	9	2173	36° 13.847	33° 54.165	x			x	x	x	x	x
	06:53	M176/2_7	20107	11	2160	36° 13.847	33° 54.165								
	06:53	M176/2_7	20108	12	2160	36° 13.847	33° 54.165	x	x	x	x	x	x	x	x
	06:56	M176/2_7	20109	13	2122	36° 13.847	33° 54.165	x	x	x	x	x	x	x	x
	06:59	M176/2_7	20111	15	2094	36° 13.847	33° 54.165	x			x	x	x	x	x
	07:03	M176/2_7	20113	17	2040	36° 13.847	33° 54.165				x	x	x	x	x
	07:14	M176/2_7	20119	23	1778	36° 13.847	33° 54.165	x	x	x	x	x	x	x	x
14.09.2021	06:55	M176/2_8	20121	1	2283	36° 14.076	33° 53.979							x	x
	07:00	M176/2_8	20125	5	2216	36° 14.076	33° 53.979							x	x
	07:03	M176/2_8	20127	7	2177	36° 14.076	33° 53.979							x	x
	07:17	M176/2_8	20137	17	2022	36° 14.076	33° 53.979							x	x
	07:26	M176/2_8	20143	23	1894	36° 14.076	33° 53.979							x	x
15.09.2021	06:51	M176/2_9	20145	1	2475	36° 16.583	33° 53.694	x	x	x	x	x	x	x	x

clean lab container															
Date	**Sampling Time [UTC]**	**Station ID**	**Bedford Number**	**Niskin Bottle**	**Depth [m]**	**Latitude [N]**	**Longitude [W]**	**FeL**	**ZnL**	**CuL**	**Pt**	**Cr-Spec. 0.2 µm**	**V-Spec.**	**HFSE**	**TM**
	06:57	M176/2_9	20147	3	2398	36° 16.583	33° 53.694				x	x	x	x	x
15.09.2021	07:00	M176/2_9	20149	5	2297	36° 16.583	33° 53.694	x			x	x	x	x	x
	07:03	M176/2_9	20151	7	2198	36° 16.583	33° 53.694	x			x	x	x	x	x
	07:05	M176/2_9	20153	9	2173	36° 16.583	33° 53.694	x	x	x	x	x	x	x	x
	07:07	M176/2_9	20155	11	2150	36° 16.583	33° 53.694	x			x	x	x	x	x
	07:11	M176/2_9	20159	15	2099	36° 16.583	33° 53.694	x			x	x	x	x	x
	07:13	M176/2_9	20161	17	2074	36° 16.583	33° 53.694				x	x	x	x	x
	07:16	M176/2_9	20165	21	2023	36° 16.583	33° 53.694	x	x	x	x	x	x	x	x
	07:20	M176/2_9	20167	23	1899	36° 16.583	33° 53.694	x	x	x	x	x	x	x	x
16.09.2021	07:14	M176/2_10	20169	1	2644	36 °16.693	36 °16.693							x	x
	07:18	M176/2_10	20171	3	2586	36 °16.693	36 °16.693							x	x
	07:22	M176/2_10	20173	5	2488	36 °16.693	36 °16.693							x	x
	07:26	M176/2_10	20175	7	2387	36 °16.693	36 °16.693							x	x
	07:30	M176/2_10	20177	9	2338	36 °16.693	36 °16.693							x	x
	07:32	M176/2_10	20179	11	2287	36 °16.693	36 °16.693							x	x
	07:34	M176/2_10	20181	13	2237	36 °16.693	36 °16.693							x	x
	07:36	M176/2_10	20183	15	2188	36 °16.693	36 °16.693							x	x
	07:38	M176/2_10	20185	17	2139	36 °16.693	36 °16.693							x	x
	07:45	M176/2_10	20191	23	1890	36 °16.693	36 °16.693							x	x
17.09.2021	06:37	M176/2_11	20193	1	2380	36° 14.806	33° 53.844	x	x	x	x	x	x	x	x
	06:42	M176/2_11	20195	3	2295	36° 14.806	33° 53.844				x	x	x	x	x
	06:47	M176/2_11	20197	5	2194	36° 14.806	33° 53.844	x			x	x	x	x	x
	06:50	M176/2_11	20199	7	2146	36° 14.806	33° 53.844	x			x	x	x	x	x
	06:53	M176/2_11	20201	9	2122	36° 14.806	33° 53.844	x	x	x	x	x	x	x	x
	06:55	M176/2_11	20203	11	2096	36° 14.806	33° 53.844	x			x	x	x	x	x
	06:57	M176/2_11	20205	13	2070	36° 14.806	33° 53.844	x			x	x	x	x	x
	06:59	M176/2_11	20207	15	2045	36° 14.806	33° 53.844	x	x	x	x	x	x	x	x

clean lab container															
Date	Sampling Time [UTC]	Station ID	Bedford Number	Niskin Bottle	Depth [m]	Latitude [N]	Longitude [W]	FeL	ZnL	CuL	Pt	Cr-Spec. 0.2 µm	V-Spec.	HFSE	TM
	07:02	M176/2_11	20209	17	2019	36° 14.806	33° 53.844	x			x	x	x	x	x
17.09.2021	07:06	M176/2_11	20213	21	1947	36° 14.806	33° 53.844				x	x	x	x	x
	07:09	M176/2_11	20215	23	1897	36° 14.806	33° 53.844	x	x	x	x	x	x	x	x
18.09.2021	07::15	M176/2_13	20217	1	2500	36° 15.517	33° 50.216							x	x
	07:22	M176/2_13	20221	5	2295	36° 15.517	33° 50.216							x	x
	07:25	M176/2_13	20223	7	2197	36° 15.517	33° 50.216							x	x
	07:27	M176/2_13	20225	9	2146	36° 15.517	33° 50.216							x	x
	07:29	M176/2_13	20227	11	2120	36° 15.517	33° 50.216							x	x
	07:30	M176/2_13	20229	13	2095	36° 15.517	33° 50.216							x	x
	07:31	M176/2_13	20231	15	2070	36° 15.517	33° 50.216							x	x
	07:33	M176/2_13	20233	17	2046	36° 15.517	33° 50.216							x	x
	07:36	M176/2_13	20237	21	1997	36° 15.517	33° 50.216							x	x
	07:40	M176/2_13	20239	23	1899	36° 15.517	33° 50.216							x	x
19.09.2021	06:45	M176/2_14	20241	1	2623	36.2363°N	33.8350 ° W							x	x
	06:52	M176/2_14	20243	3	2490	36.2363°N	33.8350 ° W							x	x
	06:55	M176/2_14	20245	5	2394	36.2363°N	33.8350 ° W							x	x
	06:58	M176/2_14	20247	7	2295	36.2363°N	33.8350 ° W							x	x
	07:00	M176/2_14	20249	9	2240	36.2363°N	33.8350 ° W							x	x
	07:02	M176/2_14	20251	11	2196	36.2363°N	33.8350 ° W							x	x
	07:04	M176/2_14	20253	13	2144	36.2363°N	33.8350 ° W							x	x
	07:06	M176/2_14	20255	15	2095	36.2363°N	33.8350 ° W							x	x
	07:09	M176/2_14	20257	15	2045	36.2363°N	33.8350 ° W							x	x
	07:15	M176/2_14	20263	23	1897	36.2363°N	33.8350 ° W							x	x
20.09.2021	07:17	M176/2_15	20265	1	3034	36° 13.509	33° 48.380	x	x	x	x	x	x	x	x
	07:27	M176/2_15	20267	3	2792	36° 13.509	33° 48.380				x	x	x	x	x
	07:32	M176/2_15	20269	5	2592	36° 13.509	33° 48.380	x			x	x	x	x	x
	07:37	M176/2_15	20271	7	2393	36° 13.509	33° 48.380	x			x	x	x	x	x

clean lab container															
Date	**Sampling Time [UTC]**	**Station ID**	**Bedford Number**	**Niskin Bottle**	**Depth [m]**	**Latitude [N]**	**Longitude [W]**	**FeL**	**ZnL**	**CuL**	**Pt**	**Cr-Spec. 0.2 µm**	**V-Spec.**	**HFSE**	**TM**
	07:43	M176/2_15	20273	9	2196	36° 13.509	33° 48.380				x	x	x	x	x
20.09.2021	07:49	M176/2_15	20275	11	2145	36° 13.509	33° 48.380	x	x	x	x	x	x	x	x
	07:51	M176/2_15	20277	13	2096	36° 13.509	33° 48.380	x	x	x	x	x	x	x	x
	07:53	M176/2_15	20279	15	2069	36° 13.509	33° 48.380	x			x	x	x	x	x
	07:54	M176/2_15	20281	17	2044	36° 13.509	33° 48.380				x	x	x	x	x
	08:01	M176/2_15	20287	23	1896	36° 13.509	33° 48.380	x	x	x	x	x	x	x	x
22.09.2021	07:04	M176/2_17	20313	1	2600	36° 13.509	33° 48.380							x	x
	07:16	M176/2_17	20317	5	2297	36° 13.509	33° 48.380							x	x
	07:19	M176/2_17	20319	7	2250	36° 13.509	33° 48.380							x	x
	07:22	M176/2_17	20321	9	2204	36° 13.509	33° 48.380							x	x
	07:23	M176/2_17	20323	11	2177	36° 13.509	33° 48.380							x	x
	07:25	M176/2_17	20325	13	2152	36° 13.509	33° 48.380							x	x
	07:27	M176/2_17	20327	15	2128	36° 13.509	33° 48.380							x	x
	07:29	M176/2_17	20329	17	2102	36° 13.509	33° 48.380							x	x
	07:34	M176/2_17	20331	19	2077	36° 13.509	33° 48.380							x	x
	07:40	M176/2_17	20335	23	1900	36° 13.509	33° 48.380							x	x
23.09.2021	09:14	M176/2_18	20337	1	2388	36° 16.149	33° 44.022	x			x	x	x	x	x
	09:22	M176/2_18	20339	3	2299	36° 16.149	33° 44.022				x	x	x	x	x
	09:24	M176/2_18	20341	5	2249	36° 16.149	33° 44.022	x			x	x	x	x	x
	09:27	M176/2_18	20343	7	2196	36° 16.149	33° 44.022	x			x	x	x	x	x
	09:28	M176/2_18	20345	9	2171	36° 16.149	33° 44.022	x			x	x	x	x	x
	09:30	M176/2_18	20347	11	2147	36° 16.149	33° 44.022	x			x	x	x	x	x
	09:32	M176/2_18	20349	13	2120	36° 16.149	33° 44.022	x			x	x	x	x	x
	09:34	M176/2_18	20351	15	2093	36° 16.149	33° 44.022	x			x	x	x	x	x
	09:36	M176/2_18	20353	17	2057	36° 16.149	33° 44.022				x	x	x	x	x
	09:40	M176/2_18	20359	23	1783	36° 16.149	33° 44.022	x			x	x	x	x	x
25.09.2021	07:19	M176/2_21	20385	1	2272	36° 23.248	33° 37.599							x	x

clean lab container																
Date	Sampling Time [UTC]	Station ID	Bedford Number	Niskin Bottle	Depth [m]	Latitude [N]	Longitude [W]	FeL	ZnL	CuL	Pt	Cr-Spec. 0.2 µm		V-Spec.		HFSE	TM
	07:21	M176/2_21	20387	3	2245	36° 23.248	33° 37.599									x	x
25.09.2021	07:23	M176/2_21	20389	5	2222	36° 23.248	33° 37.599									x	x
	07:24	M176/2_21	20391	7	2197	36° 23.248	33° 37.599									x	x
	07:26	M176/2_21	20393	9	2172	36° 23.248	33° 37.599									x	x
	07:27	M176/2_21	20395	11	2146	36° 23.248	33° 37.599									x	x
	07:29	M176/2_21	20397	13	2121	36° 23.248	33° 37.599									x	x
	07:31	M176/2_21	20399	15	2096	36° 23.248	33° 37.599									x	x
	07:33	M176/2_21	20401	17	2071	36° 23.248	33° 37.599									x	x
	07:40	M176/2_21	20407	23	1896	36° 23.248	33° 37.599									x	x
27.09.2021	07:22	M176/2_24	20433	1	2878	36.5571	33.5781	x	x	x	x	x		x		x	x
	07:26	M176/2_24	20435	3	2797	36.5571	33.5781				x	x		x		x	x
	07:32	M176/2_24	20437	5	2597	36.5571	33.5781	x			x	x		x		x	x
	07:38	M176/2_24	20439	7	2398	36.5571	33.5781	x			x	x		x		x	x
	07:42	M176/2_24	20441	9	2300	36.5571	33.5781	x	x	x	x	x		x		x	x
	07:42	M176/2_24	20442	10	2300	36.5571	33.5781										
	07:45	M176/2_24	20445	11	2197	36.5571	33.5781	x			x	x		x		x	x
	07:48	M176/2_24	20445	13	2146	36.5571	33.5781	x	x	x	x	x		x		x	x
	07:49	M176/2_24	20447	15	2094	36.5571	33.5781	x			x	x		x		x	x
	07:51	M176/2_24	20449	17	2043	36.5571	33.5781				x	x		x		x	x
	08:00	M176/2_24	20455	23	1799	36.5571	33.5781	x	x	x	x	x		x		x	x
							SUM	**64**	**28**	**28**	**91**	**81**		**81**		**151**	**151**